

2016

An Integrated Full-bridge Class-DE Ultrasound Transducer Driver for HIFU Application

Song, Ruiqi

<http://knowledgecommons.lakeheadu.ca/handle/2453/751>

Downloaded from Lakehead University, Knowledge Commons

AN INTEGRATED FULL-BRIDGE CLASS-DE ULTRASOUND TRANSDUCER DRIVER FOR HIFU APPLICATIONS

by
Ruiqi Song

Supervised by Dr. Carlos E. Christoffersen, and Dr. Laura Curiel

A thesis submitted in partial fulfilment of the requirement of the
M. Sc. degree in
Electrical and Computer Engineering department of
Lakehead University
Thunder Bay, Ontario

May 3, 2016

Abstract

This thesis presents a CMOS integrated transducer driver for high intensity focused ultrasound (HIFU) applications. Because this driver will be used in a magnetic resonance imaging (MRI) environment, no magnetic components such as inductors and transformers have been used in this design. The transducer is directly connected to the driver without a matching network. The output stage of this driver is a full-bridge Class DE RF amplifier which is able to deliver more power than the previous design that has a half-bridge Class DE amplifier.

The driver was also designed to be used in a transducer array. A digital control unit was integrated with the power amplifier that allows to program the driver's phase shift and duty ratio. A strategy to drive a ultrasound transducer array using the designed driver is also presented in this thesis.

This design was implemented using the AMS H35B4 CMOS technology using the Cadence suite of design tools and occupies a die area of 2mm by 1.5mm with 20 input and output pads. Simulation and initial experimental results are presented in this work. The proposed integrated CMOS driver has an efficiency of 89.4% with 3.60 W of output power. Results are a little bit different for each transducer.

Acknowledgements

This thesis was supported by Lakehead University and CMC Microsystems.

It gives me great pleasure in acknowledge my supervisor, Dr. Carlos E. Christoffersen, and my co-supervisor, Dr. Laura Curiel, for allowing me to work on this research project and for their support by providing insightful guidance.

I also would like to thank my family for their encouragement, patience and understanding.

Ruiqi Song

rsong1@lakeheadu.ca

Contents

1	Introduction	1
1.1	Objectives and Motivation of this study	1
1.2	Thesis Overview	3
2	Background Information and Literature Review	4
2.1	Introduction	4
2.2	Characterization of Ultrasound Transducer	4
2.3	Switched RF Amplifiers	7
2.3.1	Class-D Amplifiers	7
2.3.2	Class-E Amplifiers	11
2.3.3	Class-DE Amplifier	12
2.3.4	Step-up Driving Circuit	14
2.3.5	Flyback Topology	14
2.3.6	Push-pull driving circuit	14
2.4	Literature Review	16
2.5	Previous Design by Our Group	20
2.6	Summary	30
3	Strategy to Drive a Transducer array in Class-DE Mode	32
3.1	Characterization of the Transducer Array	34
3.2	The Transducer Array Driving Strategies	35
3.2.1	Using an External Parallel Capacitor	38
3.2.2	Using the Average frequency	42
3.3	Summary	42

4	Ultrasonic Transducer Driver Design	45
4.1	Introduction	45
4.2	Full-bridge Class-DE Amplifier	46
4.3	The Gate driver	49
4.4	Digital Logic Unit	50
4.4.1	The Structure of Each Block	50
4.4.2	Operating procedure of the digital logic unit	56
4.4.3	Additional Safety Logic Block	60
4.4.4	Simulation Results of Digital Logic Unit	62
4.5	The Layout Design	65
5	Simulation and Experimental Results	67
5.1	Simulation Results with Optimum Parameters	67
5.2	Experimental Setup	70
5.3	Experimental Results	72
6	Conclusions and Future Work	77
6.1	Conclusions	77
6.2	Future Work	77
A	Pin Diagram of the Full-Bridge Class-DE Driver	79
B	Parameter Calculations of MOSFETs	80
B.1	Gate Capacitance of MOSFETs	80
B.2	K' and Threshold Voltage	82
B.2.1	Calculation of on-resistance	86
C	Schematic Diagrams	87
D	Layout View	91

List of Figures

1.1	Block diagram of driving an Ultrasound transducer array	2
2.1	Structure of an ultrasound transducer [2]	5
2.2	BVD equivalent circuit of a resonator near its resonance frequency [1,2]	5
2.3	Impedance and admittance plots of the equivalent circuit of transducers	6
2.4	Plots of measured reflection coefficient and equivalent circuit model's reflection coefficient on a Smith Chart	8
2.5	Schematic of the CMOS integrated Class-D RF amplifier [6]	9
2.6	Input and output waveforms of the CMOS integrated Class-D RF amplifier [6]	9
2.7	Topology of the CMOS integrated Class-D full-bridge RF amplifier	10
2.8	Topology of the CMOS integrated Class-E RF amplifier.	11
2.9	Input and output waveforms of the CMOS integrated Class-E RF amplifier. [6]	12
2.10	Schematic of the CMOS integrated Class-DE RF amplifier	13
2.11	Schematic of the step-up driving circuit	13
2.12	Topology of the flyback transducer driver [8]	15
2.13	Schematic of the Push-pull driving circuit	15
2.14	Schematic of the transducer driver which was proposed by Cain and Hall [9].	16
2.15	Schematic of the driver that is used by Tang and Clement [7]	17
2.16	Input waveform of the driver that is used by Tang and Clement [7]	18
2.17	Schematic of driver that is proposed by Yang and Xu [10].	18
2.18	Schematic of high voltage pulser that is proposed by Zhao and Tian [11].	19
2.19	Block diagram of A. Bozkurk and O. Farhanieh's driver IC [12]	20
2.20	Schematic of staircase-wave driver that is proposed by K. Moro and J. Okada. [13]	21
2.21	Input and output voltage waveforms of the staircase-wave driver [13]	22
2.22	Schematic of driver that is proposed by Wai Wong. [5]	23

2.23	Output waveforms of half-bridge Class-DE amplifier [5]	23
2.24	Equivalent circuits of Class-DE amplifier in each interval. [6]	24
2.25	Variations of f_r and f_x with duty ratio of an ultrasound transducer	27
2.26	f_r and f_x plots of transducer Tx.3	29
2.27	Effect of duty ratio on efficiency,output power and current peak with variable duty ratios	29
2.28	Output waveforms for transducer Tx.3	30
3.1	Multi-element ultrasound transducer array that was designed by J. L. Kivinen [4] . .	32
3.2	Half-bridge Class-DE amplifier which was proposed by Wai Wong [1, 2, 5]	33
3.3	Output voltage and current waveforms of all the six elements that are driven by Class-DE amplifier	36
3.4	Output voltage and current waveforms of element B that is driven under 1024kHz which is a non-optimum frequency for element B	37
3.5	Half-bridge Class-DE amplifier with the parallel external capacitor	38
3.6	$C_{ext,r}$ and $C_{ext,x}$'s plots of element E in Kivinen's transducer array	39
3.7	Output waveforms of all the elements that are driven by the using the external capacitor method	41
3.8	Output waveforms of all the elements that are driven by the average of their optimum frequencies	43
4.1	Block diagram of the proposed integrated transducer driver [5]	45
4.2	Symbols of the MOSFETs (a) HV PMOS; (b) HV NMOS; (c) LV PMOS; (d) LV NMOS	46
4.3	Topology of the full-bridge Class-DE amplifier	47
4.4	Inputs and output waveforms of the full-bridge Class-DE amplifier, (a), (b), (c) and (d) The switch-on diagram of transistors M1, M2, M3 and M4. (e) The voltage waveform across the load	48
4.5	Schematic of MOSFETs' gate driver [2, 16].	50
4.6	Input signal and output signal of the gate driver.	51
4.7	Structure of the digital logic unit.	51
4.8	Structure of 10-bit-counter.	53
4.9	Schematic of 30-bit-register.	54
4.10	Transducer array driving method.	54
4.11	Schematic of the 10-bit-comparator.	55
4.12	Schematic of the pulse-trains-generator.	56

4.13	Block diagrams of the relationship of the frequency divider, phase shift and duty ratio controller and pulse train generator.	57
4.14	Block diagram of the frequency divider.	57
4.15	Output diagrams of the frequency divider.	58
4.16	Block diagram of the phase shift and duty ratios controller.	59
4.17	Output diagrams of the phase shift and duty ratios controller.	59
4.18	Input and output diagrams of the pulse trains generator.	61
4.19	Schematic of the additional safety logic block [2].	62
4.20	Outputs waveforms of the digital logic unit, its input clock signal's frequency is 200MHz, phase shift is 10%, duty ratio is 20%	64
4.21	Layout view of the driver	66
5.1	Simulation results of the full-bridge Class-DE driver that is proposed in this thesis. Brown: output voltage (Output1-Output2); Red: potential of Output1; Pink: potential of Output2; Orange: load current	68
5.2	Simulation results of the half-bridge Class-DE driver that was designed by our group [5]. Brown: output voltage ; Red: load current	69
5.3	Fabricated driver in a testing circuit.	70
5.4	Logic test result of the driver.	71
5.5	Block diagram of the testing setup of the driver	72
5.6	Simulation results of driving the transducer with $C_{ext} = 128$ pF by 1028 kHz, 0° phase shift and 25% duty ratio pulse trains. Brown: output voltage (Output1-Output2); Red: potential of Output1; Pink: potential of Output2; Orange: load current	74
5.7	Experimental result of driving the transducer by 1036 kHz and 25% duty ratio pulse trains.	75
5.8	Simulation results of driving the transducer with $C_{ext} = 128$ pF by 1036 kHz, 0° phase shift and 25% duty ratio pulse trains. Brown: output voltage (Output1-Output2); Red: potential of Output1; Pink: potential of Output2; Orange: load current	76
A.1	Pin diagram of the full-bridge Class-DE driver	79
B.1	Gate capacitance extraction circuit	81
B.2	Gate voltage plot of NMOS	81
B.3	Gate voltage plot of PMOS	82
B.4	Schematic of a MOSFET's parameters extraction [2]	83

B.5	$\sqrt{I_D}$ plots of a real MOSFET and a theoretical model, the red line is the real MOSFET's plot and the black line is the theoretical model's plot [2]	84
B.6	$\sqrt{I_D}$ plots the PMOS, the blue line is the theoretical square root of drain current $\sqrt{I_{Dt}}$ and the red line is the real model's square root of drain current $\sqrt{I_D}$	85
B.7	$\sqrt{I_D}$ plots the NMOS, the blue line is the theoretical square root of drain current $\sqrt{I_{Dt}}$ and the red line is the real model's square root of drain current $\sqrt{I_D}$	85
C.1	Block diagrams of simulation circuit of the full-bridge Class-DE amplifier.	88
C.2	Block diagrams of the logic control unit	89
C.3	Block diagrams of the Class-DE amplifier with gate drivers	90
D.1	Layout of the 10-bit-comparator	92
D.2	Layout of the 10-bit-counter	93
D.3	Layout of the pulse trains generator	94
D.4	Layout of the 30-bit-register	95
D.5	Layout of the NMOS's gate driver that designed by Wai Wong	96
D.6	Layout of the PMOS's gate driver that designed by Wai Wong	97
D.7	Layout of the gate drivers' current mirror that designed by Wai Wong	98
D.8	Layout of a branch of Class-DE amplifier that designed by Wai Wong	99
D.9	Layout of the additional safety logic block that designed by Wai Wong	100

List of Tables

1	List of Symbols	IX
2.1	Equivalent circuit's parameters of an ultrasound transducer.	26
2.2	Optimum Class-DE switching frequencies and duty ratios of the instance transducer.	27
2.3	Equivalent circuit components' values of Tx.3	28
2.4	DC supply power, output power and efficiency for transducer Tx.3	29
2.5	Comparison of some published works	31
3.1	f_S , f_P and $ Z $ values of each element of Kivinen's transducer array	34
3.2	Equivalent circuit parameters of all the six elements of Kivinen's transducer array	34
3.3	Operation frequencies and duty cycles of all elements in the transducer array	35
3.4	Simulation results of all the elements in the transducer array	37
3.5	External capacitance values of all the elements in Kivinen's transducer array	40
3.6	Efficiencies of all the elements that are driven at 1.0242MHz with C_{ext}	40
3.7	Efficiencies of all the six elements that are driven at 1.0242MHz without C_{ext}	40
3.8	Efficiencies of all elements which are driven by average frequency	42
4.1	Half-bridge Class-DE amplifier's width and length parameters [5]	47
4.2	Truth table of the additional safety logic block [2]	63
5.1	Equivalent circuit parameters of the transducer [5]	67
5.2	DC supply power, output power and efficiencies of driving the transducer by full-bridge and half-bridge Class-DE drivers	70
B.1	Step signal responds of gate voltage of the PMOS and NMOS that used in the amplifier	81
B.2	Summary of extracted parameters values of the PMOS and NMOS	86

Table 1: List of Symbols

Symbols	Meaning
Z	Impedance
C_P	Parallel capacitance
C_S	Series capacitance
R_S	Series resistance
L_S	Series inductance
ω	Angular frequency
ω_r	Angular frequency obtained from real part of impedance
ω_x	Angular frequency obtained from imaginary part of impedance
f_s	Series resonance frequency
f_p	parallel resonance frequency
Y	Admittance
G	Real part of admittance
R	Real part of impedance
V_{DS1}	Voltage across the M1
V_{DS2}	Voltage across the M2
i_1	Instantaneous current of M1
i_2	Instantaneous current of M2
i_3	Instantaneous current of M3
i_4	Instantaneous current of M4
i_C	Instantaneous current of C_p
i_L	Instantaneous current of series capacitor
V_1	The fundamental component of V_{DS2}
I_1	The fundamental component of i
Z_L	Load impedance
Z_S	Impedance of series branch
R_L	Real part of Z_L
X_L	Imaginary part of Z_L
f_r	Frequency obtained from real part of impedance
f_x	Frequency obtained from imaginary part of impedance
D	Duty ratio
C_{ext}	External capacitance
$C_{ext,r}$	External capacitance solved from real part of impedance
$C_{ext,x}$	External capacitance solved from imaginary part of impedance
ϕ	Phase angle related to the duty ratio
v_{OUT}	Output voltage
C_{gate}	Gate capacitance of MOSFET
C_{ox}	Oxide capacitance per unit area
t_{ox}	Gate oxide thickness
ϵ	Permittivity
ϵ_0	Permittivity of free space
ϵ_r	Relative permittivity
L_D	Lateral diffusion
W	Width of MOSFET's gate
L	Length of MOSFET's gate
I_{Dt}	Theoretical drain current
I_D	Drain current
V_{GS}	Voltage across the gate and source
V_{th}	Threshold Voltage
R_{ch}	Channel resistance of MOSFETs

Chapter 1

Introduction

1.1 Objectives and Motivation of this study

High Intensity Focused Ultrasound (HIFU) is a surgical technique that ablates human tissues by using the thermal energy that is generated by focused ultrasound [1,2]. It is a kind of non-invasive technique that can be used for the ablation of tumours or other kind of damaged tissues in human bodies. The ablation process is very precise. A movement of patient's body would cause the displacement of the focal zone of the HIFU, and then other tissues that are around the tumour could be damaged. In order to avoid that, Magnetic Resonance Imaging (MRI) can be used [1,2] to guide the HIFU operation by monitoring the tissues' temperature, so that the focal zone can be located and the patient's body movements can be compensated in real time. Multi-element ultrasound transducer array is required to allow electronic steering of the focal point. Every element in the transducer array is driven by different phase information to create sufficient acoustic pressure level on the focal zone [1,2]. But the transducer driver cannot include any magnetic components, such as inductors, because they would interfere with the MRI.

Wai Wong has designed an integrated CMOS ultrasound transducer driver for the HIFU operation [1]. The output stage of it is a Class-DE RF amplifier whose efficiency is over 90%, it can deliver 1W of power from the power source to the loaded transducer and it does not have any magnetic components. In this design, the driver needs a pair of pulse trains to drive the PMOS and the NMOS in Class-DE amplifier, so we must provide programmed external pulse trains for the driver.

If we generate the pulse trains inside of the driver, the connection setup of it will be highly simplified. Also, for more flexibility the driver should deliver more power to the load. Therefore, the objective is to design an integrated CMOS transducer driver that can generate the pulse trains and

deliver more than 1W of power to the load transducer. All the challenges of designing the intended driver are listed below:

1. The driver should occupy minimum possible area.
2. We cannot use any magnetic components because of MRI conditions.
3. The phase angle, duty ratios and operating frequencies of Class-DE amplifier's driving pulse trains can be programmable.
4. It should be able to deliver more than 1W of power to the load, if possible

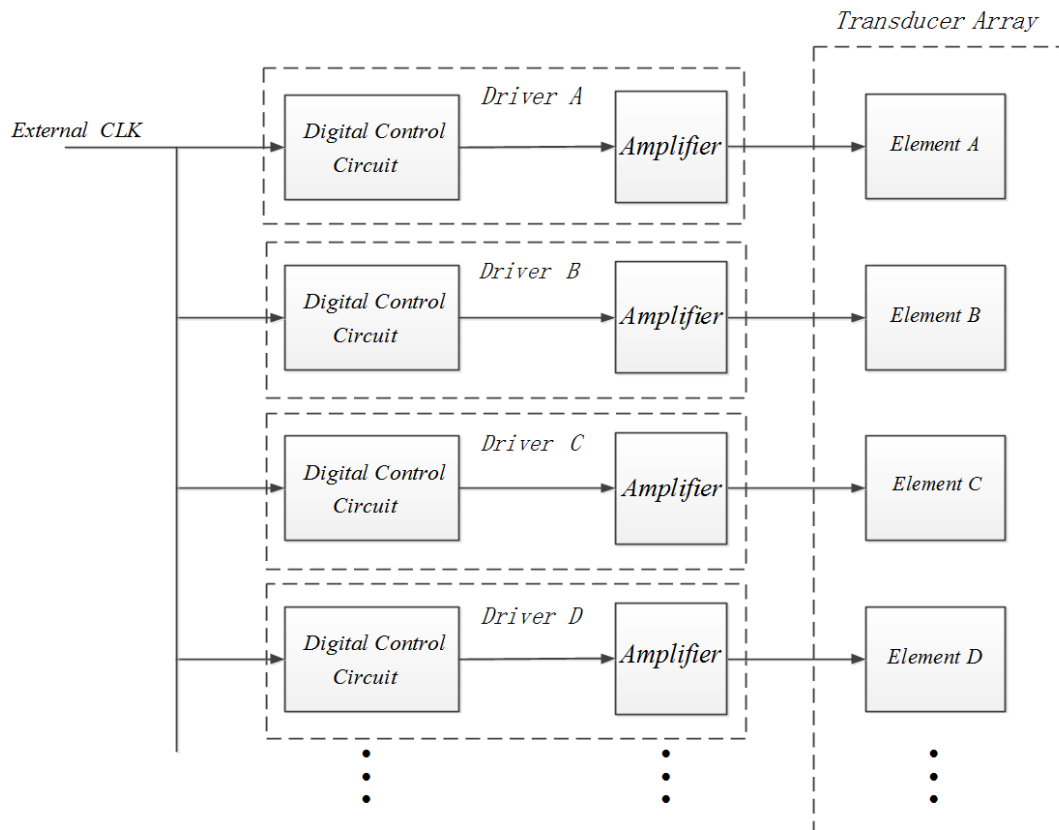


Figure 1.1: Block diagram of driving an Ultrasound transducer array

Figure 1.1 shows the intended block diagram of driving a transducer array. Each element of the array will be driven by a driver and a digital control circuit will make the pulse trains, phase shifts and duty ratio programmable. The control circuit along with a full-bridge Class-DE amplifier will be fabricated on a single chip. All drivers will be driven by an external clock signal and share a

common power source. Also we would like to make a feedback from each driver to measure power delivered to load.

1.2 Thesis Overview

In this thesis, Chapter 2 describes the applicability of switched RF amplifiers, especially Class-DE amplifier, characterization of ultrasound transducer which are used in HIFU application, as well as some published works on the subject of this project. Chapter 3 discusses two strategies of driving a transducer array in Class-DE mode. Chapter 4 discusses the characteristics and design procedure of full-bridge Class-DE amplifiers and its driving strategies and also includes the digital logic control unit of the driver and the functions of each component. Chapter 5 summarizes the experimental results of the driver.

Chapter 2

Background Information and Literature Review

2.1 Introduction

In common ultrasound therapy, people usually use analog amplifiers to drive the ultrasound transducers, especially Class-A RF amplifiers. But the analog amplifiers' efficiency is not high enough to preclude overheating. So in many published works on this subject, it is proposed to use switched amplifiers to drive the transducers. In this Chapter, the characterization of ultrasound transducers, some switched amplifiers and some published works on this subject will be reviewed.

This Chapter is organized as follows: Section 2.2 reviews the background information about characterization of ultrasound transducers; Section 2.3 covers the topologies of some switched amplifiers; Section 2.4 reviews some published works; Section 2.5 introduces the previous design by our group and Section 2.6 summarizes drivers that were reviewed in this chapter.

2.2 Characterization of Ultrasound Transducer

The ultrasound wave that is used in HIFU applications is often generated by piezoelectric transducers. The structure of a transducer is shown in Figure 2.1. As we can see in this Figure, the right most component is called piezoelectric crystal which is the resonator, and the ultrasound wave generator. Electrodes are coated on both sides of resonator for the electrical connections. The leftmost part which is the outer case is called housing. It protects the internal circuitry and resonator from the physical environment.

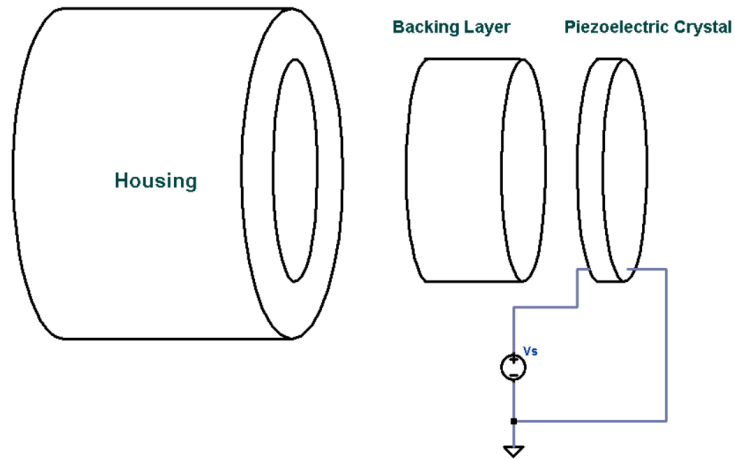


Figure 2.1: Structure of an ultrasound transducer [2]

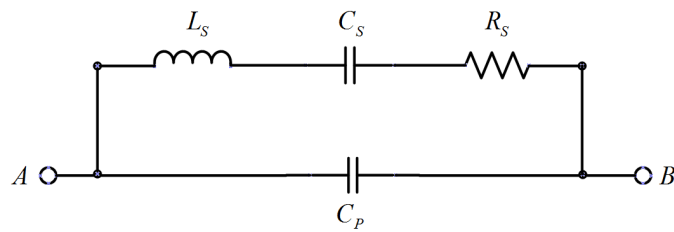


Figure 2.2: BVD equivalent circuit of a resonator near its resonance frequency [1,2]

The Butterworth Van Dyke (BVD) equivalent circuit of a piezoelectric resonator near its own resonance frequency is shown in Figure 2.2 [1, 2]. This equivalent circuit is a combination of a parallel capacitance C_p and a series resonance branch. The parallel capacitance C_p describe the static capacitor of the piezoelectric resonator and is determined by the physical characteristics of the resonator. The series branch which is made up by L_s , C_s and R_s represent the mechanical oscillator near the resonator's resonance frequency. The two terminals A and B that we can see in the Figure 2.1 are the input terminals of the resonator. Usually, one of them is connected to the output of the driver and another one is connected to the ground or the reference point of the circuit. Mathematically, the impedance of the BVD equivalent circuit can be expressed as below:

$$Z = \frac{\frac{1}{j\omega C_P} (\frac{1}{j\omega C_S} + R_S + j\omega L_S)}{\frac{1}{j\omega C_P} + \frac{1}{j\omega C_S} + R_S + j\omega L_S} \quad (2.1)$$

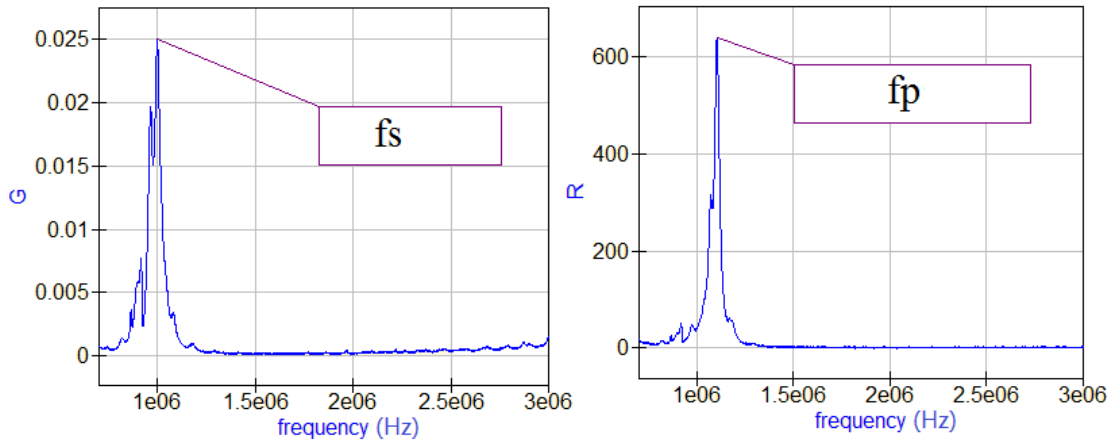


Figure 2.3: Impedance and admittance plots of the equivalent circuit of transducers

where the ω is the angular frequency and the $j = \sqrt{-1}$. In Equation (2.1), we can see that the impedance of this equivalent circuit is a function of the frequency f ($\omega = 2\pi f$). The admittance of the impedance is denoted by Y ($Y = 1/Z$). If we let the real part of impedance $Re(Z) = R$ and real part of admittance $Re(Y) = G$, and then plot them in a certain frequency range, we obtain Figure 2.3. In Figure 2.3, f_p is the parallel resonance frequency in which R (the real part of the resonator's impedance) reaches its maximum value [4]; f_s is the series resonance frequency when G (the real part of admittance of the resonator) is at its maximum [4].

The expressions of the values of all components [1, 3] are shown below:

$$C_S = C_P \left[\left(\frac{f_P}{f_S} \right)^2 - 1 \right] \quad (2.2)$$

$$L_S = \frac{1}{(2\pi f_S)^2 C_S} \quad (2.3)$$

$$C_P = \frac{-Im(Z_S)}{2\pi f_S |Z_S|^2} \quad (2.4)$$

$$R_S = \frac{|Z_S|^2}{Re(Z_S)} \quad (2.5)$$

where the Z_s is the resonator's impedance at its series resonance frequency. Once C_p is found using Equation (2.4), apply Equations (2.2), (2.3) and (2.5) to find the values in the series resonance branch.

By using a vector network analyzer, we can get the reflection coefficient plots of the transducer's resonator on a Smith chart (Figure 2.4). In this figure, the blue solid line is the measured reflection coefficient plot and the red, dashed line is the equivalent circuit model's reflection coefficient plot.

2.3 Switched RF Amplifiers

In RF amplifier family, there are two categories of amplifier: 1. Analog RF amplifiers; and 2. Switched amplifiers. The analog amplifiers (such as Class-A, Class-B and Class-AB amplifiers) power efficiency are not as high as the switched amplifiers, so the overheating problem is the main drawback of analog amplifiers. Because of that reason, analog amplifiers do not meet our requirements, and this section reviews switched amplifiers. In contrast, the power efficiency of switched amplifiers (such as Class-D, Class-E and Class-DE amplifiers) is very high, they can achieve almost 100% theoretically.

2.3.1 Class-D Amplifiers

Due to their simple circuitry and high efficiency, switched amplifiers are commonly used in many applications. In contrast with analog amplifiers, a switched amplifier operates its transistors as switches. When the switch is turned on, it will apply all voltage to the load. When the switch is turned off, no voltage will be applied to the load [6].

Figure 2.5 shows the schematic of a Class-D CMOS RF amplifier, in which a PMOS MOSFET M_1 and a NMOS MOSFET M_2 are used as switching devices. This kind of amplifier circuitry can be integrated for high-frequency applications, such as RF transmitters for wireless communications.

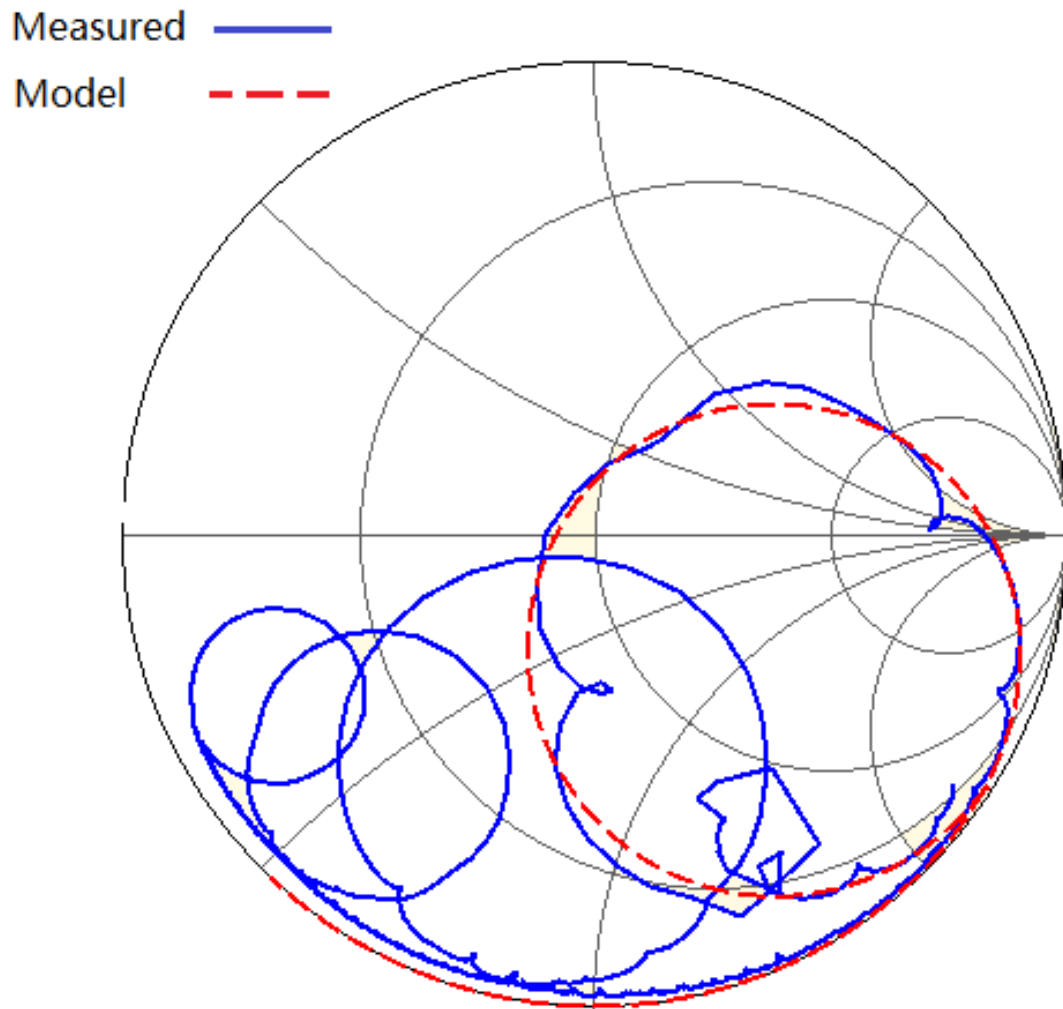


Figure 2.4: Plots of measured reflection coefficient and equivalent circuit model's reflection coefficient on a Smith Chart

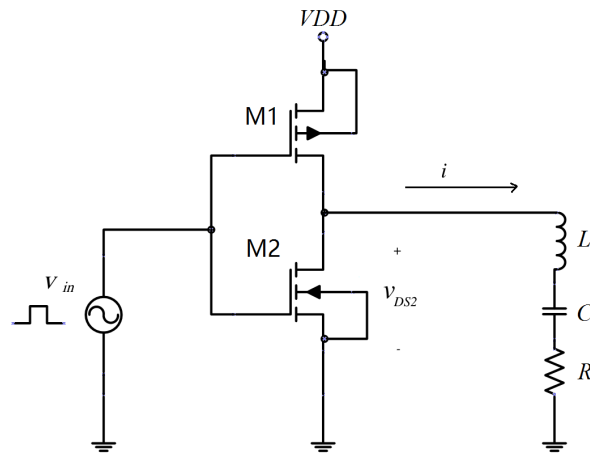


Figure 2.5: Schematic of the CMOS integrated Class-D RF amplifier [6]

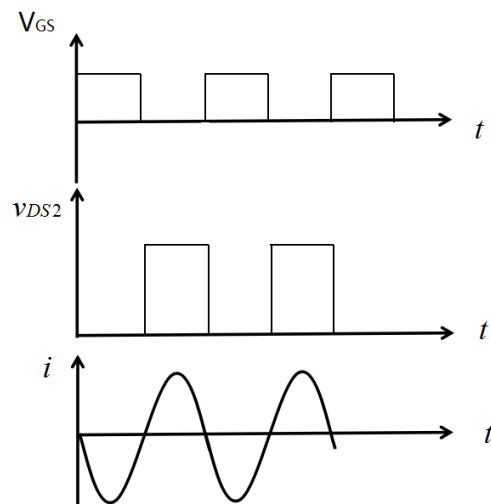


Figure 2.6: Input and output waveforms of the CMOS integrated Class-D RF amplifier [6]

It only requires one driver. However, cross-conduction of both transistors during the MOSFETs transitions may cause spikes in the drain currents. Non-overlapping gate-to-source voltages may reduce this problem, but driver will become very complex. The peak-to-peak value of the gate-to-source drive voltage which is also the input signal V_{GS} is equal or close to the dc supply voltage V_{DD} , like in CMOS digital gates. Therefore, this circuit is appropriate only for low values of the dc supply voltage V_{DD} , usually below 20V. At high values of the dc supply voltage V_{DD} , the gate-to-source voltage should also be high, which may cause voltage breakdown of the gate [6].

The operating procedure of the Class-D amplifier is the transistor M1 and M2 will be turned on alternatively with 50% duty ratio in the operation, to output the square wave that charges and discharges the load. The load of Class-D amplifiers is a series resonance circuit whose quality factor Q is high enough so that the load current is sinusoidal. The harmonics at the output of the Class-D amplifier are thus suppressed. Theoretically the efficiency of the Class-D amplifier can reach 100%, but in practice the efficiency is reduced because of the switching loss. When the transistors are turned on, the voltage across the transistors are not zero, and also the derivative of the voltage are not zero. The input and output waveforms of Class-D amplifiers are shown in the Figure 2.6. [6]

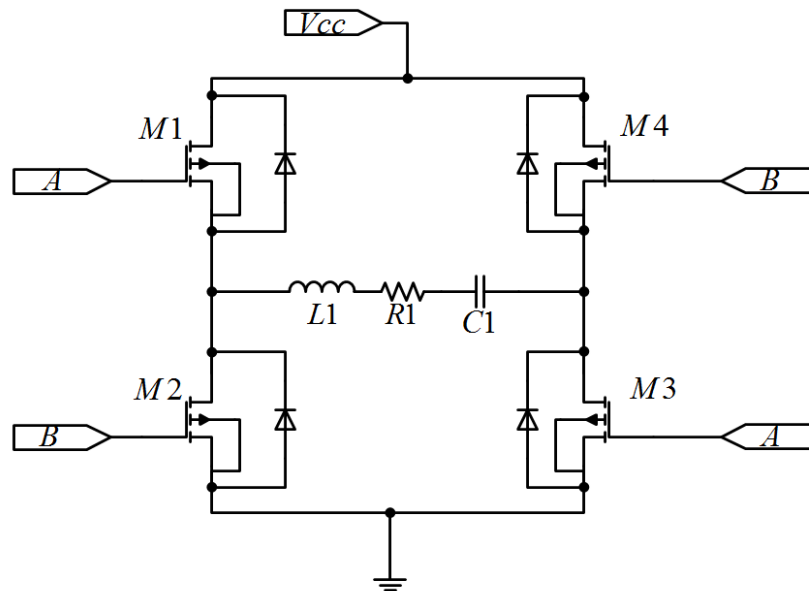


Figure 2.7: Topology of the CMOS integrated Class-D full-bridge RF amplifier

The schematic of full-bridge Class-D amplifier is shown in Figure 2.7, it consist of 4 transistors M1, M2, M3 and M4. This full-bridge Class-D amplifier's operating strategy is the same as the half-bridge one that we discussed before. M1 and M2 are turned on and off alternatively at same

time as the half-bridge Class-DE amplifier that discussed before, the main difference is the M3 will be turned on and off at same time as M1 and M4 will be turned on and off at same time as M2. So the output voltage swing will be doubled compared to the half-bridge Class-DE amplifier (from $-V_{DD}$ to $+V_{DD}$). [6]

In general, the Class-D amplifier is a very popular choice for ultrasound therapy. However, it need a tuned filter to attenuate the harmonics to achieve the highest efficiency which will interfere with the MRI operation. [2]

2.3.2 Class-E Amplifiers

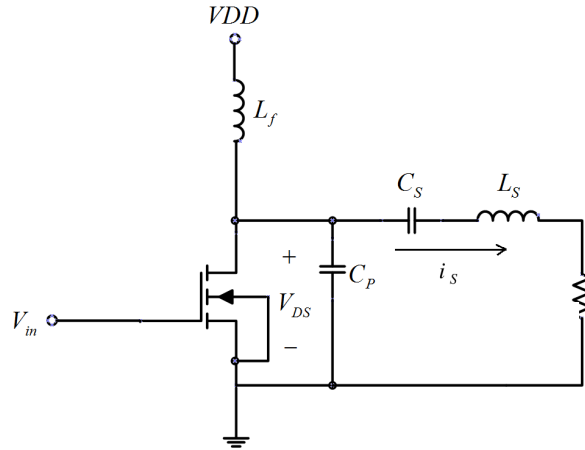


Figure 2.8: Topology of the CMOS integrated Class-E RF amplifier.

The Class-E amplifier is also called Class-E DC-AC inverter. The schematic of it is shown in Figure 2.8. It consists of a MOSFET operating as a switch, LCR series resonance circuit, shunt capacitor C_P and a choke inductor L_f . In this circuit the choke inductance L_f is assumed to be high enough to eliminate the AC current ripple on the DC supply V_{DD} 's current. A small inductance will result in a large current ripple. [6]

Circuit with hard-switching operation of semiconductor components, such as the Class-D amplifiers and digital gates, always suffer from switching losses. The voltage waveform in these circuits decrease abruptly from a high value (often equal to the dc supply V_{DD}) to almost zero, when a switching device, such as a MOSFET, turns on. When the switch is turned on, the current is circulating through the switch's on-resistance and all the stored energy is lost in the on-resistance as heat. This switching loss energy is independent of the transistor on-resistance. [6]

The switching losses can be avoided if the voltage across the transistor V_{DS} is zero. The main

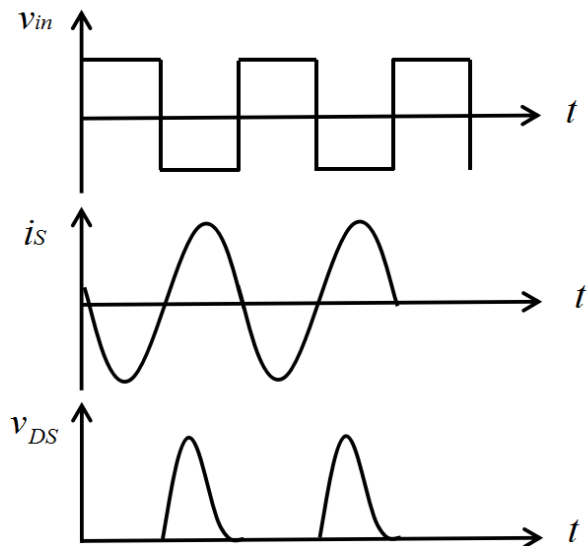


Figure 2.9: Input and output waveforms of the CMOS integrated Class-E RF amplifier. [6]

idea of the Class-E RF amplifier is that the transistor turns on as a switch at zero voltage, resulting in zero switching loss and high efficiency. The Class-E amplifier contains a single transistor, it turns on at zero voltage switching (ZVS), and it also turns on at zero derivative switching (ZDS). In general, this type of operation is called soft-switching. The input and output waveforms of the Class-E amplifier are shown in Figure 2.9. [6]

The major drawback of the Class-E amplifier is that it needs a large choke inductance to eliminate the DC current ripples. Because of that it is not a suitable choice for the integrated driver to be used in MRI conditions. [2]

2.3.3 Class-DE Amplifier

The schematic of the Class-DE amplifier is shown in Figure 2.10. It is the combination of the topology of Class-D amplifiers and the switching condition of Class-E amplifiers. The theoretical efficiency is 100%. In Figure 2.10, the M1 and M2 turns on and off with a duty ratio of 25% which means that the duty ratio of the dead time is also 25% to let the ZVS and ZDS happen. It doesn't have any switching loss theoretically. Our previous design which was proposed by Wong et al. [2] used this kind of RF amplifier as the output stage of the driver. A detailed analysis is provided in Section 2.4.

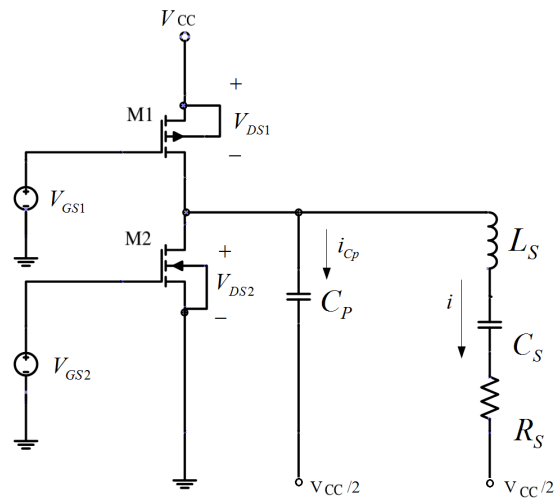


Figure 2.10: Schematic of the CMOS integrated Class-DE RF amplifier

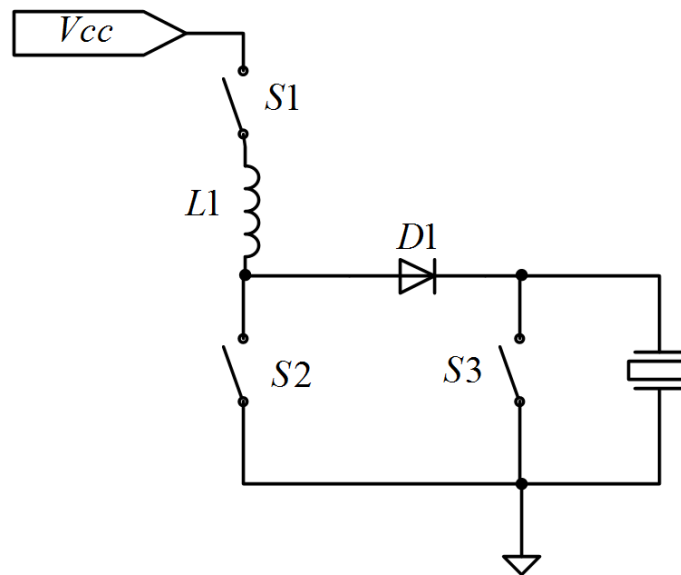


Figure 2.11: Schematic of the step-up driving circuit

2.3.4 Step-up Driving Circuit

The step-up driving circuit's schematic is shown in the Figure 2.11. It is derived directly from the classical step-up DC/DC circuit which is also known as boost-buck converter. The only difference is the charge storage capacitor is replaced by the parallel capacitor in the equivalent circuit of the transducer (C_P). The voltage on the transducer terminals depends in the pumping pulse train switching frequency, duty ratio, inductance L_1 and the switch S_1, S_2 on-resistance [8].

The operating process is: first, both the S_1 and S_2 turns on to charge up the inductance L_1 . Then S_2 turns off to let the energy that was stored in the inductor to be transferred to the transducer. At last, S_1 turns off and S_3 turns on to discharge the transducer. Because it includes 3 transistors in the step-up driving circuit, its timing and control circuit can be very complicated and the diode used in this circuit introduces additional losses [8].

2.3.5 Flyback Topology

The schematic of the flyback topology is shown in Figure 2.12., in this figure, the L_P and L_S operate as a transformer, L_P connects the supply voltage and switch and L_S connects ground and transducer. By turning switch on and off, that will make the voltage change across the transducer [8].

The major advantage of the flyback topology is that it just needs one transistor to generate the pulse signal to the transducer [2]. But a major drawback of this topology is that this circuit has a secondary winding resonance generated by the transducer parasitic capacitance C_P , which will cause long ringing after the switch is open and it needs a transformer which is a magnetic component, thus it cannot be used in the MRI conditions [8].

2.3.6 Push-pull driving circuit

The push-pull topology is almost the same as the flyback topology, the schematic is shown in Figure 2.13. This topology uses two switches that turn on and off at different times. At start, both switches are turned off, then the S_1 is turned on for the half of the transducer excitation pulse period. After that it is turned off, but the S_2 is turned on [8].

In this topology, the transformer is used to match the impedance of the transducer to maximize power transfer, but it will occupy a large portion of area and it cannot be used in the MRI conditions, so this kind of topology will not be applied in our design.

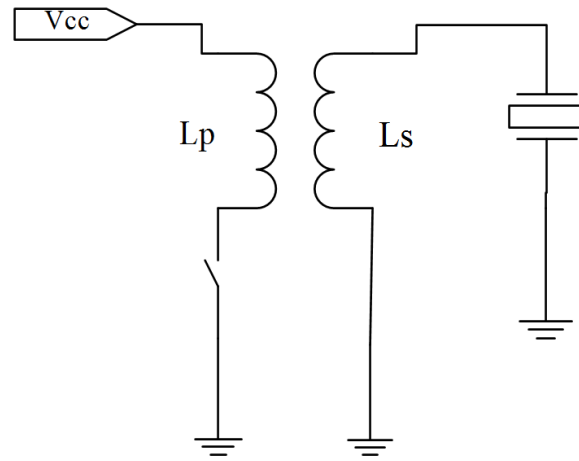


Figure 2.12: Topology of the flyback transducer driver [8]

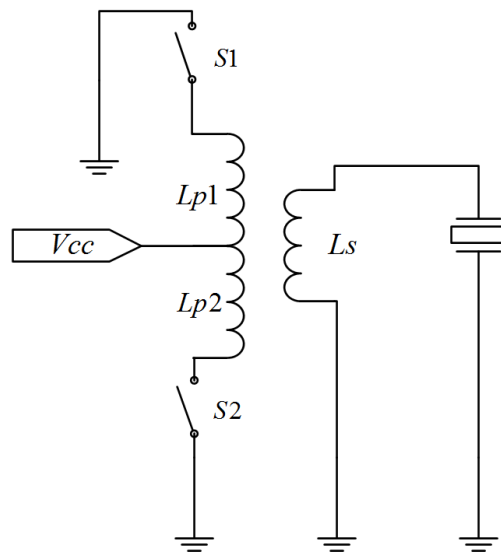


Figure 2.13: Schematic of the Push-pull driving circuit

2.4 Literature Review

Hall and Cain [9] proposed a Class-D amplifier, whose efficiency is 90% and output power is 20 W, operating frequency is 1 MHz, for a 512-channel transducer array. Its schematic is shown in Figure 2.14. The two transistors in this schematic form an inverter with the addition of transistor gate drivers. The duty ratio is decided by the input TTL signal which is a square wave. Tuned filter inductor L_1 and capacitor C_1 cancel out the higher harmonics of the square wave. [9]

The advantage of this topology is simplicity and low cost. But there are two resistors (R_1 and R_2) in this design, which will occupy a lot of area if we use them in an integrated circuit. Also the inductor L_1 in the filter cannot be used in the MRI conditions. So this kind of topology is not suitable to our objective.

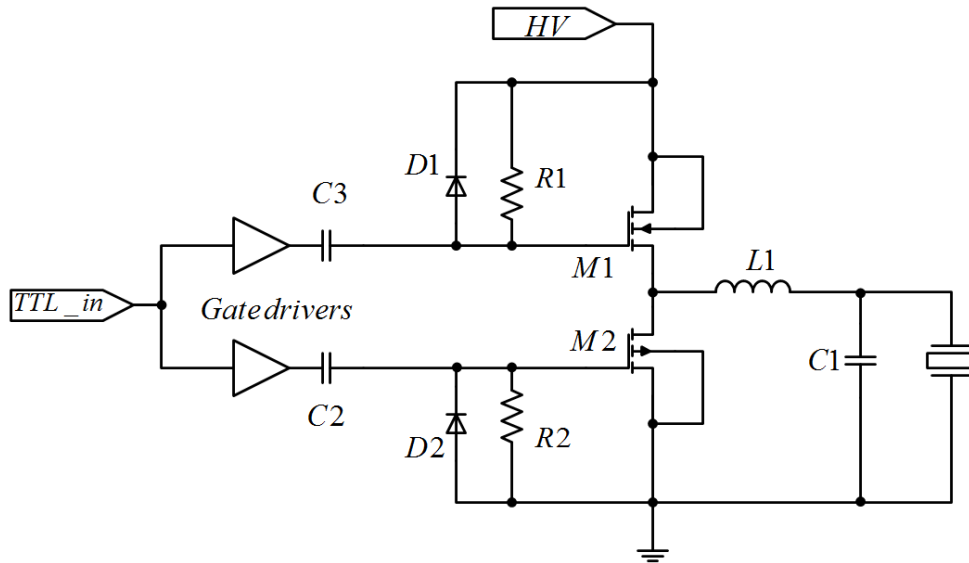


Figure 2.14: Schematic of the transducer driver which was proposed by Cain and Hall [9].

Tang and Clement [7] discussed the harmonic cancellation technique for a therapeutic ultrasound transducer in HIFU applications. The schematic of the driver that they used is shown in Figure 2.15. It contains two power converters in cascade and the operating frequency is 1 MHz. [7]

In their work, they point out that driving a piezoelectric ultrasound transducer in HIFU applications with a signal that contains harmonics will distort the shape of the ultrasound focal zone. This is because the harmonic in the driving signal will lead the transducer to generate unwanted sidelobes in the acoustic field. These sidelobes have extra energy and will distort the shape of the focal zone. So the harmonic cancellation technique was introduced to solve this problem. [7]

The harmonic cancellation technique uses a pre-calculated firing angle of the driving signal which

is a square wave pulse train. As shown in Figure 2.16, the square wave has a firing angle of $\pi/3$ which eliminates the third harmonic. This technique does not require an LC filter circuit. [7]

However this design requires two transformers in the circuit which is not suitable for MRI. Also this harmonic cancellation technique must be very precise. Rise time and fall time must be minimized, otherwise, the unwanted harmonic will appear at the output of the driver. So this design is not suitable for our objective. [7]

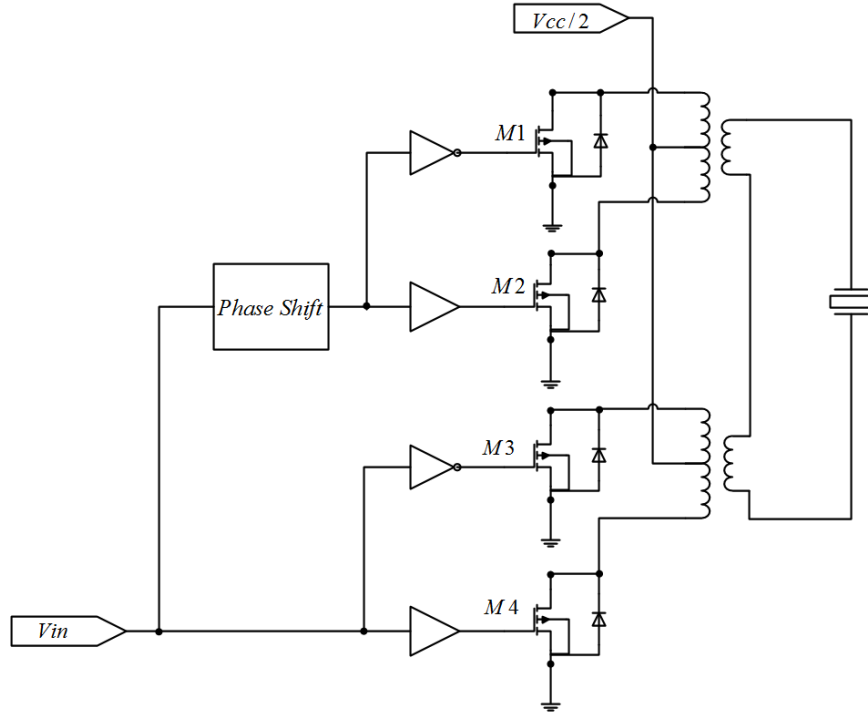


Figure 2.15: Schematic of the driver that is used by Tang and Clement [7]

Yang and Xu [10] used a Class-D full-bridge amplifier to drive an Audio Beam system. The schematic of this driver is shown in Figure 2.17. The switching operating frequency is 600 kHz, and the Audio Beam System can generate a highly concentrated audio signals between 20 kHz to 60 kHz. There are two resistors R_1 and R_2 and an operational amplifier in this circuit to cooperate with the gate driver IC to make an over current protection for the MOSFETs at the output stage. Inductors L_1 and L_2 are connected with the transducer to make a reduction of instantaneous current that flows through the loaded transducer.

Because of the inductors and the resistors in this design, it will occupy a large portion of area and interfere the operation of MRI, so we cannot employ this design in our project.

D. Zhao *et al.* [11] proposed a high voltage pulser for ultrasound medical imaging applications. The schematic of their design is shown in Figure 2.18. This circuit is a Class-D amplifier with a

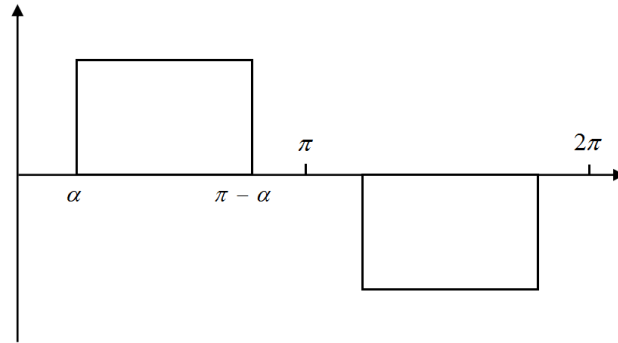


Figure 2.16: Input waveform of the driver that is used by Tang and Clement [7]

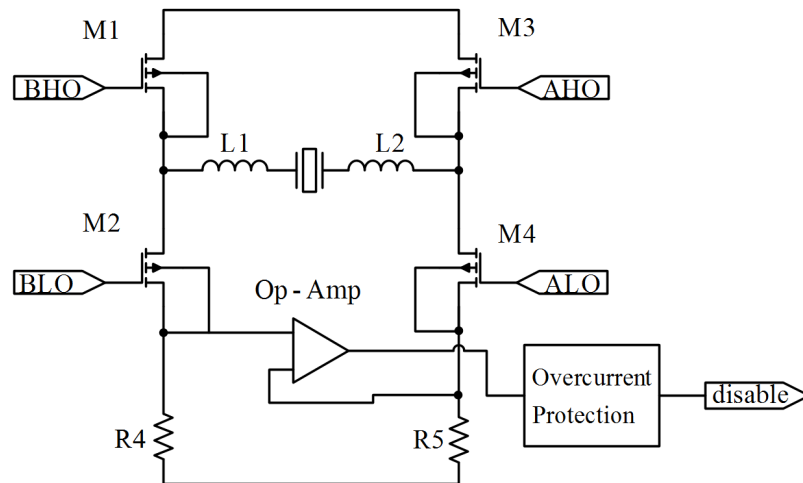


Figure 2.17: Schematic of driver that is proposed by Yang and Xu [10].

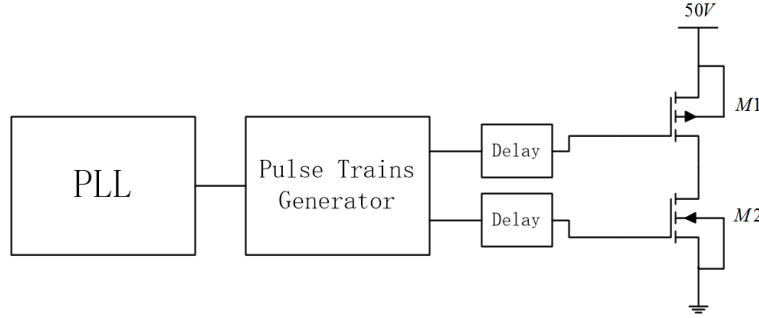


Figure 2.19: Block diagram of A. Bozkurk and O. Farhanieh’s driver IC [12]

K. Moro and J. Okada [13] designed a staircase-wave drive circuit to drive therapeutic array transducers. Their circuit is shown in Figure 2.20 and the waveforms of the schematic are shown in Figure 2.21. In the schematic, the V_{PP1} is higher than V_{PP2} . As shown in the Figure 2.21, the M3 is turned on first, so the output voltage is equal to V_{PP2} , and then M1 is turned on and off for a while, it generates a higher voltage pulse which is equal to V_{PP1} . When the M1 is turned off, the output voltage waveform falls back to V_{PP2} . In this process, a half period of staircase-wave is presented at the output. If we turned on and off M3 and M4 by the same procedure, a negative staircase-wave will be presented at the output. By using this stair-wave, the third and fifth harmonics will be reduced to zero, but the switching loss cannot be eliminated. It also needs a large portion of area to fit the 4 resistors in this design if we fabricate this circuit in a chip.

2.5 Previous Design by Our Group

Our previous ultrasound transducer driver design was proposed by W. Wong *et al.* [1,2,5]. A Class-DE amplifier is driven by two gate drivers (Figure 2.22). This driver is implemented by using AMS H35B4 CMOS technology.

The operation of the Class-DE amplifier can be divided in 4 intervals. Figure 2.23 shows the voltage and current waveforms of the whole operation period and Figure 2.20 shows the equivalent circuits for each interval.

Interval 1

Between ωt_0 radians and π . Transistor M1 turns on and M2 turns off. The equivalent circuit is shown in Figure 2.24(a). The current i_{M1} slowly increases from 0 until its peak and then decreases until $\omega t = \pi$. The drain potential of M2 is at highest potential(V_{cc}) in this whole interval, so no

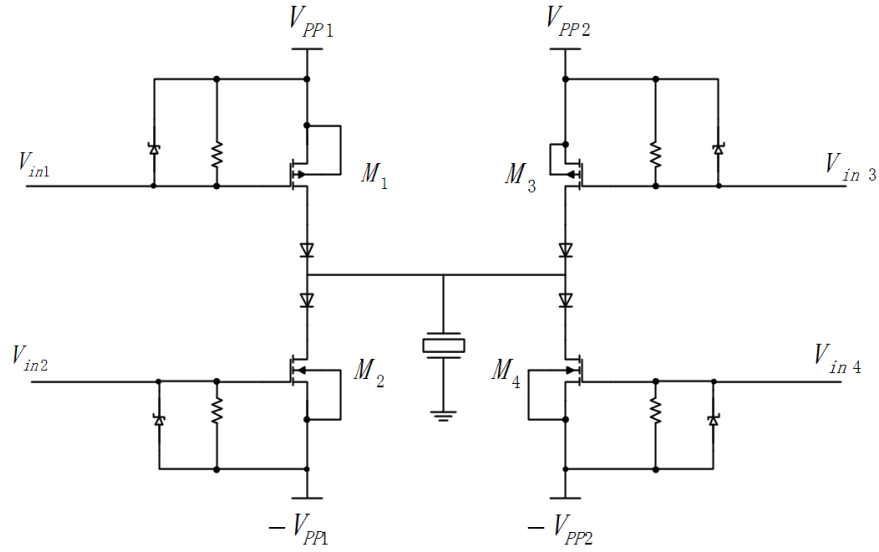


Figure 2.20: Schematic of staircase-wave driver that is proposed by K. Moro and J. Okada. [13]

current flow through the parallel capacitor C_P . The current i_{M1} will be the only current that charges the series resonance branch [2]. In this interval the output voltage is V_{cc} .

Interval 2

Between π and $\pi + \omega t_0$. Both transistors M1 and M2 are turned off. The equivalent circuit of this interval is shown in Figure 2.24(b). There is no current flow through the transistors in this interval. So the parallel capacitor will provide the current to the series resonance branch, because the L_s and C_s maintains the continuity of the load current. Because of that, the load current falls down sinusoidally to 0 at $\pi + \omega t_0$. Since the C_P charges the series resonance branch in this interval, the voltage across the M2 will be decreased slowly, from V_{cc} until 0 at $\pi + \omega t_0$. The V_{DS1} will be decreased to $-V_{cc}$ at this moment.

Interval 3

Between $\pi + \omega t_0$ and 2π . In this interval the M2 is turned on and M1 is turned off. The equivalent circuit of this interval is shown in Figure 2.24(c). M2 is turned on when the V_{DS2} is zero, so the ZVS and ZDS conditions are reached. Because of the M2 being turned on, the V_{DS1} is maintained at $-V_{cc}$ and no current flows through the C_P . The series resonance branch will discharge through M2, its current keeps decreasing until its lowest peak.

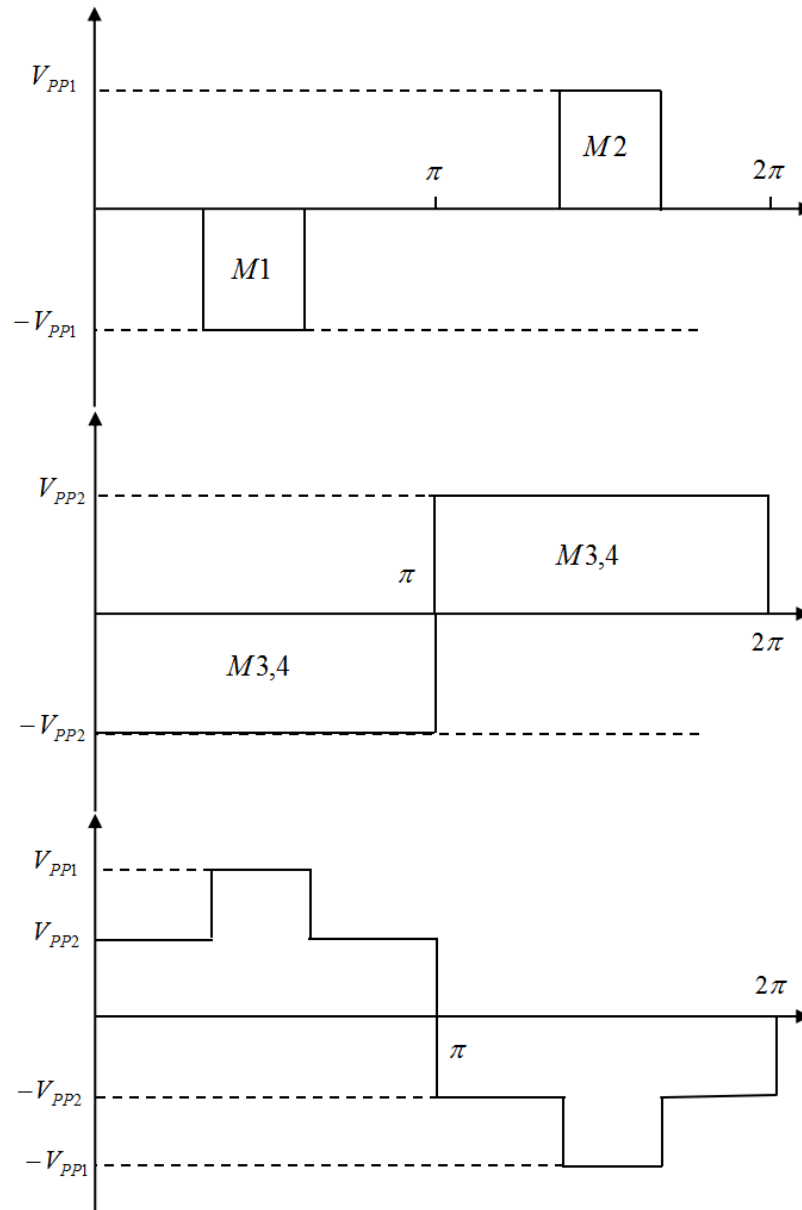


Figure 2.21: Input and output voltage waveforms of the staircase-wave driver [13]

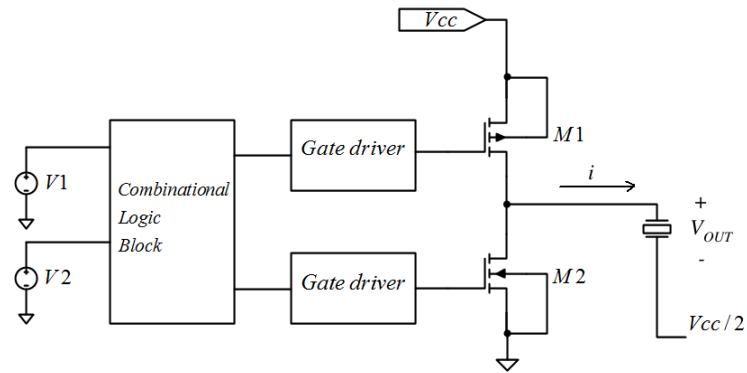


Figure 2.22: Schematic of driver that is proposed by Wai Wong. [5]

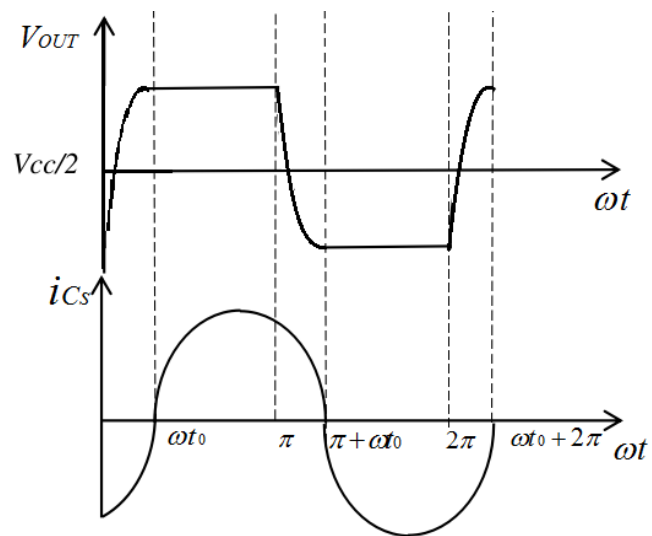


Figure 2.23: Output waveforms of half-bridge Class-DE amplifier [5]

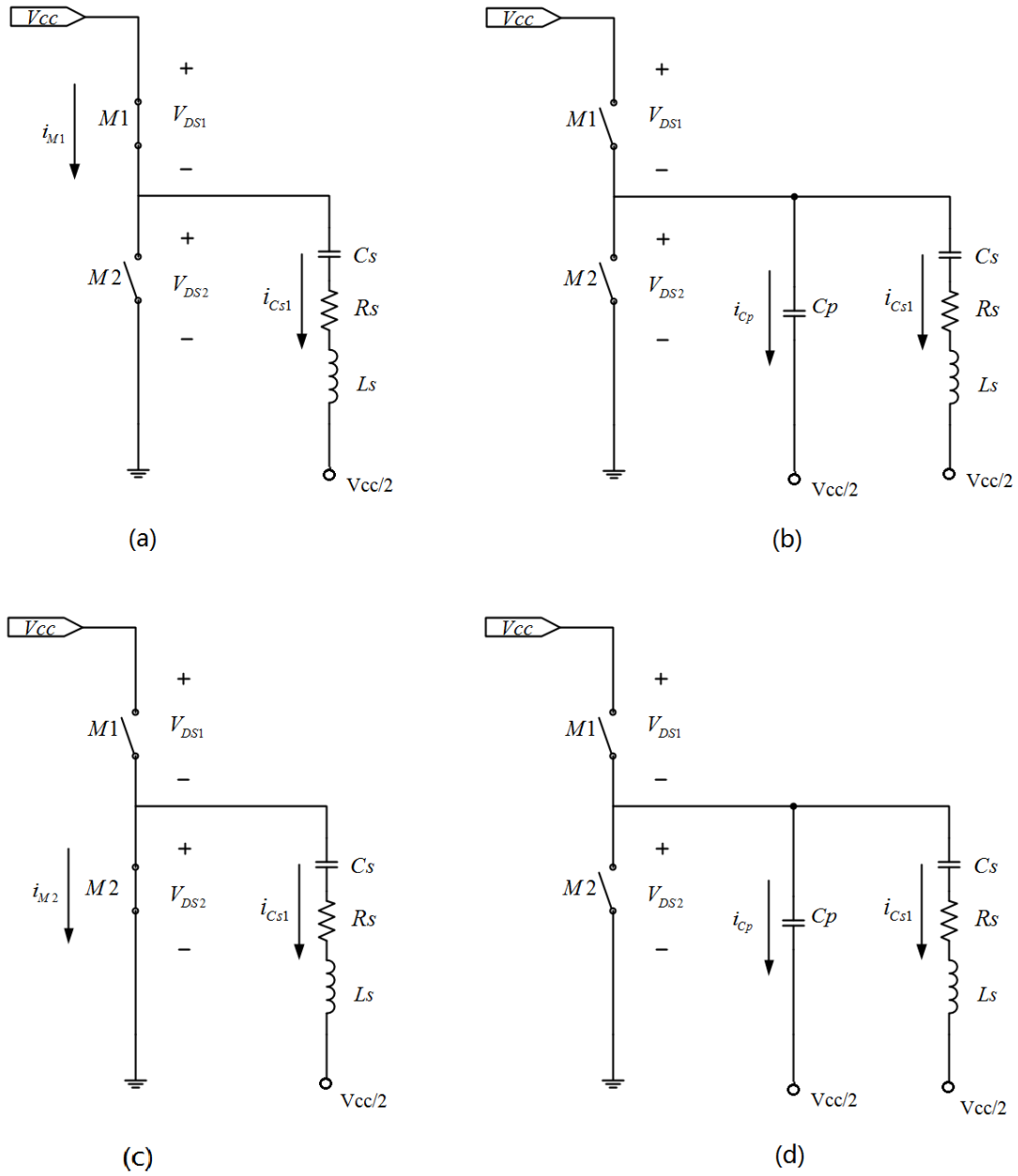


Figure 2.24: Equivalent circuits of Class-DE amplifier in each interval. [6]

Interval 4

Between 2π and $2\pi + \omega t_0$. In this interval both M1 and M2 are turned off. The equivalent circuit of this interval is shown in Figure 2.24(d). Because of C_s and L_s , the series resonance branch keep discharging in this interval. Because of M2 being turned off, the load current will flow through C_P to charge it and let the V_{DS2} increase, at the end of this interval which is at $2\pi + \omega t_0$, the V_{DS2} will reach its highest point that is V_{cc} . After 2π , its the fifth interval which is same as the first one, the M1 will be turned on and M2 will be turned off. At the moment that M1 is turned on which is at $\omega t = 2\pi + \omega t_0$ the V_{DS1} is equal to zero which matches the ZVS and ZDS conditions again.

If we want to drive an ultrasound transducer by using this design, we must decide its operating frequency (f) and corresponding duty ratio (D) to maximize the power transmission efficiency. The expression of the output voltage and load current of the Class-DE amplifier in the interval 2 and 4 is [14]:

$$v_{OUT} = V_{CC} \frac{2\cos(\omega t - \phi) - (1 + \cos\phi)}{2(1 - \cos\phi)} \quad t \in [0 + k\pi, t_0 + k\pi], k = 0, 1, 2 \dots \quad (2.6)$$

$$i = I_m \sin(\omega t - \phi) \quad (2.7)$$

where the ϕ is an angle that relate to the duty ratio D by equation $\phi = \pi(1 - 2D)$, the ϕ cannot be zero, because when $\phi = 0$ the duty ratio is 50%, then the Class-DE condition is no longer exist. Then we can get the fundamental component of V_{OUT} and load current i by using Fourier analysis [14]:

$$V_1 = \frac{4}{T} \left(\int_0^{t_0} v_{DS2}(t) \exp(-j\omega t) dt + \int_{t_0}^{T/2} \frac{V_{CC}}{2} \exp(-j\omega t) dt \right) \quad (2.8)$$

$$I_1 = \frac{2}{T} \int_0^T I_m \sin(\omega t - \phi) \exp(-j\omega t) dt \quad (2.9)$$

The fundamental components of the output voltage V_{OUT} and load current i are shown below (please note that $V_{CC} = \frac{1}{C_P} \int i(t) dt$) [14]:

$$V_1 = V_{CC} \frac{\phi \cos\phi - \sin\phi - j\phi \sin\phi}{\pi(1 - \cos\phi)} \quad (2.10)$$

$$I_1 = -\frac{\omega C_P V_{CC}(\sin\phi + j\cos\phi)}{1 - \cos\phi} \quad (2.11)$$

If we substitute the equation (2.10) and (2.11) to equation $Z = V/I$, we can get the expression of the load impedance Z_L [5, 14]:

$$Z_L = \frac{V_1}{I_1} = \frac{1 - \cos(2\phi)}{2\pi\omega C_P} + j\frac{2\phi - \sin(2\phi)}{2\pi\omega C_P} \quad (2.12)$$

In Equation 2.12, the real part and imaginary part of Z_L are [5]:

$$R_L = \frac{1 - \cos(2\phi)}{2\pi\omega C_P} \quad (2.13)$$

$$X_L = \frac{2\phi - \sin(2\phi)}{2\pi\omega C_P} \quad (2.14)$$

From Equation (2.1)

$$Z_L = R_S + j\omega L_S + \frac{1}{j\omega C_S} \quad (2.15)$$

So, let the $R_L = R_S$, $X_L = j\omega L_S + \frac{1}{j\omega C_S}$ and solve them for frequency [5]:

$$f_r = \frac{1 - \cos(2\phi)}{4\pi^2 C_P R_S} \quad (2.16)$$

$$f_x = \frac{1}{2\pi} \sqrt{\frac{2\phi - \sin(2\phi)}{2\pi C_P L_S} + \frac{1}{C_S L_S}} \quad (2.17)$$

where the f_r is the frequency that we get from the real part of the impedance and f_x is the frequency that we get from the imaginary part of impedance. Equations (2.16) and (2.17) are functions of duty ratio D . If we plot these two equations in a duty ratio range [0.1,0.4], we can get the operation frequency and corresponding duty ratio of the Class-DE amplifier. For instance, in Figure 2.25 we plot f_r and f_x for a transducer that has the equivalent circuit values that are shown in Table 2.1: In this Figure the black line represents the plot of the f_r and red line represent the

C_P	C_S	L_S	R_S
827pF	183pF	139uH	40.25Ω

Table 2.1: Equivalent circuit's parameters of an ultrasound transducer.

plot of f_x . As we can see, there are two intersection points of these two lines in this figure, these are

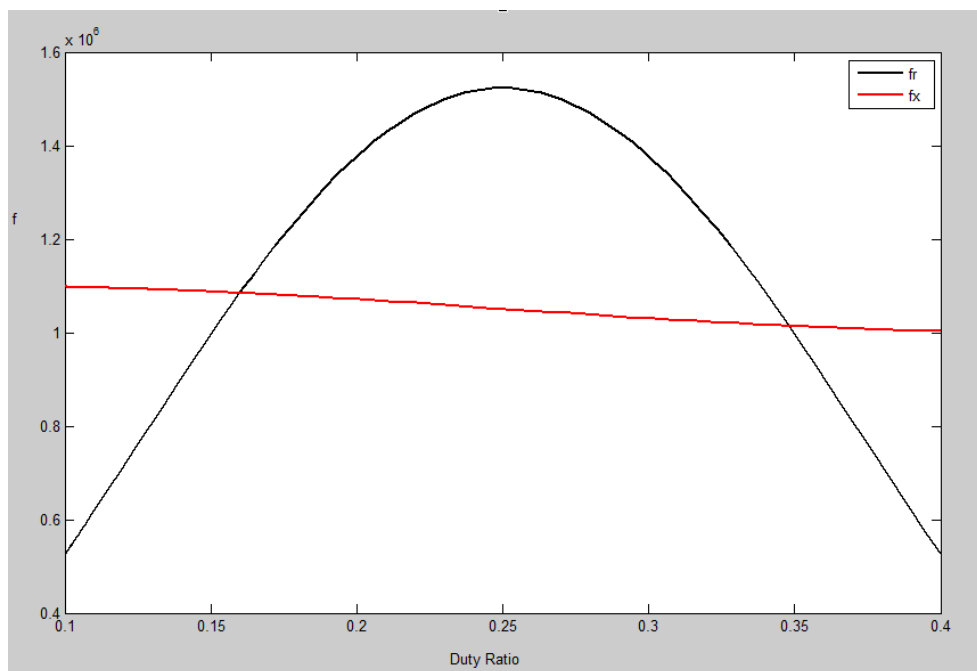


Figure 2.25: Variations of f_r and f_x with duty ratio of an ultrasound transducer

the points that Class-DE mode switching happens ($f_r = f_x$). If we substitute equations (2.16) and (2.17) into $f_r = f_x$, we can find the optimum Class-DE switching frequencies and the corresponding duty ratios for this transducer. The optimum frequencies and corresponding duty ratios are shown in Table 2.2.

$D_1 = 0.160$	$f_1 = 1084kHz$
$D_2 = 0.348$	$f_2 = 1014kHz$

Table 2.2: Optimum Class-DE switching frequencies and duty ratios of the instance transducer.

Because of the series resonance frequency of this transducer being $f_s = 1/(2\pi\sqrt{L_s C_s}) \approx 1MHz$, the operating frequency must be closest to it. That means we should use the f_2 and D_2 as the operating frequency and duty ratio. Also, because the D_2 is larger than D_1 , using D_2 and f_2 will let the transistors turned on time is longer than using D_1 and f_1 , which means more output power [5].

The efficiency of the transducer driver designed in [5] is 90% and there is no magnetic components, such as inductors and transformers, in this circuit, which means that we can use this driver in MRI conditions. Also the circuitry of this design is very simple, it won't occupy a large portion of area, so we can integrate it in a chip. The power will be delivered to the transducer by the driver is over 1 W which means we have achieved our minimum goal [5].

However, in this design the driving signals, which are pulse trains, of both transistors in the Class-DE amplifier are not generated by the driver itself. Instead external signals must be provided to the transducer driver. Because of that, the connection setup of the driver would be very complex in a large transducer array. If we want to decrease the complexity of the connection setup, we should internally generate the pulse trains that drive the switches of the Class-DE amplifier. The phase shift and duty ratios should be digitally programmable through an interface that is common to all drivers in an array (phase shifts determines when *phi* is get started and duty ratio determines the value of ϕ).

Some of transducers do not have Class-DE switching points, which means that they cannot be driven by Class-DE amplifiers. For instance, a transducer such as the one described in Table 2.3(Tx.3) [15].

$C_P(pF)$	$C_S(pF)$	$L_S(mH)$	$R_S(k\Omega)$
473	15	6.5	1.116

Table 2.3: Equivalent circuit components' values of Tx.3

If we substitute these values to the equation 2.16 and 2.17 and plot them, we obtain curves of f_r and f_x that do not intersect (see Figure 2.26. In this case, if we want to drive this transducer by using Class-DE amplifiers, either an external matching network is required or the amplifier has to be driven in sub-optimal conditions near the series resonance frequency of the transducer, since at the series resonance frequency the transducer can get highest power delivery. Due to the MR environment concern, we can not use an external matching network in this case, which means driving it in sub-optimal condition is the only choice. In order to find the best duty ratio in this case, a duty ratio sweep can be used. Figure 2.27 shows the effect of duty ratio on efficiency, output power and current peak when the transducer is driven at the series resonance frequency. We can then use this sweep to use the operating duty cycle that allow for the maximum efficiency despite the sub-optimum condition.

As we can see in this figure, the transducer Tx.3's efficiency reaches its maximum when duty ratio is near 0.25, so we choose 0.25 as the operating duty ratio for driving the transducer Tx.3. The output waveforms are shown in Figure 2.28. The amplifier is not operating in Class-DE mode and the output current waveform has high peaks, caused by the MOSFETs turning on when the voltage across the drain and source is not zero. The average current peak value is 1.06A, the current peaks width ($41.22764\mu s - 41.19224\mu s = 0.0354\mu s$) is shown in this Figure. Table 2.4 summarizes DC supply power, output power and efficiency for transducer Tx.3.

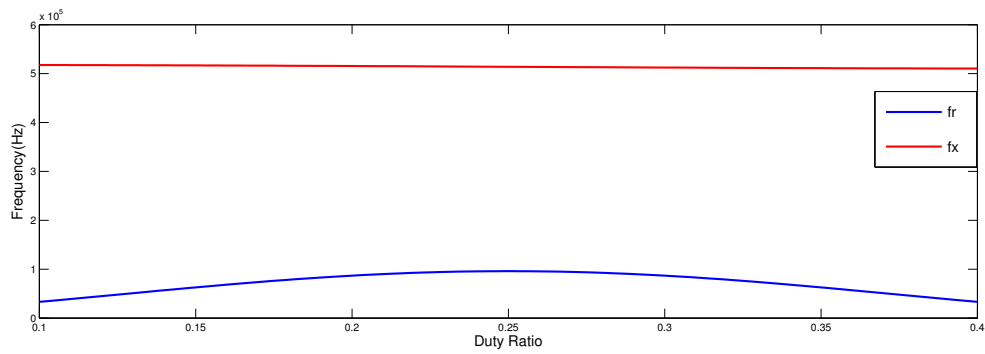


Figure 2.26: f_r and f_x plots of transducer Tx.3

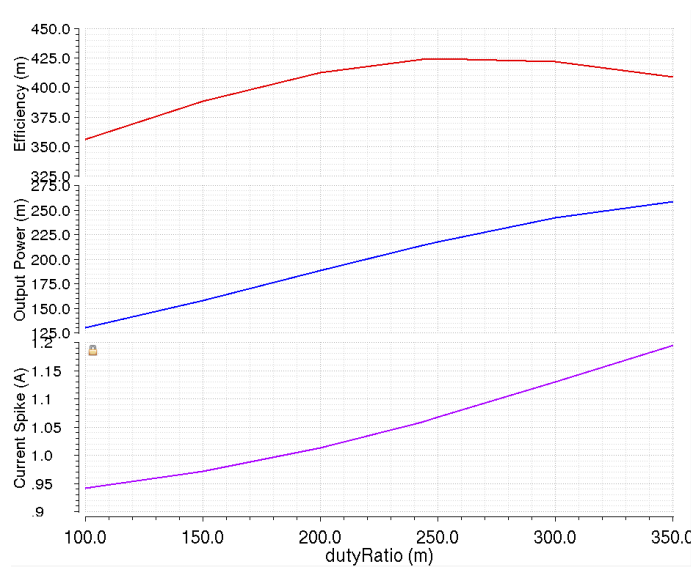


Figure 2.27: Effect of duty ratio on efficiency,output power and current peak with variable duty ratios

DC supply power(mW)	Output power (mW)	Efficiency(%)
524	227	43.3

Table 2.4: DC supply power, output power and efficiency for transducer Tx.3

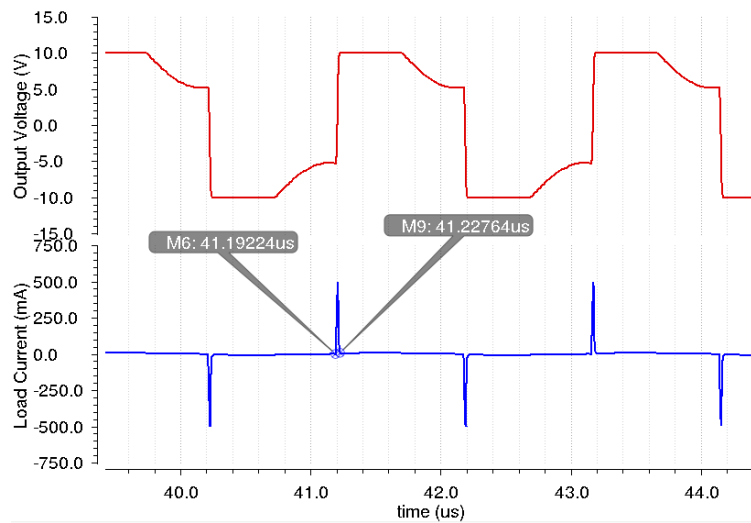


Figure 2.28: Output waveforms for transducer Tx.3

2.6 Summary

Overall, the Class-DE amplifier that was used in [5] is more suitable for our objectives than others. Because of that, the works that are presented in this thesis intend to upgrade that design to include the phase shift, driving frequency and duty ratios as programmable parameters. Furthermore, we intend to make the driver capable of delivering more power to the transducer. The comparison of the reviewed works is shown in Table 2.5.

Topology or Reference	Waveforms	Efficiency	Power	Comments
Hall and Cain's design [9]	PWM Wave	Over 90%	20W	Need a LC matching network.
Tang and Clement's design [7]	Sinusoidal Wave	90%	Unknown	Needs a transformer.
Yang and Xu's design [10]	PWM	Unknown	Unknown	Needs a inductor
Zhao <i>et al.</i> 's design [11]	Square Wave	Unknown	Unknown	Switching loss is high
Moro and Okada's design [13]	Staircase Wave	Unknown	Unknown	Switching loss is high and need a large portion of area for the resistors
A. Bozkurk and O. Farhanieh's design [12]	Square Wave	Unknown	530mW	Output power is not high enough
W.Wong and C.Christoffersen's design [2, 5]	Class-DE Wave	90%	1W	Duty ratios and phase shifts non-programmable

Table 2.5: Comparison of some published works

Chapter 3

Strategy to Drive a Transducer array in Class-DE Mode



Figure 3.1: Multi-element ultrasound transducer array that was designed by J. L. Kivinen [4]

In last chapter, it was stated that the half-bridge Class-DE amplifier proposed in [5] is suitable to the objectives, it can deliver enough power and the efficiency is high. If we want to apply this ultrasound transducer driver in a MRI conditions for HIFU applications, we must use it to drive a multi-element transducer array which might include over 1000 elements. Since the transducers in

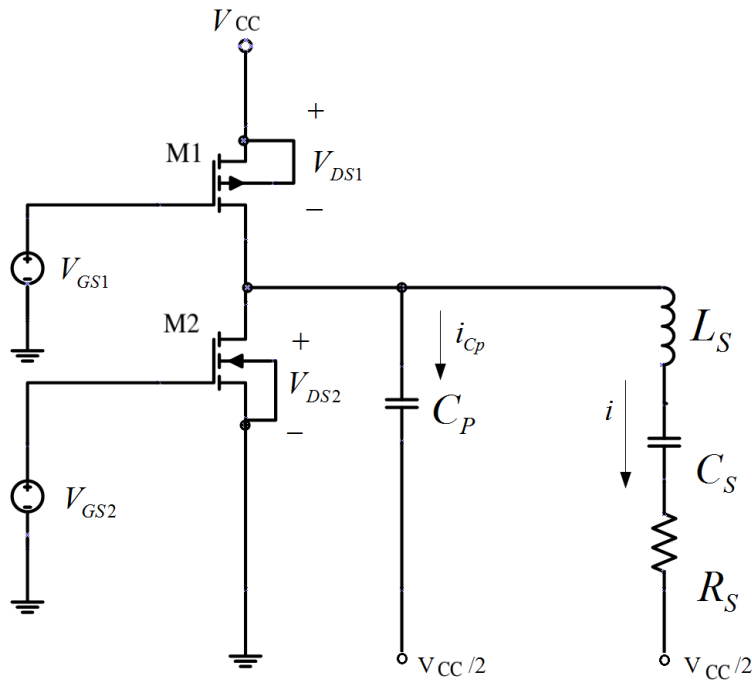


Figure 3.2: Half-bridge Class-DE amplifier which was proposed by Wai Wong [1, 2, 5]

an array are not exactly equal, the optimum driving parameters will be different for each individual transducer. However, all these elements will be driven at the same frequency. Therefore, a strategy must be developed to drive an ultrasound transducer array with elements which have different optimum driving frequencies.

In this Chapter, we will use an ultrasound transducer array designed by J. L. Kivinen [4] (Figure 3.1) and the half-bridge Class-DE amplifier proposed by Wai Wong [1, 5] (Figure 3.2). To develop the multi-element transducer array's driving strategy. Although this transducer array's elements can be used in HIFU applications, but it cannot focus the acoustic waves because of their arrangement pattern. It is however a good model to help us derive an array driving strategy since it has multiple piezoelectric elements.

The outline of this Chapter is: Section 3.1 introduced a transducer array and derived its equivalent circuit parameters; Section 3.2 introduced two strategies to drive a transducer array; The Section 3.3 summarizes this Chapter.

3.1 Characterization of the Transducer Array

We can plot each element's real part of the impedance and the real part of admittance of Kivinen's transducer array by using a vector network analyzer to find the series resonance frequency (f_S) and the parallel resonance frequency (f_P) of each element and their magnitude of impedance ($Z|_{\omega=\omega_S} = R + jX$). The f_S , f_P and $|Z|$ are shown in Table 3.1.

Based on these parameters we can get all the equivalent circuit value of these six elements by

Element	f_S (kHz)	f_P (kHz)	$R(\Omega)$	$X(\Omega)$
A	997.5	1102.5	38.6	8.04
B	997.0	1100.0	45.32	8.65
C	1000.0	1110.0	42.3	7.78
D	1000.0	1110.0	38.4	9.27
E	1000.0	1110.1	40.8	7.16
F	1000.0	1110.3	38.0	8.82

Table 3.1: f_S , f_P and $|Z|$ values of each element of Kivinen's transducer array

using the Equations 2.2 to 2.5, all the parameters of are shown in Table 3.2, the differences among transducers can be observed in Table 3.1 and 3.2:

Transducers	C_P (pF)	C_S (pF)	L_S (uH)	R_S (Ω)
A	827	183	139	40.25
B	699	152	167.8	45.32
C	669	155	163.04	43.73
D	945	219	115.43	40.64
E	664	154	164.33	42.06
F	922	214	118.31	40.05

Table 3.2: Equivalent circuit parameters of all the six elements of Kivinen's transducer array

3.2 The Transducer Array Driving Strategies

We can get the optimum operation frequency and duty cycles (a transducer will reach its maximum efficiency when it is driven by its optimum frequency and duty ratio) for all elements in the transducer array using Equations (2.16) and (2.17). They are shown in the Table 3.3. If every element is driven

Transducer	Duty Cycle	Operation Frequency(kHz)
A	$D = 0.348$	$f = 1014$
B	$D = 0.354$	$f = 1012$
C	$D = 0.361$	$f = 1014$
D	$D = 0.328$	$f = 1024$
E	$D = 0.366$	$f = 1013$
F	$D = 0.334$	$f = 1022$

Table 3.3: Operation frequencies and duty cycles of all elements in the transducer array

by its own optimum frequency and duty cycle separately, the output voltage and load current waveforms are shown in Figure 3.3. As we can see, all the elements are driven in Class-DE mode, but there are some small spikes on the output current waveform, because the input pulse trains need a rise time or fall time to reach their highest value and lowest value to turn on the transistors so that the transistors cannot be turned on at the exact time that they should be turned on. The efficiency when all elements are driven by their own optimum frequencies and duty cycles is shown in Table 3.4

In the table, DC supply power is the power that is provided by power supply and output power is the power that is delivered to the transducer. As we can see in Table 3.4, all the efficiencies are close to 92% and the output powers are close to 1 W. In practice, however, we must drive all the elements at the same frequency (the duty cycle can be different for each element). If we drive a transducer by using a non-optimum frequency, the switching loss of the Class-DE amplifier will be higher. The output waveforms of element B when it is driven under a non-optimum frequency 1024kHz is shown in Figure 3.4, the output waveforms show it is not in Class-DE mode (there are some distortions in the current waveform). So, to eliminate the switching loss and drive all the elements under a same frequency, we derived the following two strategies.

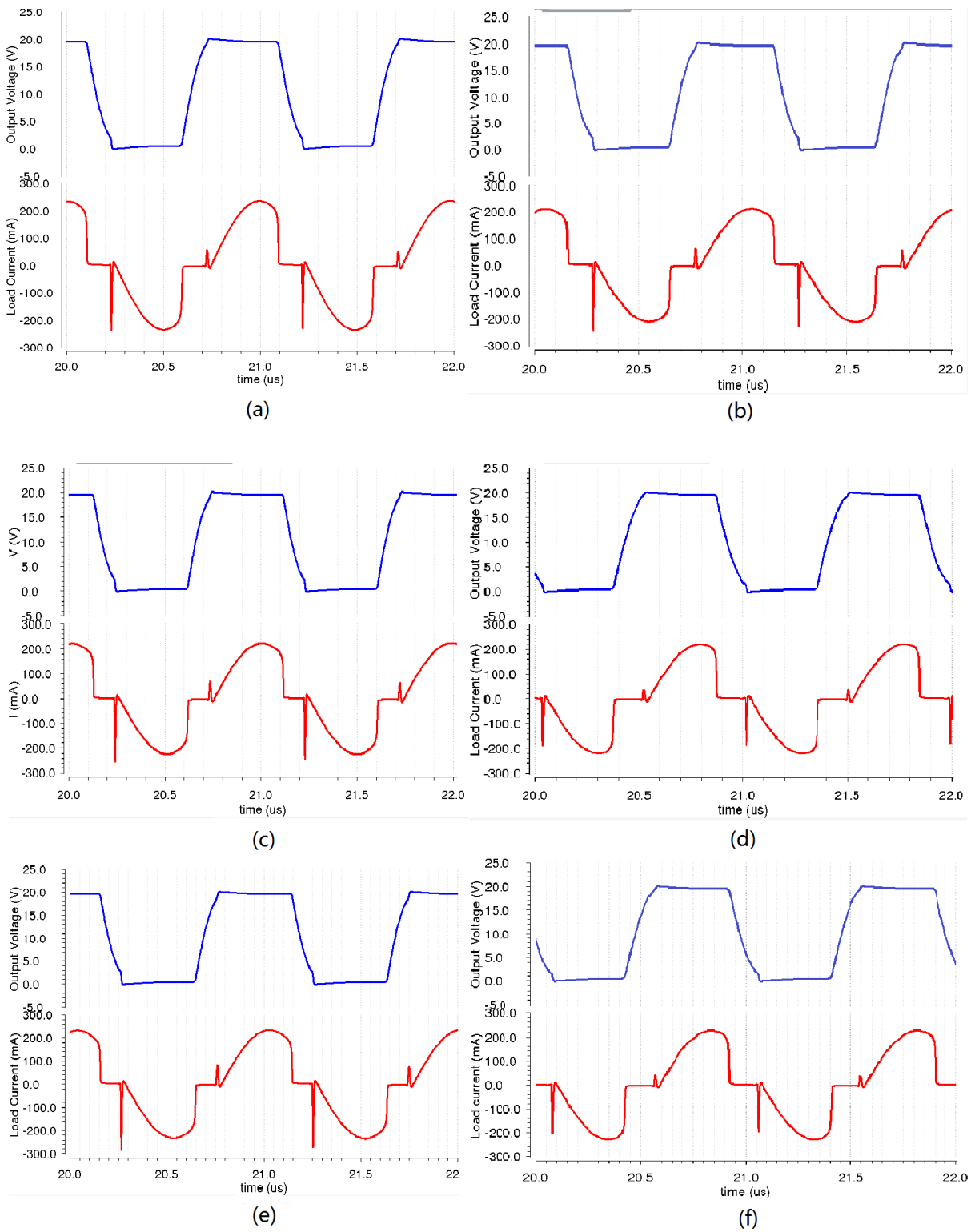


Figure 3.3: Output voltage and current waveforms of all the six elements that are driven by Class-DE amplifier

Transducers	DC supply power(mW)	Output power (mW)	Efficiency(%)
A	1242	1144	92.1
B	1161	1071	92.2
C	1238	1142	92.3
D	1071	984.4	91.9
E	1300	1200	92.3
F	1145	1053	92

Table 3.4: Simulation results of all the elements in the transducer array

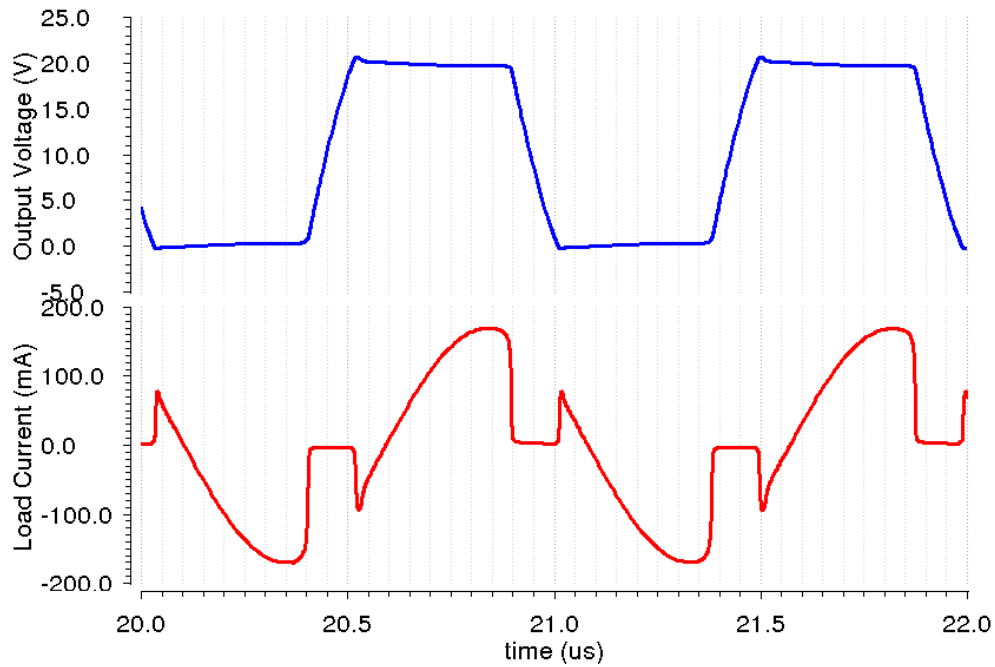


Figure 3.4: Output voltage and current waveforms of element B that is driven under 1024kHz which is a non-optimum frequency for element B

3.2.1 Using an External Parallel Capacitor

As we can see in the Figure 2.25, there are two intersection points of the plots of f_r and f_x which are the Class-DE switching points f_1 and f_2 . If the external capacitance C_{ext} increased, the f_1 will increase and f_2 will decrease until they meet each other [5]. As mentioned before, the f_2 always is the optimum frequency, so we can increase a transducer's optimum operation frequency by adding an external capacitor that is in parallel with the load. The modified circuit is shown in Figure 3.5. So we can use the highest optimum operation frequency among these six elements, and add external capacitors to the other five elements to match this frequency. In these six elements, the highest optimum operation frequency is 1024 kHz which corresponds to Transducer D.

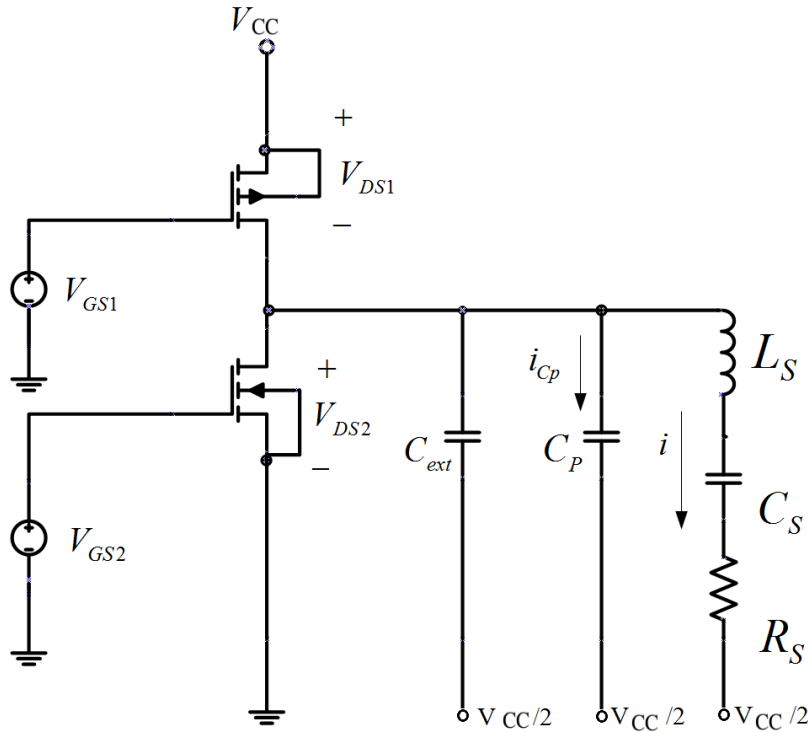


Figure 3.5: Half-bridge Class-DE amplifier with the parallel external capacitor

Based on Equations (3.1) and (3.2), let the f_r and f_x be equal to 1024 kHz and replace C_P by $C_P + C_{ext}$. Then solve them for C_{ext} , we can get following equations:

$$C_{ext,r} = \frac{1 - \cos(4\pi D)}{4\pi^2 f R_S} - C_P \quad (3.1)$$

$$C_{ext,x} = \frac{2\pi(1 - 2D) - \sin(2\pi D)}{2\pi L_S [(2\pi f)^2 - 1/(C_S L_S)]} - C_P \quad (3.2)$$

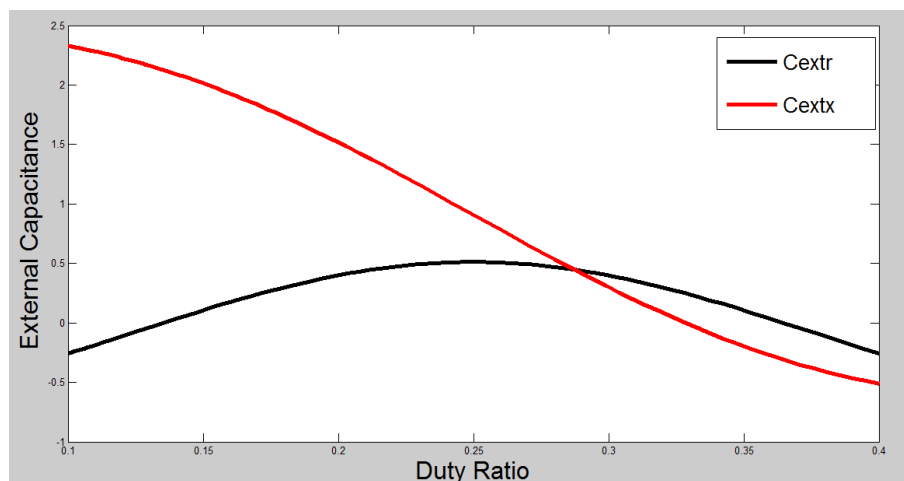


Figure 3.6: $C_{ext,r}$ and $C_{ext,x}$'s plots of element E in Kivinen's transducer array

Where $C_{ext,r}$ is the external parallel capacitance which is obtained from solving the equation for the real part of the transducer's impedance and $C_{ext,x}$ is the external parallel capacitance that is obtained from solving the equation for the imaginary part of transducer's impedance. Then if we let the $C_{ext,r} = C_{ext,x}$ and solve this equation, we can get the value of this external parallel capacitance with its corresponding duty ratio.

Let's use element E as an instance. In Equations (3.1) and (3.2), set $f = 1024kHz$ and plot $C_{ext,r}$ and $C_{ext,x}$ versus the duty ratio D respectively. We obtain Figure 3.6 where the black line is the plot of the $C_{ext,r}$ and the red line is the plot of the $C_{ext,x}$. There is an intersection of these two plots, the intersection point is the value of the external capacitance with its corresponding duty ratio. In this instance, the element E's external capacitance and its corresponding duty ratio is 449pF and 0.287.

Based on above method, we can get all the external capacitance values of these six elements and their corresponding duty ratios. These values are shown in Table 3.5. The output voltage and current waveforms of all the 6 elements are shown in Figure 3.7. In this Figure, the periods of all the transducer elements are same, but their duty ratios are different. Their efficiency results are shown in Table 3.6. If we compare the efficiency results from Table 3.6 to the efficiency results of all the elements are driven under same frequency without the C_{ext} , which are shown in Table 3.7, the efficiencies have been increased.

However, the output power of this method is in some cases much lower than 1 W. Because the duty ratios are smaller than the optimum duty ratios, the turn on time of each transistor is shorter and less power is transferred to the load.

Element	D	C_{ext}
A	0.291	323pF
B	0.279	356pF
C	0.293	380pF
D	0.328	0
E	0.287	449pF
F	0.323	69pF

Table 3.5: External capacitance values of all the elements in Kivinen's transducer array

Transducers	DC supply power(mW)	Output power (mW)	Efficiency(%)
A	797	726.8	91.1
B	641.8	579.5	90.3
C	754.7	686.8	91
D	1071	984.4	91.9
E	736.8	669.4	90.9
F	1047	961.1	91.8

Table 3.6: Efficiencies of all the elements that are driven at 1.0242MHz with C_{ext}

Transducers	DC supply power(mW)	Output power (mW)	Efficiency(%)
A	855.5	778.9	91
B	692.9	622.6	89.9
C	817.5	741.2	90.7
D	1071	984.4	91.9
E	816.1	736	90.2
F	1065	977.7	91.8

Table 3.7: Efficiencies of all the six elements that are driven at 1.0242MHz without C_{ext}

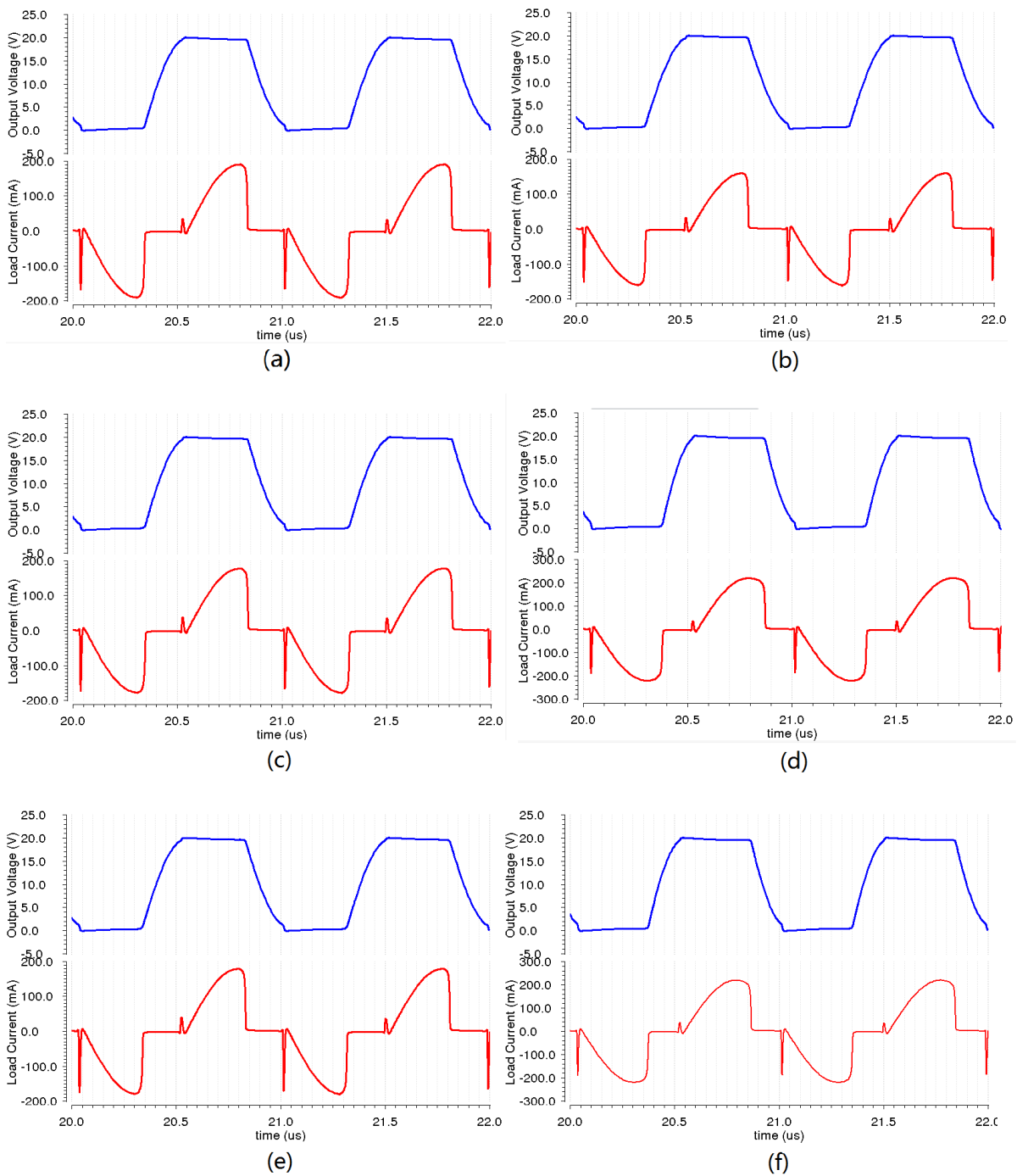


Figure 3.7: Output waveforms of all the elements that are driven by the using the external capacitor method

3.2.2 Using the Average frequency

We can obtain more output power with acceptable efficiency by using the average frequency and optimum duty ratios of each element.

The average of all the optimum operating frequencies of all the six elements is 1017 kHz. Under this operating frequency, all the elements should have some distortions on their output Voltage and current waveforms. This will cause more switching loss during the Class-DE switching. However, if the switching loss is not very high, it should be acceptable. The output voltage and currents of all the six elements are shown in Figure 3.8. As we can see, there are some distortions on all the output current waveforms except D compared with the Figure 3.3. Table 3.8 shows the efficiency results of all the six elements that are driven at the average frequency, all the output power are higher than the external capacitor method and the efficiency is almost the same. Comparing the results of average frequency driving to the optimum frequency driving which is shown in Table 3.4, the total delivered power is the same and the efficiencies are only slightly lower.

Transducers	DC supply power(mW)	Output power (mW)	Efficiency(%)
A	1151	1059	92
B	972.3	891.1	91.7
C	1125	1037	92.1
D	1340	1229	91.8
E	1137	1046	92
F	1345	1236	91.9

Table 3.8: Efficiencies of all elements which are driven by average frequency

3.3 Summary

In this section we introduced two strategies to drive a transducer array under the same frequency, one uses an external capacitor to make all the elements operate at a higher frequency and the other drives the elements by using the average of the optimum operating frequencies of all elements. The external capacitor strategy can remove all the distortions of all the output waveforms and keep elements operating in high efficiencies. But the major drawback of this strategy is that the output power is reduced. The average driving strategy cannot remove all the distortions on the output

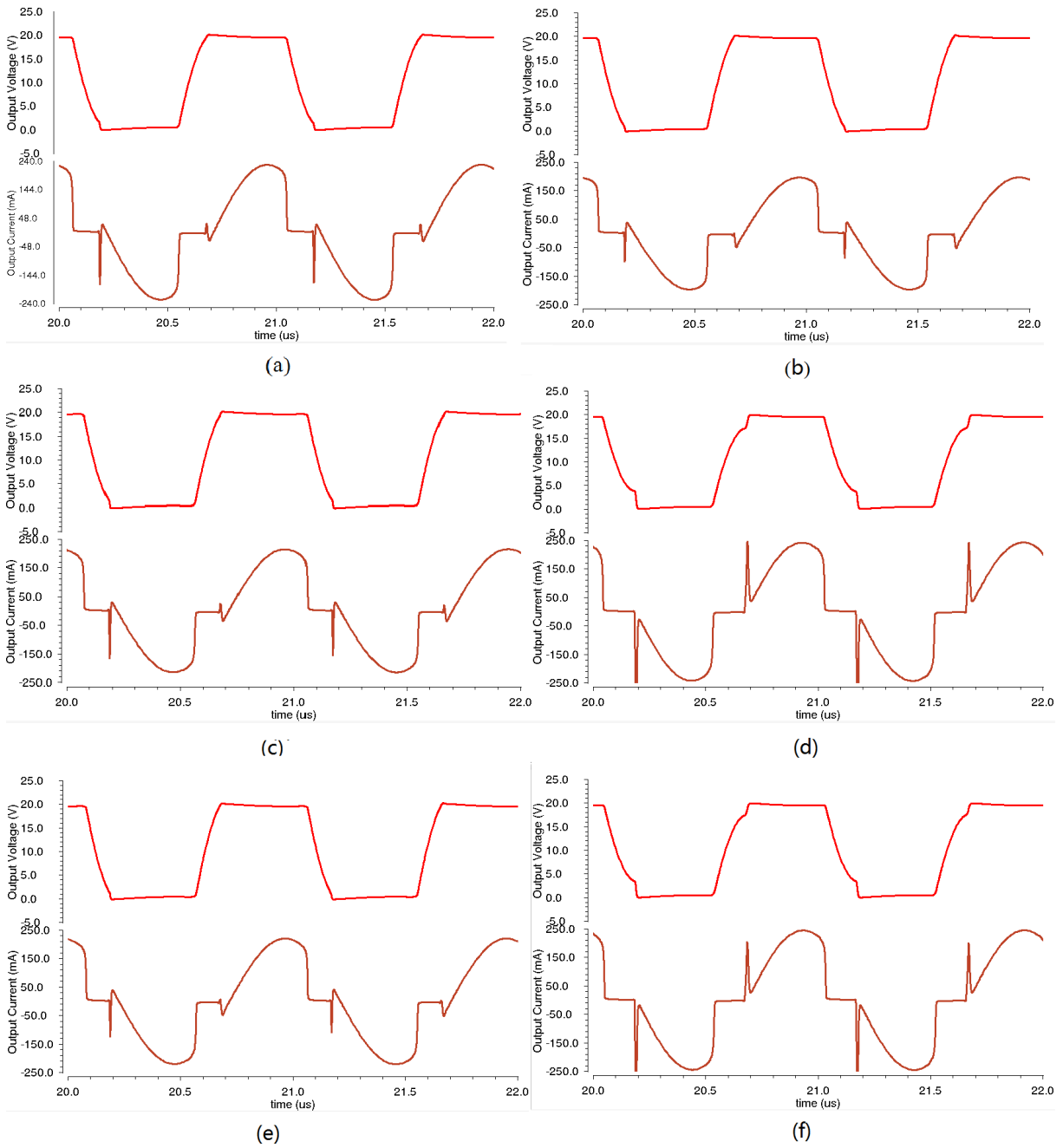


Figure 3.8: Output waveforms of all the elements that are driven by the average of their optimum frequencies

waveforms, but it still can let the elements operate at high efficiencies while keeping the output power at a higher level.

Chapter 4

Ultrasonic Transducer Driver Design

4.1 Introduction

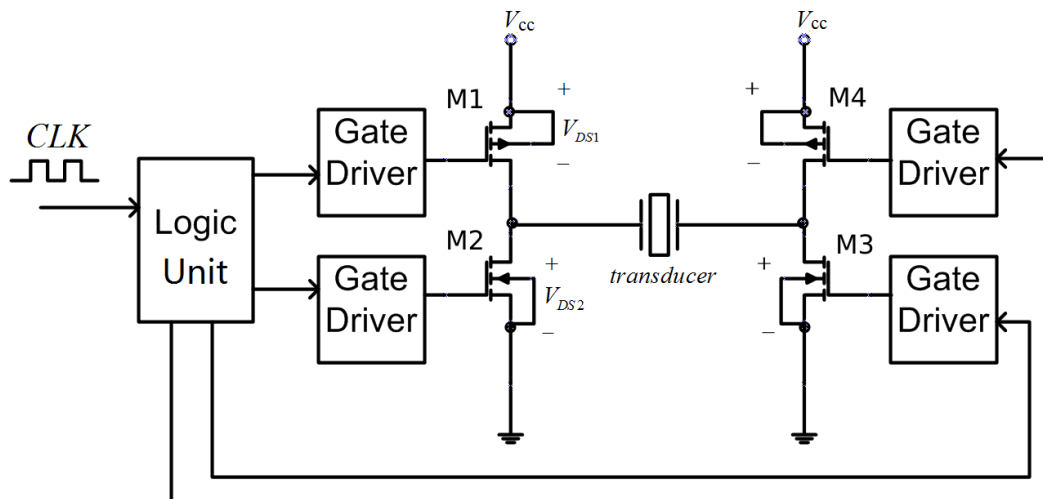


Figure 4.1: Block diagram of the proposed integrated transducer driver [5]

As previously discussed, the final design is a full-bridge Class-DE amplifier with integrated logic and gate drivers. The block diagram of the final design is shown in Figure 4.1. In this design,

we integrated the output stage, gate drivers and digital logic control part in the same chip. The output stage is a full-bridge Class-DE amplifier which is composed of 4 transistors. The gate driver is composed by a level shifter and a output stage to amplify the 5 V pulse trains to 20 V pulse trains. The digital logic control unit is composed by a counter, 3 comparators , a register and a pulse trains generator. The driver was implemented with Austria Microsystems' AMS AG H35 CMOS process using the Cadence® suite of design tools.

4.2 Full-bridge Class-DE Amplifier

In our proposed design, we chose a full-bridge Class-DE amplifier as the output stage. Its efficiency is just slightly lower than the half-bridge Class-DE amplifier, because of the full-bridge Class-DE amplifier's switch resistance being 2 times of the half-bridge one. On the other hand the output power can be nearly 4 times higher than the one obtained with the half-bridge. So by using the full-bridge one we can achieve one of our objectives to deliver more power to the load and keep the high efficiency at same time.

The high voltage MOSFETs' symbol is shown in Figure 4.2 (a) and (b), the low voltage MOSFETs' symbol is shown in Figure 4.2 (c) and (d).

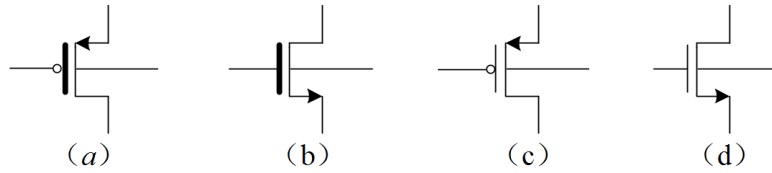


Figure 4.2: Symbols of the MOSFETs (a) HV PMOS; (b) HV NMOS; (c) LV PMOS; (d) LV NMOS

The topology of the full-bridge Class-DE amplifier is shown in Figure 4.3. In this figure, the load transducer has been replaced by its equivalent BVD circuit. The input and output waveforms of the full-bridge Class-DE amplifier are shown in Figure 4.4.

The full-bridge Class-DE amplifier also has 4 intervals in its operation. These 4 intervals' principles are similar to the half-bridge Class-DE amplifier's which was described in section 2.5, so the ZVS and ZDS conditions are also satisfied. During interval 1, M1 and M3 are turned on, $V_{OUT} = V_{CC}$; In interval 2, all transistors are turned off, C_P is charging the series resonance branch during this interval, so V_{OUT} decreases to $-V_{CC}$; During interval 3, M2 and M4 are turned on, V_{OUT} stay at $-V_{CC}$; During interval 4, all transistors are turned off again, V_{OUT} increases to V_{CC} . compare to the half-bridge Class-DE amplifier, the output voltage of full-bridge amplifier is doubled and output

power is increased 4 times.

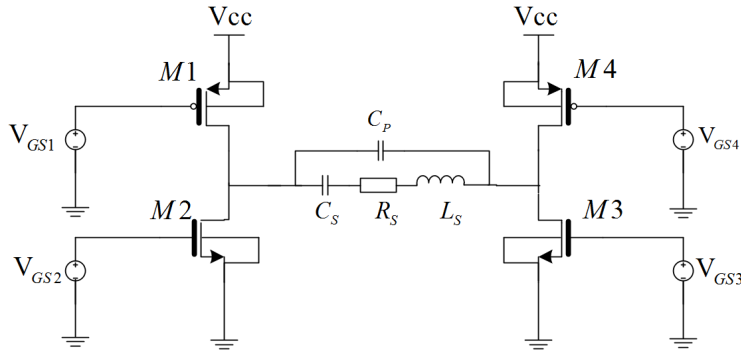


Figure 4.3: Topology of the full-bridge Class-DE amplifier

In practice, the channel resistance will produce switching loss in the transistors, and the actual efficiency of the Class-DE amplifier is not the ideal 100%. From [2] the maximum efficiency of the half-bridge Class-DE amplifier is nearly 80% and in the [5] the maximum efficiency is over 90%.

The full-bridge Class-DE amplifier is actually a combination of two half-bridge Class-DE amplifier, so we can use the same $\frac{W}{L}$ value of half-bridge Class-DE amplifier for the full-bridge one. In [5], we have the half-bridge Class-DE amplifier's width and length parameters which are listed in Table 4.1:

	PMOS	NMOS
Transistor finger $W/L(\mu m/\mu m)$	50/1.4	50/1
Number of parallel fingers	360	140
On-resistance	4.17 Ω	4.07 Ω

Table 4.1: Half-bridge Class-DE amplifier's width and length parameters [5]

Please note that $(W/L) = (W/L)_{finger} \times N_{finger} \times 2$, where (W/L) is the total aspect ratio of a transistor, $(W/L)_{finger}$ is the finger width and N_{finger} is the finger number of the transistor. So in the full-bridge Class-DE amplifier we can set $(\frac{W}{L})_{M1,M4} = 36000/1.4$ and $(\frac{W}{L})_{M2,M3} = 14000/1$. The parasitic capacitance of the switches is approximately 70 pF, so we should also consider the effect of this parasitic capacitance while determining operating frequencies and duty ratios.

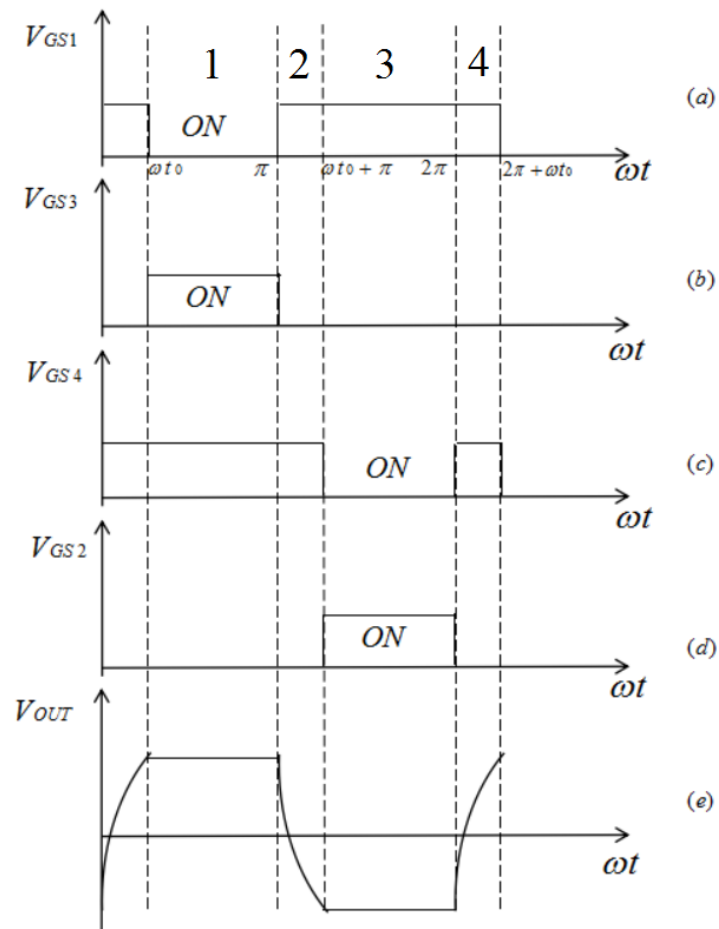


Figure 4.4: Inputs and output waveforms of the full-bridge Class-DE amplifier, (a), (b), (c) and (d) The switch-on diagram of transistors M1, M2, M3 and M4. (e) The voltage waveform across the load

4.3 The Gate driver

The switch MOSFETs operate at a different voltage level than the logic control. Also the gate capacitance of the switch MOSFETs is very large. For these reasons we need a dedicated gate driver to drive these MOSFETs in Class-DE operations. The gate driver determines the rise time and fall time of the gate voltage to let the MOSFETs to be turned on and off on time.

The schematic of the gate driver is shown in Figure 4.5 [16]. This gate driver consists a level shifter and an output stage. The output stage is composed by a HV NMOS (M4) and a HV PMOS (M3). The major advantage of the level shifter is that it offers high speed switching without the need for multiple driving signals and the major drawback is that its power consumption is nearly 2% of maximum output power [2]. The output V_{OUT} is connected to the gate terminal of a switch MOSFET. So in this design we need four gate drivers.

In gate driver's schematic, the LV PMOSs M11, M12, M13 and M14 consist of two voltage mirrors, along with two HV NMOS M7 and M8. These transistors form a level shifter. The level shifter can raise a reference 0V to 5V signal to a 0V to V_{CC} signal. The working process of this gate driver is explained below.

When the input signal V_{IN} (the 0V to V_{dd} low voltage signal) is logic high, M6 and M7 conduct and M8 is turned off and then M11 and M13 conduct and M12 and M14 are turned off, so the drain potential of M7 V_C is logic low and drain potential of M8 $V_A = V_{CC}$. Therefore M5 is turned off and M6 conducts, the output voltage $V_{OUT} = 0V$. If the V_{IN} is logic low, M8 conducts and M7 is turned off, so M12 and M14 are turned on, M11 and M13 turned off. So V_A is logic low and $V_C = V_{CC}$. Then M5 is turned on and M6 is turned off, the output voltage is $V_{OUT} = V_{CC}$. By using this method, the gate driver converts the low voltage signal to high voltage signal.

The aspect ratios of all the transistors in this gate driver is listed below [2]:

$$\left(\frac{W}{L}\right)_{11} = \left(\frac{W}{L}\right)_{12} = \left(\frac{W}{L}\right)_{13} = \left(\frac{W}{L}\right)_{14} = \frac{10\mu m}{4\mu m} \quad (4.1)$$

$$\left(\frac{W}{L}\right)_7 = \left(\frac{W}{L}\right)_8 = \frac{10\mu m}{0.5\mu m} \quad (4.2)$$

The output of this gate driver is the inverse signal of the input signal, which means when the input is logic high, the output is logic low; when the input is logic low and the output is logic high. As shown in Figure 4.6. The gate driver's parameters are taken from Wai's previous design [2]. When the input is logic low, the M8 and M14 are turned on and V_A is up to 18.45V which is just 1.55 V lower than V_{CC} , that means the M5 is in active region, but the gate driver still keeps working. The reason is that the load is a MOSFET's gate whose impedance can be assume to be infinity, so we

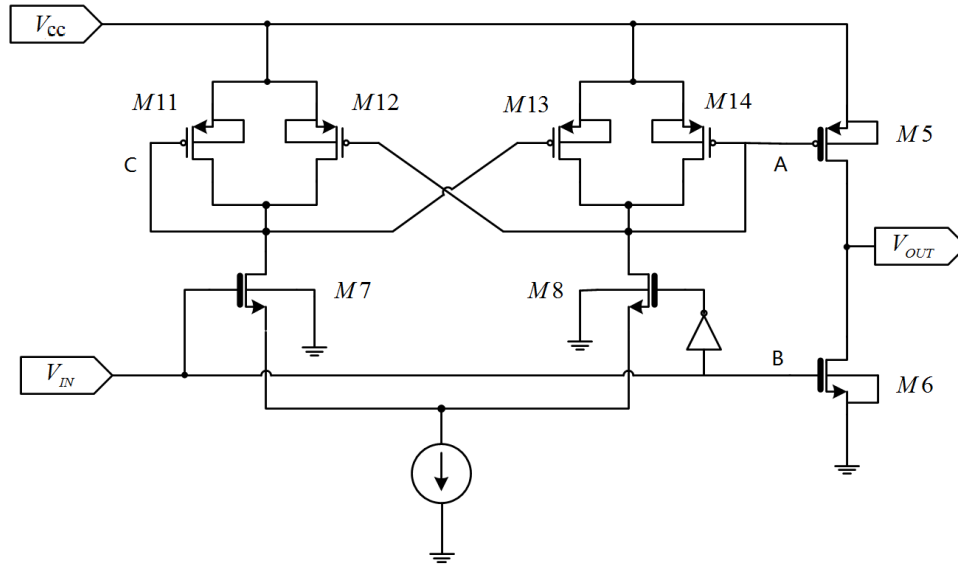


Figure 4.5: Schematic of MOSFETs' gate driver [2, 16].

just need to make the M5 conduct, no matter it is in triode region or active region.

A disadvantage of this design is that the full V_{CC} supply voltage is applied to the switch gates (V_{OUT}). This limits the high voltage that can be applied to the chip to 20V (maximum HV gate voltage) instead of the maximum drain voltage supported by the technology (50V).

4.4 Digital Logic Unit

The function of the digital logic unit is to generate pulse trains to the 4 MOSFETs in the a full-bridge Class-DE amplifier and make sure the phase shift and duty ratios of the pulse trains can be programmable. The structure of this digital logic unit is shown in Figure 4.7. It consists a 10-bit-counter, a 30-bit-register, 3 10-bit-comparators and a pulse train generator. The Digital logic unit has 7 logic input pins. Among these, CLK, EN, reg_CLK, reg_data and reset are common to all drivers in an array. Pin A and B are used to address individual drivers in the array. The power supply pins are also common to all drivers. A digital logic unit can generate 4 pulse trains for each MOSFET in a full-bridge Class-DE amplifier.

4.4.1 The Structure of Each Block

A. 10-bit-counter

The 10-bit-counter's function is to divide CLK signal's frequency by its modulus. The structure of

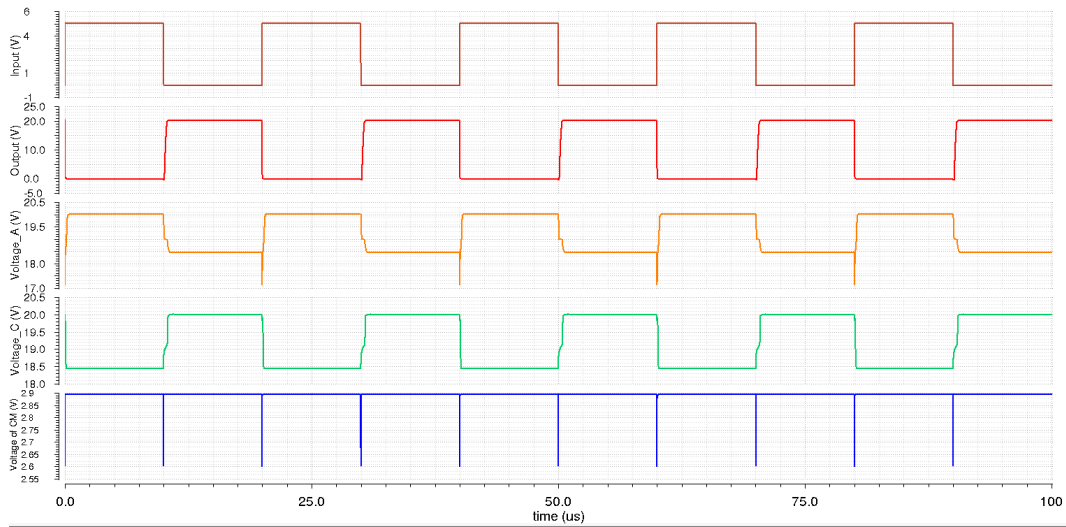


Figure 4.6: Input signal and output signal of the gate driver.

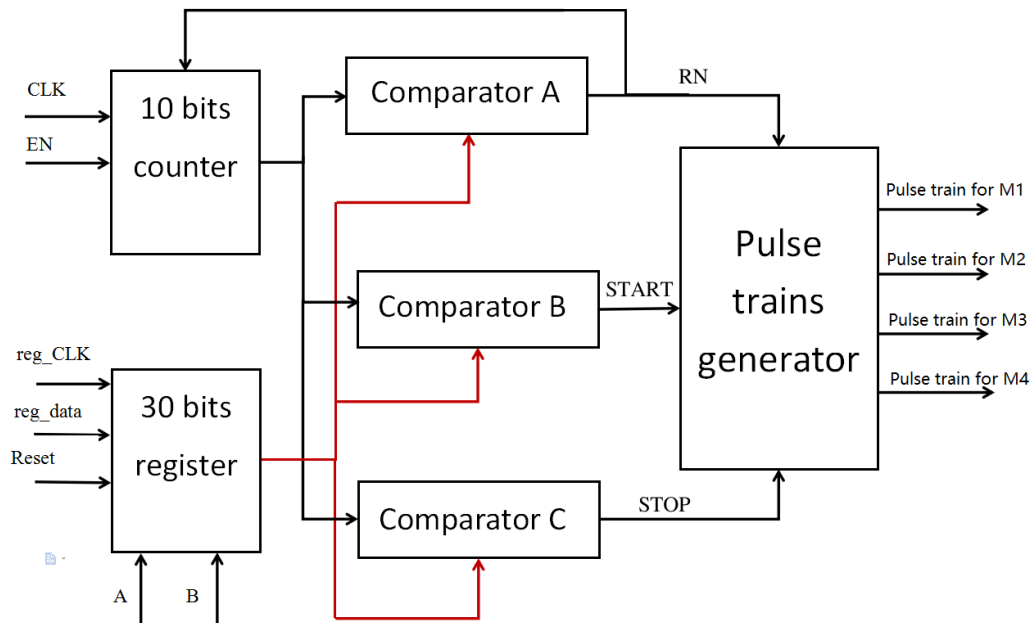


Figure 4.7: Structure of the digital logic unit.

10-bit-counter is shown in Figure 4.8. It consists 10 positive-edge triggered T flip-flops and some AND gates. This is an synchronous counter which has better performance in the high frequency range than the asynchronous counter [17], but it occupies more area in the chip. In this schematic, the external clock signal will be sent to the CLK pin, the counter will count every positive edge of the pulses. The Reset pin's function is to reset the counter by logic low, it connects the output of the comparator A and an input pin of the pulse trains generator. EN pin is the enable signal of the counter, it also connects the EN pin of the pulse trains generator. Q0 to Q9 is the output of this counter, they connect to the input pins in comparator A, B and C.

B. 30-bit-register

The schematic of the 30-bit-register is shown in Figure 4.9. This 30-bit-register consists of 30 positive-edge triggered D flip-flops and an AND gate. This register has 5 input pins which are A, B, reg_data, Reset and reg_CLK and 30 output pins which are Q0 to Q29. Pin A and B are the selection pins of the register, set both A and B to logic high will select a certain driver. In a transducer array, we can arrange the drivers as a matrix which shown as Figure 4.10. In this figure, each green square represents a driver. After set one driver's both pin A and B to logic high, we can send the data to its 30-bit-register. The data at the pin reg_data can be sent to the register when the pin reg_CLK meets a positive edge, so this register is a shift register.

The 30-bit-register has been divided into 3 parts, each part has 10 bits. The first 10 bits is the CLK pulses to be counted for half period (the reason will be mentioned later) of the output waveforms of the digital logic unit. The second and third parts are counts for turning one MOSFET on and off, respectively, in each semi-period. These values define the period, phase shift and duty ratio of the driver.

C. 10-bit-comparator

The schematic of the 10-bit-comparator is shown in Figure 4.11. It consists of 10 XOR gates, 5 two-input OR gates and a 5-input OR gate. It has 20 input pins which are Q0 to Q9 and R0 to R9. The Q0 to Q9 is connected with the 10 output pins of the 10-bit-counter and R0 to R9 is connected to the First, second or third 10 output pins in the 30-bit-register. The OUTPUT pin of this comparator is connected to the pulse trains generator. When the data at Q0 to Q9 is equal to the data at R0 to R9, the output of the 10-bit-comparator will generate a negative pulse (its pulse width is same as a CLK signal's pulse width), otherwise the OUTPUT pin remains logic high. By this method, the comparator A can send reset signal to control the 10-bit-counter's modulus, comparators B and C can generate start and stop signals of duty cycles and send them to pulse train

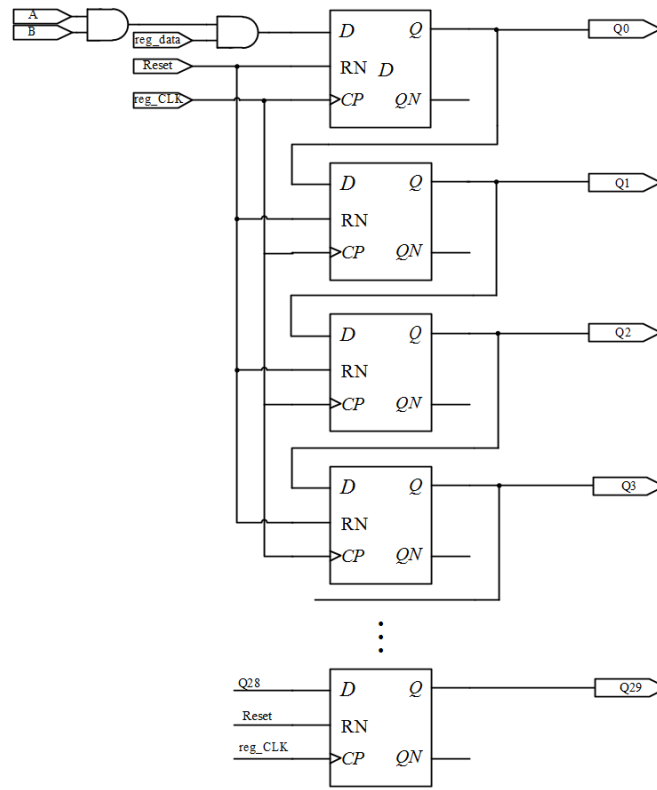


Figure 4.9: Schematic of 30-bit-register.

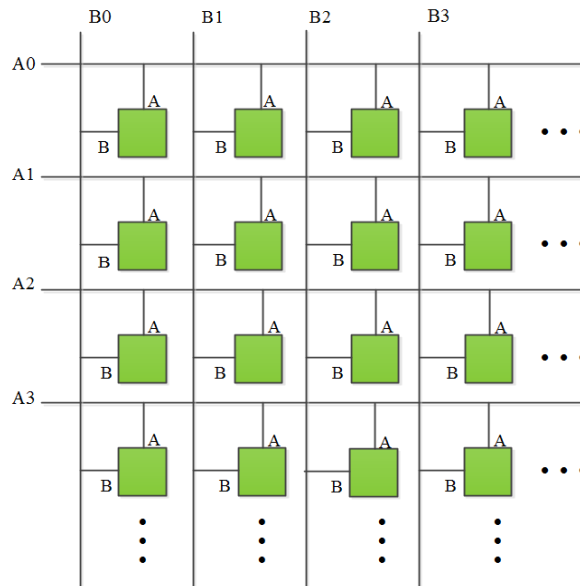


Figure 4.10: Transducer array driving method.

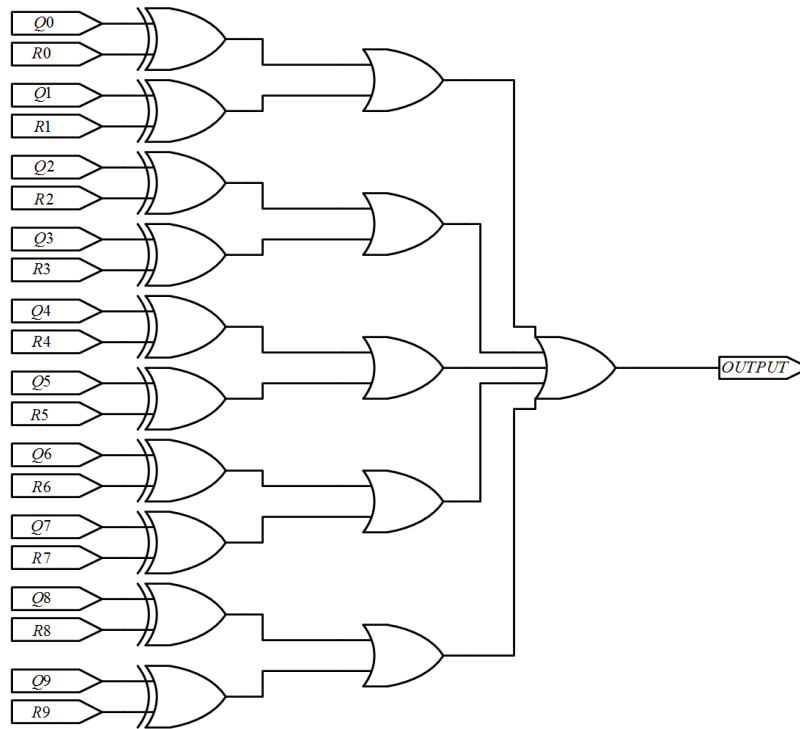


Figure 4.11: Schematic of the 10-bit-comparator.

generator.

D. Pulse Train Generator

The pulse train generator consists of two positive edge triggered T flip-flops, an inverter, a NAND gate, 2 OR gates and 2 AND gates. Its schematic is shown in Figure 4.12. It has 5 input pins which are RN, EN, VDD, START and STOP, 4 output pins which are Pulse_P1, Pulse_N1, Pulse_P2 and Pulse_N2. The EN is the enable pin, it is connected to the EN pin of the counter; RN pin is connected to the OUTPUT pin of the comparator A which is the reset signal of the 10-bit-counter, represents the period; START and STOP pins are connected to the OUTPUT pins of the comparator B and C which are the signal of the start and stop time of the pulse; the output pins Pulse_P1, Pulse_N1, Pulse_P2 and Pulse_N2 are the driving signal of the gate drivers of the M1, M2, M3 and M4 in the full-bridge Class-DE amplifier respectively.

When EN is set to logic high, the pulse train generator can work normally; if it is set to logic low, the output of the two T flip-flops will be set to zero, then the Pulse_P1 is set to high, Pulse_N1 is set to low, Pulse_P2 is set to logic high and Pulse_N2 is set to logic low, which means all the MOSFETs in the full-bridge Class-DE amplifier have been turned off. If the EN goes high, this pulse train generator can generate the objective pulse trains for the four MOSFETs in the Class-DE amplifier.

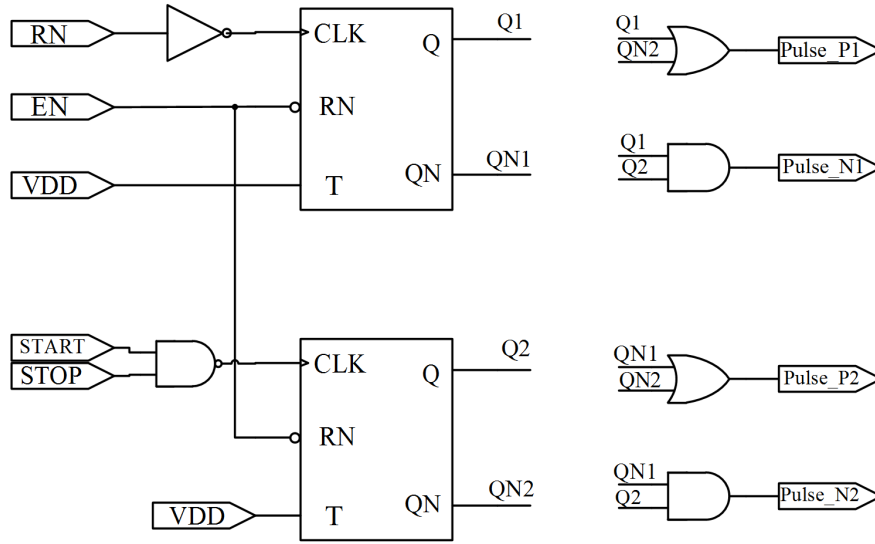


Figure 4.12: Schematic of the pulse-trains-generator.

The working procedure of the whole digital logic unit will be described in the next Sub-section.

4.4.2 Operating procedure of the digital logic unit

The digital logic unit can be divided to 3 parts, the first one is a frequency divider, the second one is a phase shift and duty ratio controller and the third one is the pulse trains generator. The block diagram of the relationship of these three parts are shown in Figure 4.13. The operating procedure is shown below:

A. Frequency Divider

The block diagram of the frequency divider is shown in Figure 4.14. First, when the EN input goes high, the 10-bit-counter counts the number of the external clock signal's pulse (CLK). The external CLK is normally set to a multiple of the transducer operating frequency. The counter's modulus controls the resolution of the duty ratio and phase shift. The output of the counter will be compared with the first 10 bits of the 10-bit-register in comparator A, if they match each other the comparator A will outputs a negative pulse to the pulse train generator and reset the counter, otherwise its OUTPUT pin will stay on logic high. The output diagrams are shown in Figure 4.15.

B. Phase Shift and Duty Ratio Controller

The block diagram of the phase shift and duty ratio controller is shown in Figure 4.16. It consists of two comparators. In the operation of the digital logic unit, the comparator B and C compare the output of the 10-bit-counter to the second and third 10 bits of the register, if the counter's output

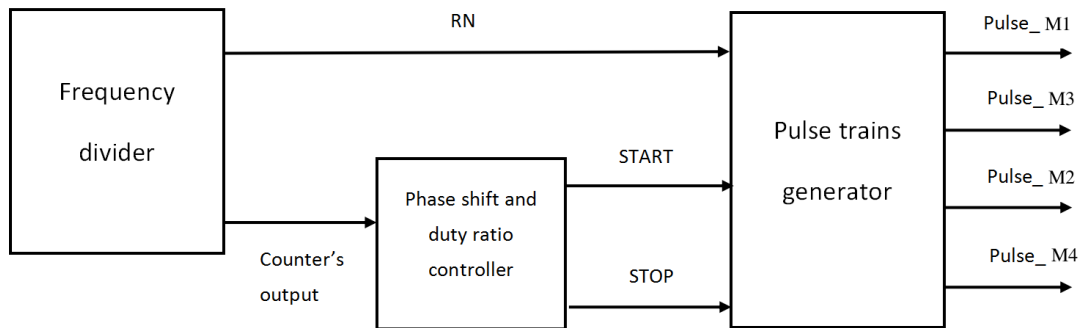


Figure 4.13: Block diagrams of the relationship of the frequency divider, phase shift and duty ratio controller and pulse train generator.

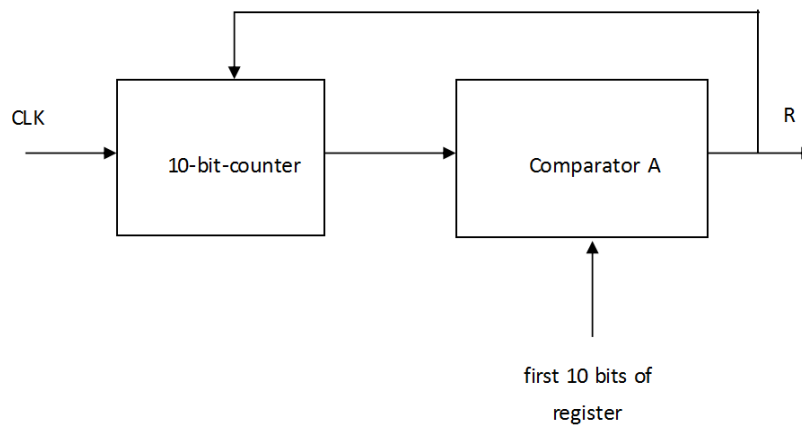


Figure 4.14: Block diagram of the frequency divider.

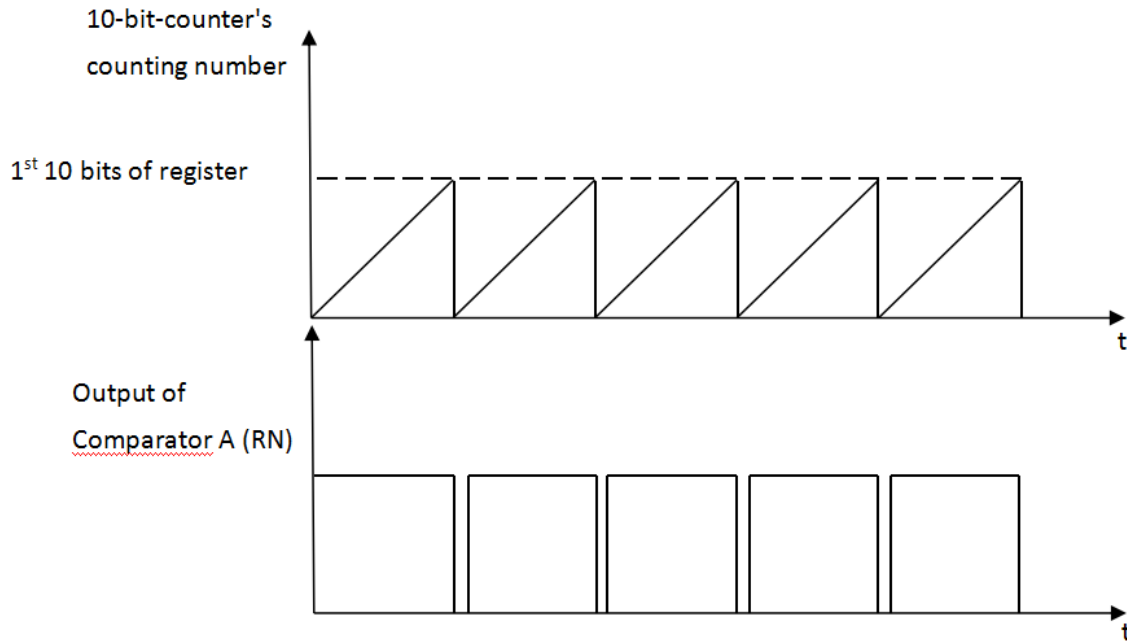


Figure 4.15: Output diagrams of the frequency divider.

matches the data stored in the second and third 10 bits of the register, these two comparators will generate negative pulses which are the start and stop signal of a duty cycle (START and STOP), otherwise their outputs will remain on logic high. Because of that, the data stored in the third 10 bits of the register must be greater than the data stored in the second 10 bits and both of them must be smaller than the data stored in first 10 bits. The output diagrams are shown in Figure 4.17.

C. Pulse Train Generator

In this part the only component is the pulse trains generator itself. The initial state of both the two T flip-flops are zero. The input and output diagrams are shown in Figure 4.18.

As shown in the Figure 4.18, when the 10-bit-counter finished the first counting round, comparator A will generate a negative pulse to the RN pin of the pulse train generator. Because we have already set the T pins of both T flip-flop to logic high (as shown in Figure 4.12), the Q1 will be logic high and QN1 will be logic low, but the Q2 still is logic low and QN2 is still logic high, so the Pulse_P1 and Pulse_P2 are logic high, Pulse_N1 and Pulse_N2 are logic low, which means all the MOSFETs are still turned off. When the START signal become logic low and STOP signal remains in logic high, which means the counter's output matches the second 10 bits of the register but still doesn't match the third 10 bits, the Q2 will be logic high and QN2 will be logic low. So the

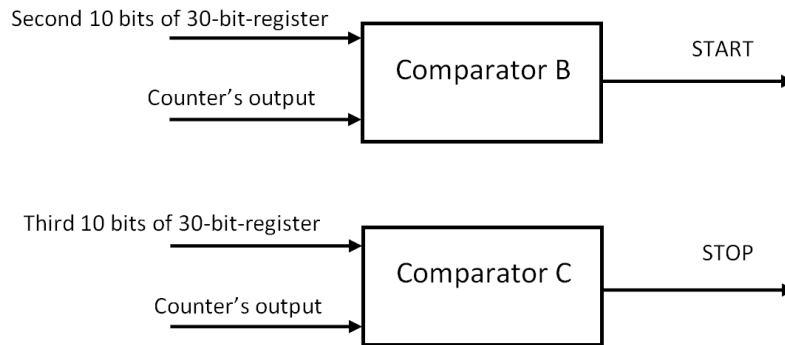


Figure 4.16: Block diagram of the phase shift and duty ratios controller.

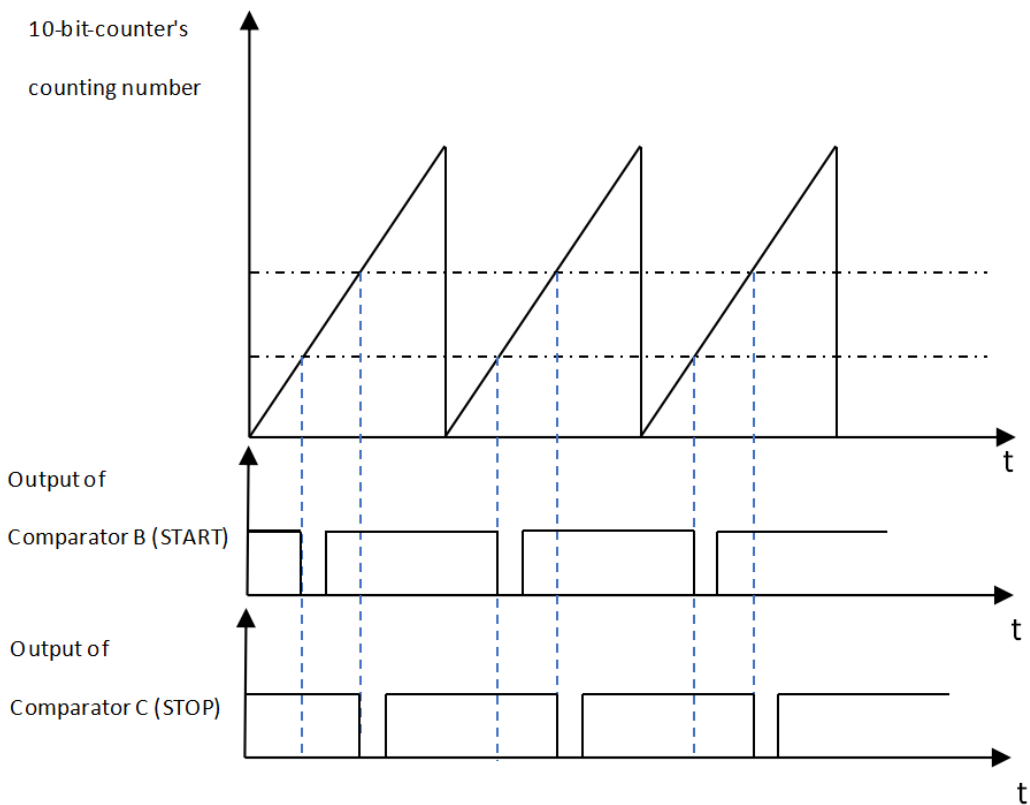


Figure 4.17: Output diagrams of the phase shift and duty ratios controller.

Pulse_P1 is logic high, Pulse_N1 is logic high, Pulse_P2 is logic low and Pulse_N2 is logic low, that means the M1 and M3 are turned off, M2 and M4 are turned on. When the output of the counter matches the data of the third 10 bits of the register, Q2 is set to logic low and QN2 is set to logic high, then Pulse_P1 and Pulse_P2 are set to logic high, Pulse_N1 and Pulse_N2 are set to logic low. Because of that all the MOSFETs are turned off.

When the 10-bit-counter finished the second round of counting , the pulse trains generator's pin RN will receive another negative pulse from the comparator A, so Q1 will be logic low and QN1 will be logic high, but the Q2 is still stays on logic low and QN2 is still stays on logic high, which means all the MOSFETs are still turned off. When the output of the counter meets the data that is stored in the second 10 bits of the register, the Q2 will be logic high and QN2 will be logic low again, so in this time the Pulse_P1 and Pulse_N1 will be logic low, Pulse_P2 and Pulse_N2 will be logic high, which means that the M1 and M3 are turned on, M2 and M4 are turned off. When the output of the counter matches the third 10 bits of the register, the Q2 is set to logic low and QN2 are logic high again, then the Pulse_P1 and Pulse_P2 go logic high, Pulse_N1 and Pulse_N2 go logic low, all the MOSFETs in the full-bridge Class-DE amplifier are turned off.

By repeating the procedure described above the M1 and M3, M2 and M4 will be turned on and off alternatively , to make the full-bridge Class-DE switching occurs.

4.4.3 Additional Safety Logic Block

Two additional safety logic block have been implemented with the digital logic unit to provide the functions of power stage enabling, output stage buffering and the faulty signal filtering, to make sure that the NMOS and PMOS in a same branch of the full-bridge Class-DE amplifier won't be turned on at same time [2]. They are located prior to the MOSFETs' gate drivers. The PMOS and NMOS in same branch share a same additional safety logic block. The schematic of the additional safety logic block is shown in Figure 4.19. This additional safety logic block's power supply is standard 5V, it has 3 input pins and 4 output pins. The input pins are EN which is connected to the EN signal of the pulse trains generator and 10-bit-counter, P which is connected to the Pulse_P1 or Pulse_P2 on the pulse train generator, N which is connected to the Pulse_N1 or Pulse_N2 on the pulse trains generator. The two outputs are Pout and Nout, the Nout is connected to the one of the gate driver's input of the NMOSs in Class-DE amplifier and Pout is connected to the one of the gate driver's input of the PMOSs in Class-DE amplifier. The P_comp and N_comp are the complimentary signals of the Pout and Nout. Because of the gate drivers' output signals are the inverse of their input signals, as we mentioned in Section 4.4, the Pout and Nout must to be the inverse signal of the input P and N; and also all the four output pins must can handle the large capacitor loads from the gate

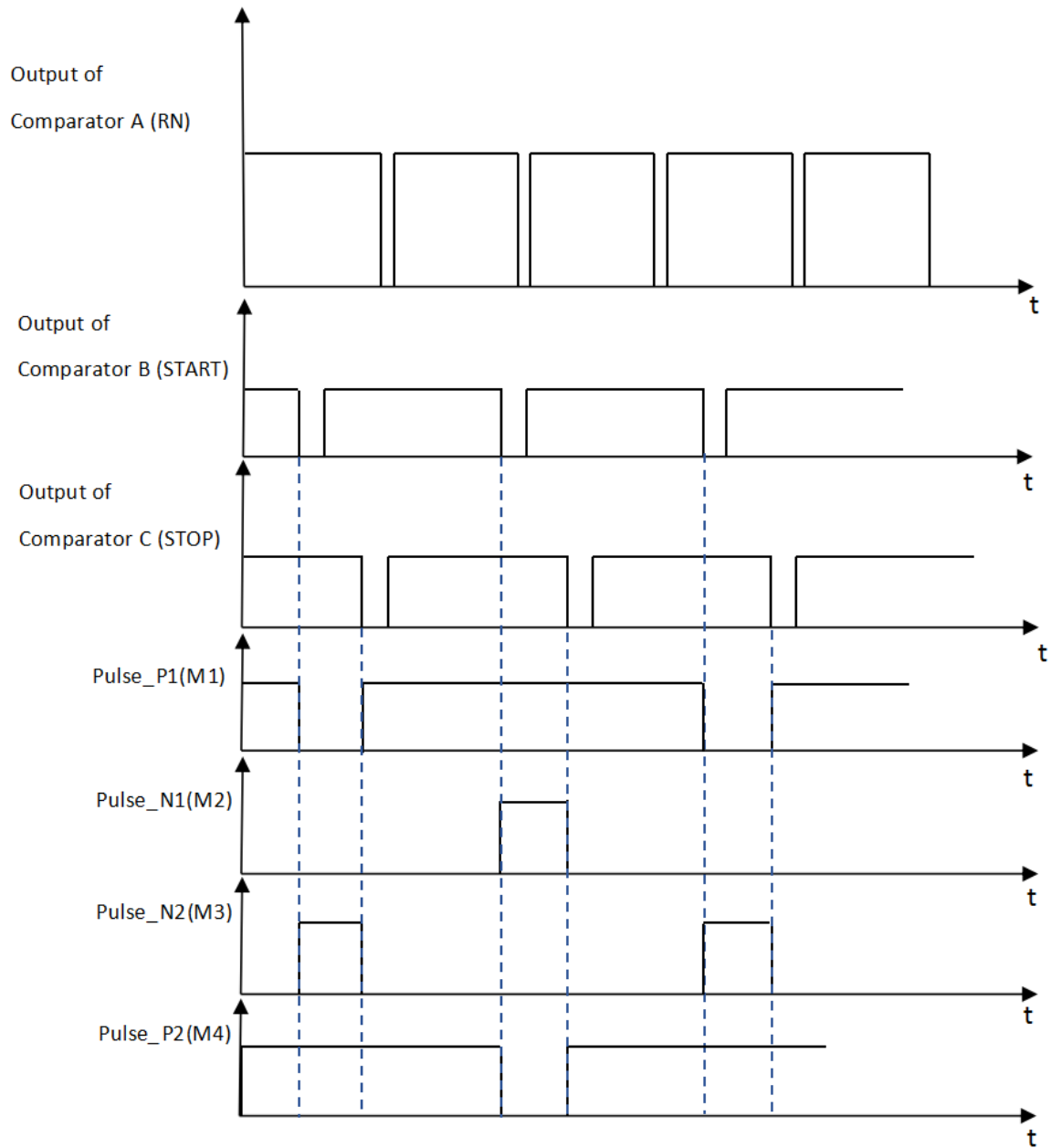


Figure 4.18: Input and output diagrams of the pulse trains generator.

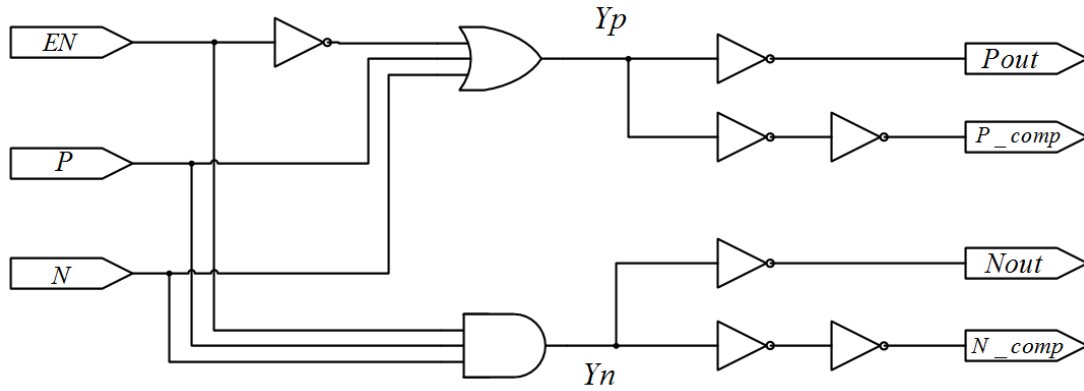


Figure 4.19: Schematic of the additional safety logic block [2].

driver.

The Yp and Yn are the output signals before inverted. If we ignore the delay, they have same phase shifts with the input signals of the PMOSs and NMOSs in the Class-DE amplifier (the input signals of the PMOSs and NMOSs are the output signals of the gate drivers). When the EN input goes low the Yp is logic high and Yn is logic low, which means the PMOSs and NMOSs are biased in cut-off mode; when the EN goes logic high, the additional safety logic block is enabled and Yn and Yp will follow the respective inputs unless the faulty inputs occurs (when P is logic low and N is logic high, which means the PMOS and NMOS in same branch are turned on at same time). When the P is logic low and N is logic high, the Yn is set to be logic low and Yp is set to be logic high, so the NMOS and PMOS in the same branch are in cut-off mode. This process will avoid the faulty state. The truth table of this additional safety logic block is shown in Table 4.2.

4.4.4 Simulation Results of Digital Logic Unit

In the simulation of the digital logic unit, we want to check not also its functionality, but also its high frequency performance. In order to make the result clear and easy to check, we used a 200 MHz external clock signal to generate 20 MHz, 36° phase shift and 72° duty ratio pulse trains for the NMOSs and PMOSs in the Class-DE amplifier.

Based on the setup strategy we mentioned before, we first set pin A and pin B to logic high and send the data that represent the frequency, start and stop time of the duty cycle to the 30-bit-register. The intended data is 3, 1 and 5 for each 10 bits of register. We put the data of stop time of the duty cycle first and the second 10 bits is the start time of the duty cycle, the third 10 bits is the parameter of the frequency. After that, set the EN pin to logic high, we can get the objective pulse trains from the output pins.

EN	P	N	Y _p	Y _n	PMOS	NMOS
0	0	0	1	0	off	off
0	0	1	1	0	off	off
0	1	0	1	0	off	off
0	1	1	1	0	off	off
1	0	0	0	0	on	off
1	0	1	1	0	off	off
1	1	0	1	0	off	off
1	1	1	1	1	off	on

Table 4.2: Truth table of the additional safety logic block [2]

The simulation results are shown in Figure 4.20. In this figure, the first signal is the external CLK signal that is sent to the counter, then the comparator A, B and C generates the second and third signals which are the negative pulses of the period, start time and the stop time of the driver's output. The last four signals are the driving signals of M1, M3, M2 and M4 respectively. As we can see, the M1 and M3 are turned on at same time, M2 and M4 are turned on at same time. The four driving signals have a little bit delay, but all the signals are passed through the same number of stages, so the delay time is almost equal for all of them.

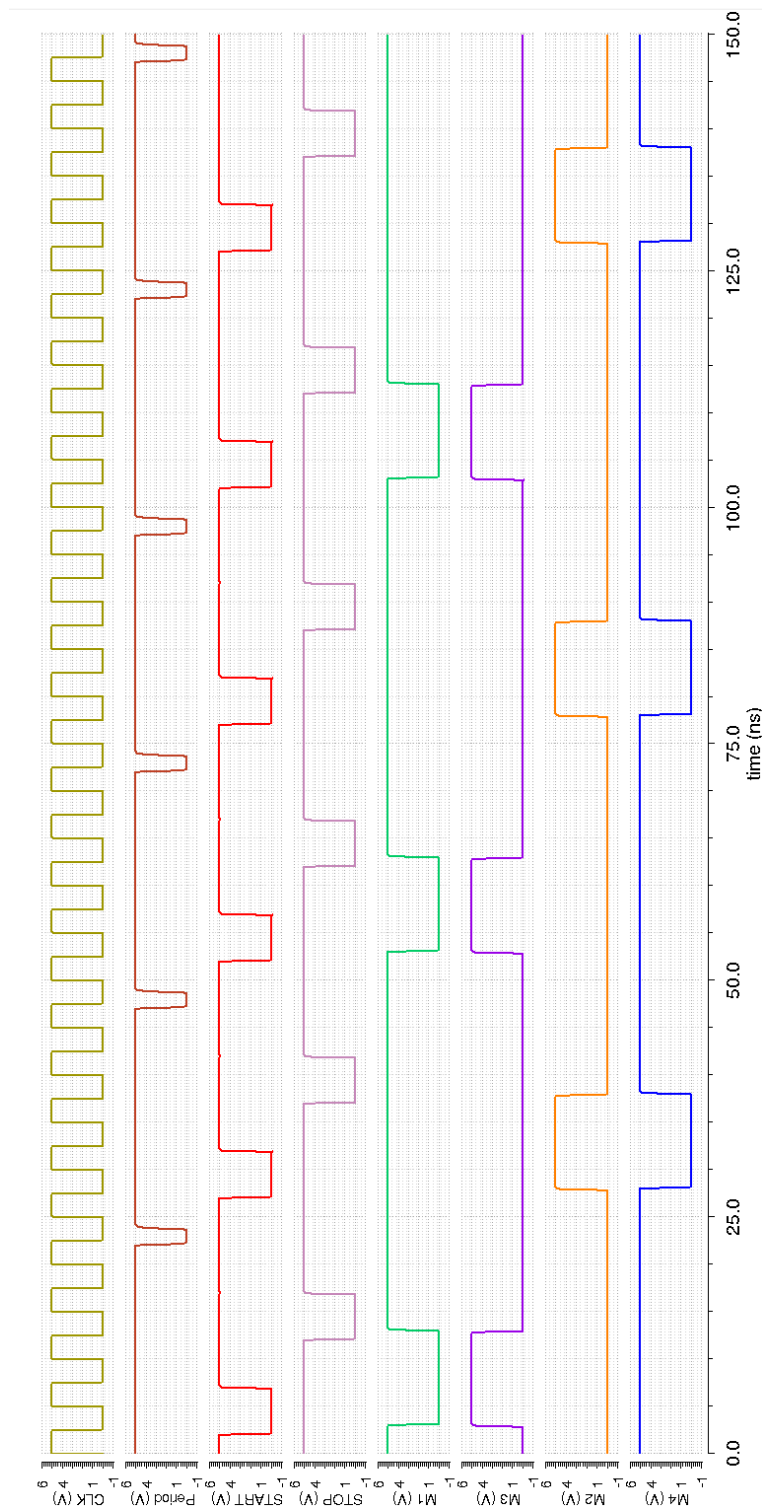


Figure 4.20: Outputs waveforms of the digital logic unit, its input clock signal's frequency is 200MHz, phase shift is 10%, duty ratio is 20% .

4.5 The Layout Design

We used a $2mm \times 1.5mm$ die area to fabricate the chip. We used a Kyocera's JLCC-28 package which can accommodate just one die because of the available pin number concern. The layout view is shown in Figure 4.21. The red blocks which have black comments are the cells described in this chapter. M1, M2, M3 and M4 are the MOSFETs that form the full-bridge Class-DE amplifier. They are sized to provide same on-resistance, so the PMOSs is much wider than the NMOSs [5]. Gate drivers are located near each MOSFET. The gate drivers that are in a same branch share a common current source. The digital logic unit consists of a 10-bit-counter, a 30-bit-register, a pulse train generator and 3 10-bit-comparators and is located near the second branch of the full-bridge Class-DE amplifier.

The blue blocks are the pins of this driver, VDD20V and GND20V are the pins of the 20V power supply of the Class-DE amplifier and gate drivers, VDD5V and GND5V are the 5V supply of the logic unit and gate drivers, Reg_D and Reg_C are the reg_data and reg_CLK of the register as we mentioned before. Psub is the connection of the substrate (ground), Vm_o and Vm_in is the output and input of the current mirror that is shared by the gate drivers. The En, CLK, A, B and Reset we have mentioned in section 4.4.

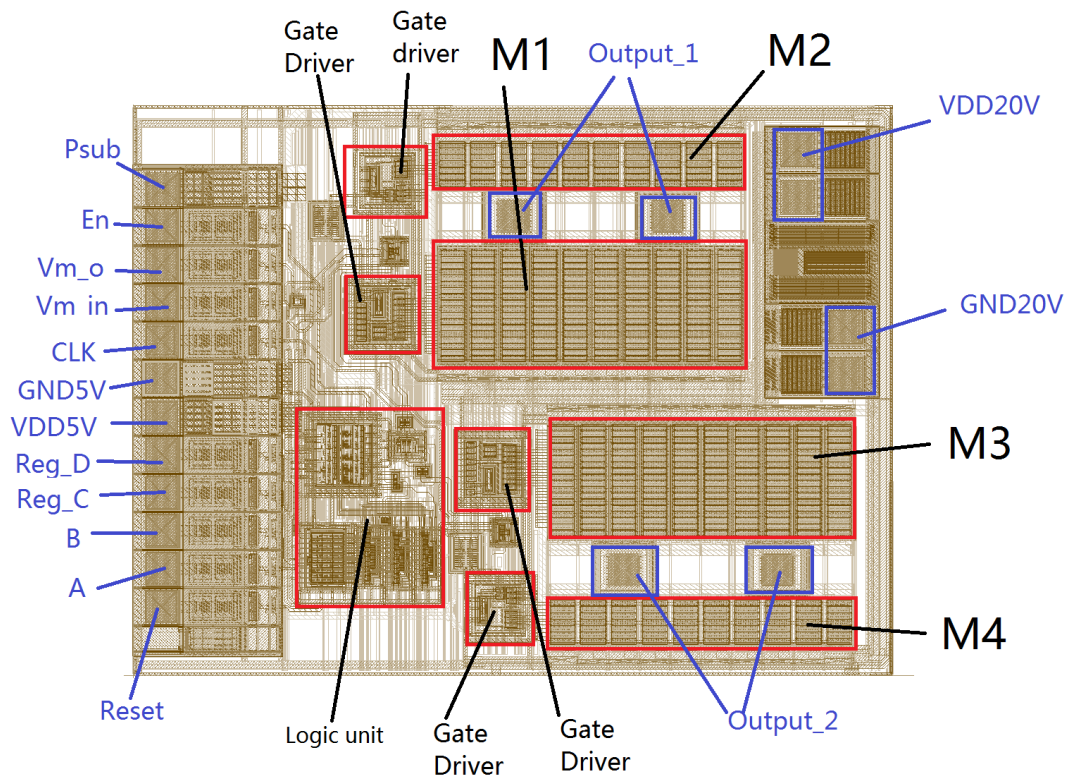


Figure 4.21: Layout view of the driver

Chapter 5

Simulation and Experimental Results

All simulations presented in this chapter were generated using the *Spectre*® simulator using the schematic view.

5.1 Simulation Results with Optimum Parameters

The full-bridge Class-DE driver's simulation results are shown in Figure 5.1. The load is the transducer from [5]. Equivalent circuit parameters are listed in Table 5.1 and optimum driving parameters are $f = 1010$ kHz and $D = 29.5\%$. The output voltage range is from -20V to 20V. Figure 5.2 shows simulation results of the half-bridge Class-DE driver for the same transducer. Its output voltage range is from 0V to 20V. Since the full-bridge Class-DE driver has 2 outputs (Output1 and Output2), there are two extra voltage waveforms which are taken from these two outputs. DC supply power, output power and efficiencies of these two drivers are shown in Table 5.2. As we can see, the efficiencies of these two drivers are close to each other, but the output power of the full-bridge driver is nearly 4 times of the half-bridge one's.

$C_P(nF)$	$C_S(pF)$	$L_S(uH)$	$R_S(\Omega)$
1.39	340	78.6	31.9

Table 5.1: Equivalent circuit parameters of the transducer [5]

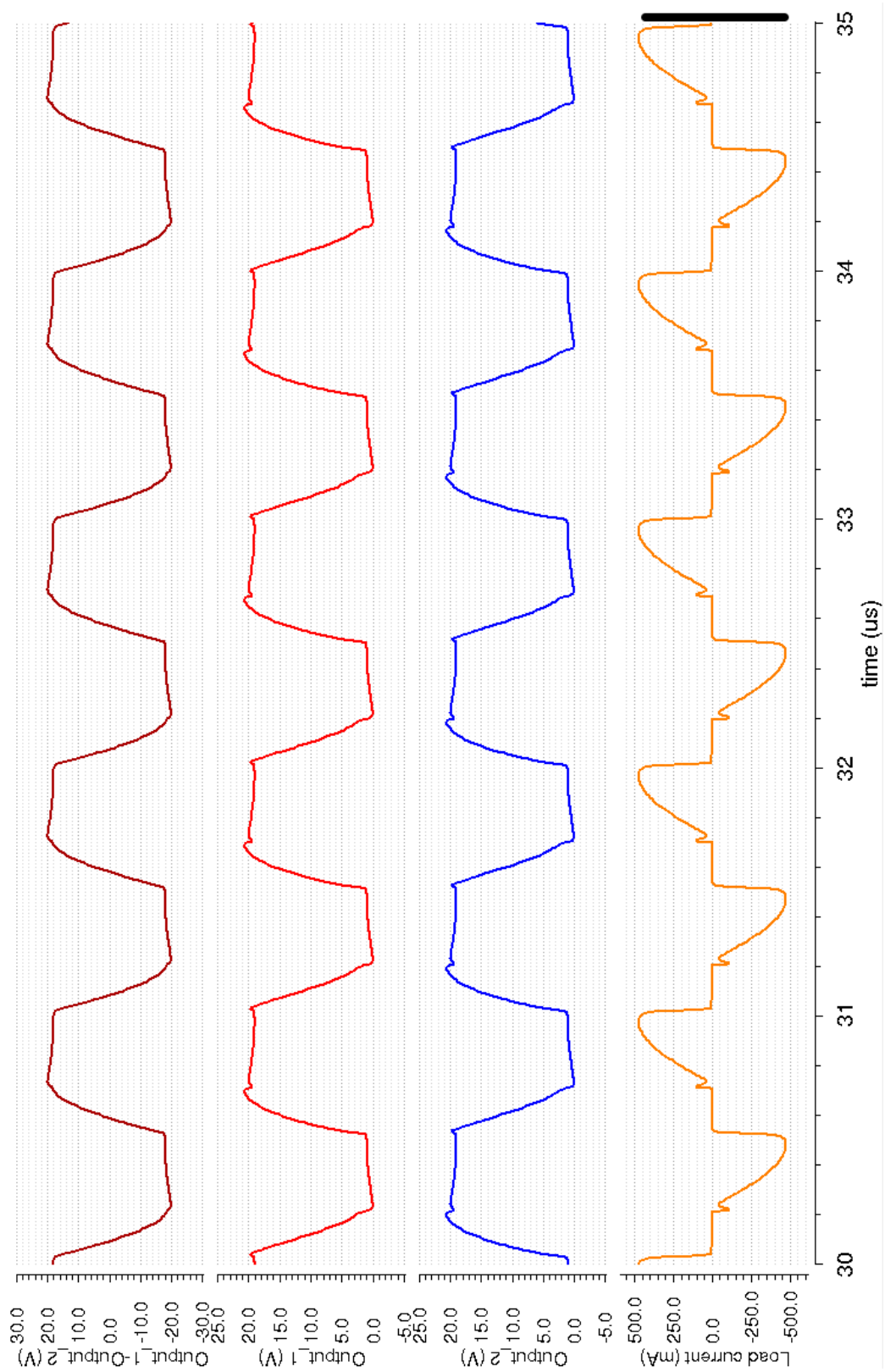


Figure 5.1: Simulation results of the full-bridge Class-DE driver that is proposed in this thesis. Brown: output voltage (Output1-Output2); Red: potential of Output1; Pink: potential of Output2; Orange: load current

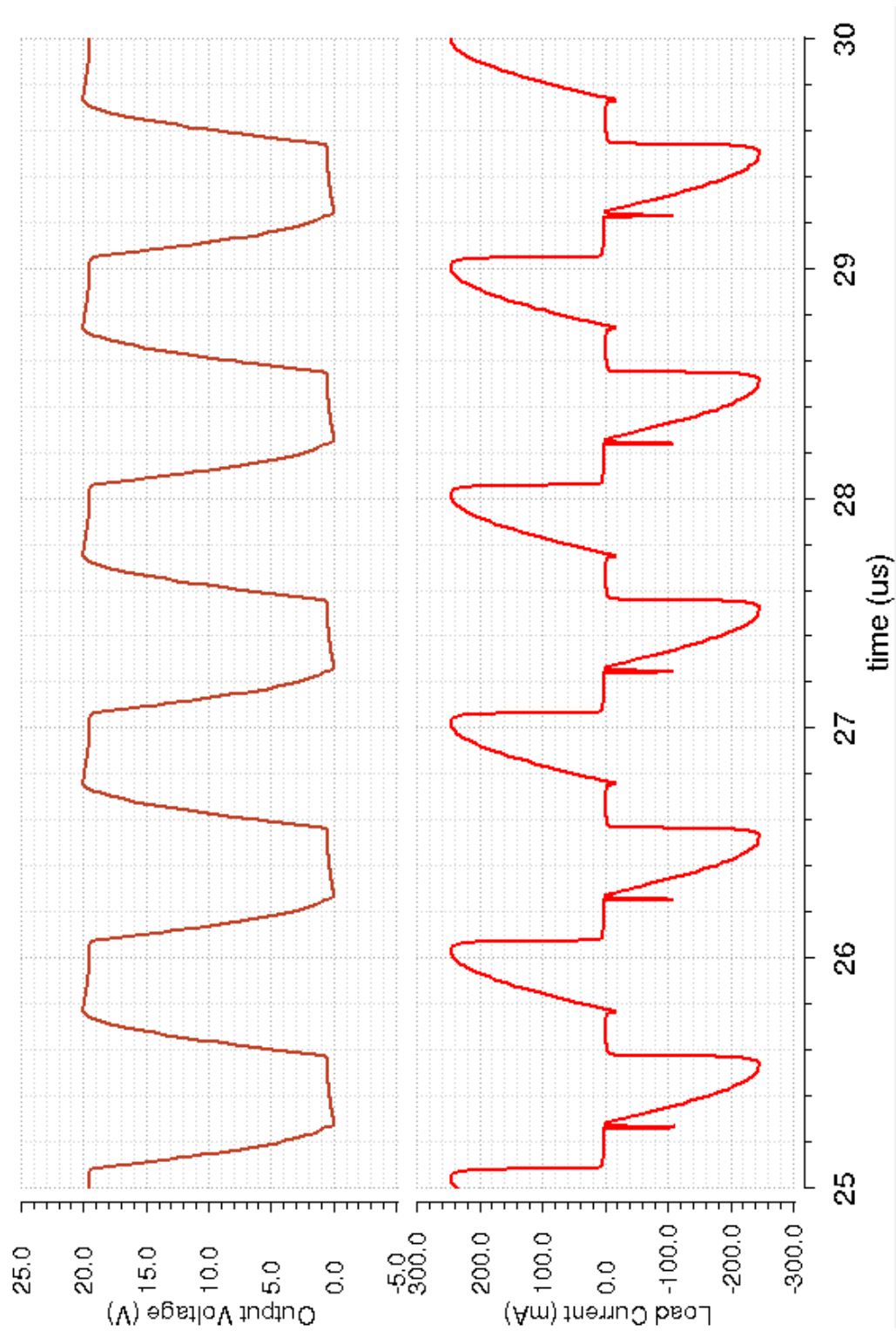


Figure 5.2: Simulation results of the half-bridge Class-DE driver that was designed by our group [5].
Brown: output voltage ; Red: load current

Driver	DC Supply Power(W)	Output Power(W)	Efficiency(%)
Full-bridge Class-DE driver	4.02	3.59	89.4
Half-bridge Class-DE driver	1.04	0.95	91.5

Table 5.2: DC supply power, output power and efficiencies of driving the transducer by full-bridge and half-bridge Class-DE drivers

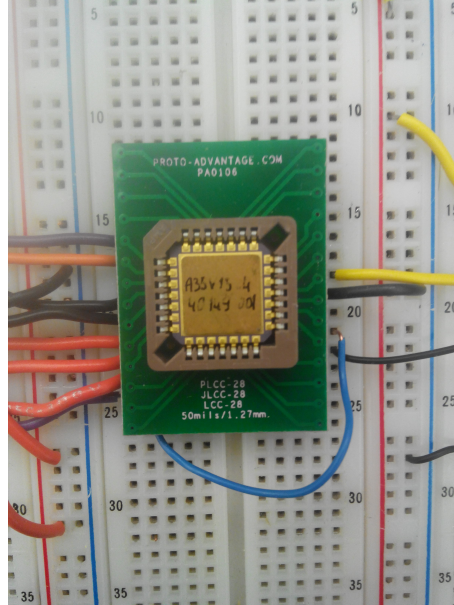


Figure 5.3: Fabricated driver in a testing circuit.

5.2 Experimental Setup

The driver has been fabricated. Initially Kyocera's LCC 02046 package was going to be used. This package should be MRI compatible because it has a gold plating instead of nickel plating. For lowering packaging cost the five packaged samples use a different package: Kyocera's JLCC-28. Unfortunately this package is not compatible with MRI imaging because it has a nickel plating under the gold plating. For this reason it may not be possible to test these packaged samples in the MRI environment. However, we still can make some tests. Figure 5.3 is the driver which is tested by using a bread board. We used a function generator (its maximum signal frequency is 15 MHz) to generate the external CLK signal and an Arduino Uno to program the duty ratios and phase shifts of the output pulse trains.

First, we tested the logic function of the driver. For example, if we want a load frequency of 187.5 kHz, 45° phase shift and 12.5% duty ratio pulse train, we should send 40, 10 and 20 to the 30-bit register when the CLK signal is 15MHz. The load is a 10k Ω (9.884k Ω) resistor and the DC supply is 10V (we used a 10 V DC supply instead of 20V to reduce overheating risk). The output waveform



Figure 5.4: Logic test result of the driver.

is shown in Figure 5.4. As we can see, the output pulse trains swing is from -10V to 10V, the duty ratio is approximately 12.5% , the distortions on the ends of pulses are caused by the total parasitic capacitance (caused by the bread board, the probe and load etc.) and switch capacitance. The combination of total parasitic capacitance and switch capacitance can be expressed as an external capacitance C_{ext} (Figure 3.5). The C_{ext} can be extracted from Figure 5.4, the 90% and 10% rise time ($t_{90\%}$ and $t_{10\%}$, respectively) of the output voltage's negative half cycle are approximately $4.98 \mu s$ and $2.20 \mu s$, respectively. These times satisfy the following equations:

$$90\%V_{CC} = V_{CC}(1 - \exp(-\frac{t_{90\%}}{R_{load}C_{ext}})) \quad (5.1)$$

$$10\%V_{CC} = V_{CC}(1 - \exp(-\frac{t_{10\%}}{R_{load}C_{ext}})) \quad (5.2)$$

If we substitute $t_{90\%} = 4.98 \mu s$ and $t_{10\%} = 2.20 \mu s$ into these equations, we can get the $C_{ext} \approx 128$ pF. Because of the switch capacitance is 70 pF (section 4.2), the total parasitic capacitance is approximately 58pF.

We tested this driver by letting it drive the transducer simulated in Section 5.1. The block diagram of the testing setup is shown in Figure 5.5. The driver drives a transducer connected using a 20 cm long coaxial cable. The optimum frequency and duty ratio of the transducer are modified

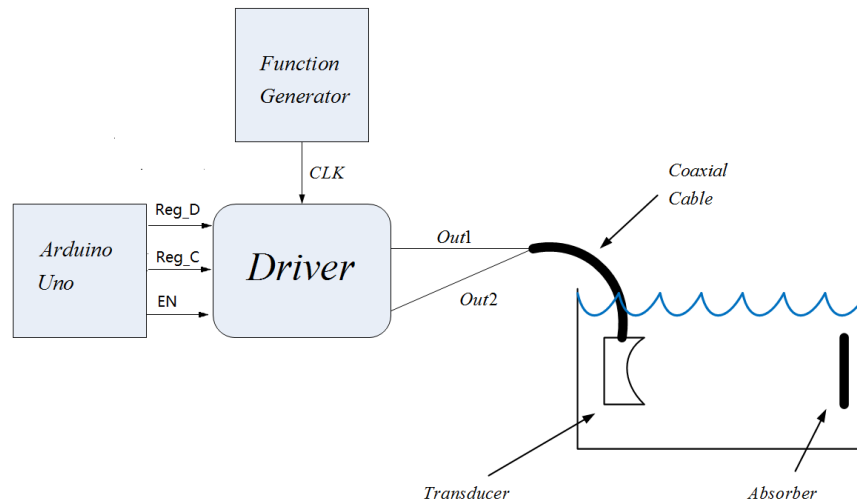


Figure 5.5: Block diagram of the testing setup of the driver

to 1028 kHz and 25.2% by C_{ext} .

We were intended to use a 102.8 MHz (which is 100 times of the transducer's optimum frequency) CLK signal, and send 50, 0 and 25 to each 10 bits of the 30-bit-register. But the maximum output frequency of the function generator is 15 MHz and also the driver is mounted on a bread board, the CLK signal's frequency cannot be too high. So we used a 8224 kHz CLK signal and sent 4, 0 and 2 to the driver's register for a 1028 kHz, 0° phase shift and 25% duty ratio (the closest condition we can get) pulse train.

5.3 Experimental Results

Figure 5.6 shows simulation results of driving the transducer simulated in Section 5.1 by using a 1028 kHz, 0° phase shift and 25% duty ratio pulse train (the parameters that were mentioned in Section 5.2). During the experimental test, we manually adjusted the frequency to obtain the best output waveforms at $f = 1036$ kHz. Experimental results are shown in Figure 5.7, the bottom waveform is taken from the pin Output2 and the middle one is taken from the pin Output1, the uppermost waveform is the Class-DE wave which drives transducer (Output1-Output2). A simulation with $f = 1036$ kHz is shown in Figure 5.8. Comparing to the simulation waveforms, the uppermost waveform is nearly a Class-DE waveform and matches the simulation result, but the waveforms of Output1 and Output2 are much worse, they have many distortions. These distortions may be caused by following two reasons:

-
1. The bread board's parasitic capacitance at the Output1 and Output2 are asymmetric.
 2. The loads of the coaxial cable's two nodes that connect the driver and transducer are asymmetric

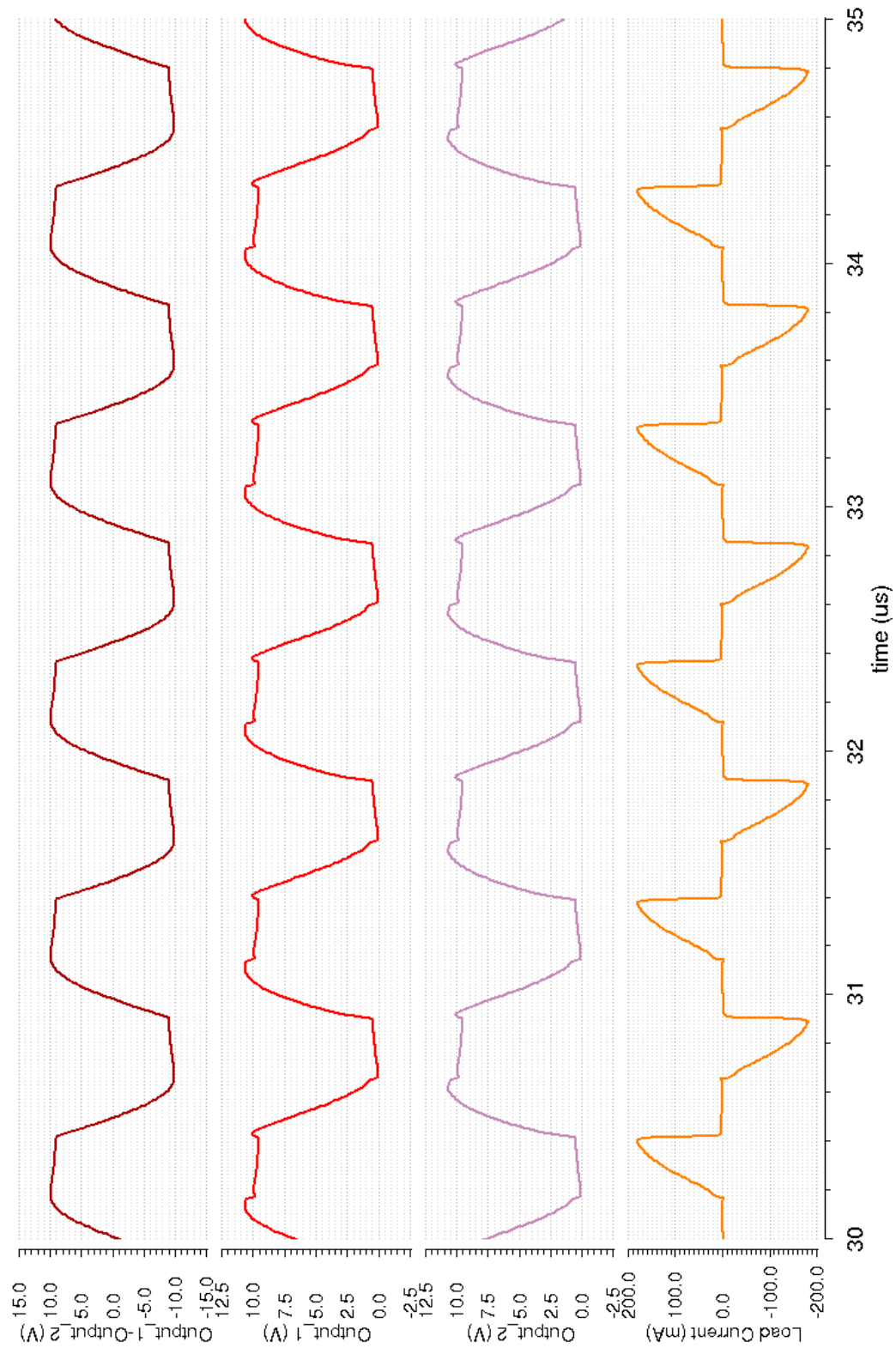


Figure 5.6: Simulation results of driving the transducer with $C_{ext} = 128$ pF by 1028 kHz, 0° phase shift and 25% duty ratio pulse trains. Brown: output voltage (Output1-Output2); Red: potential of Output1; Pink: potential of Output2; Orange: load current

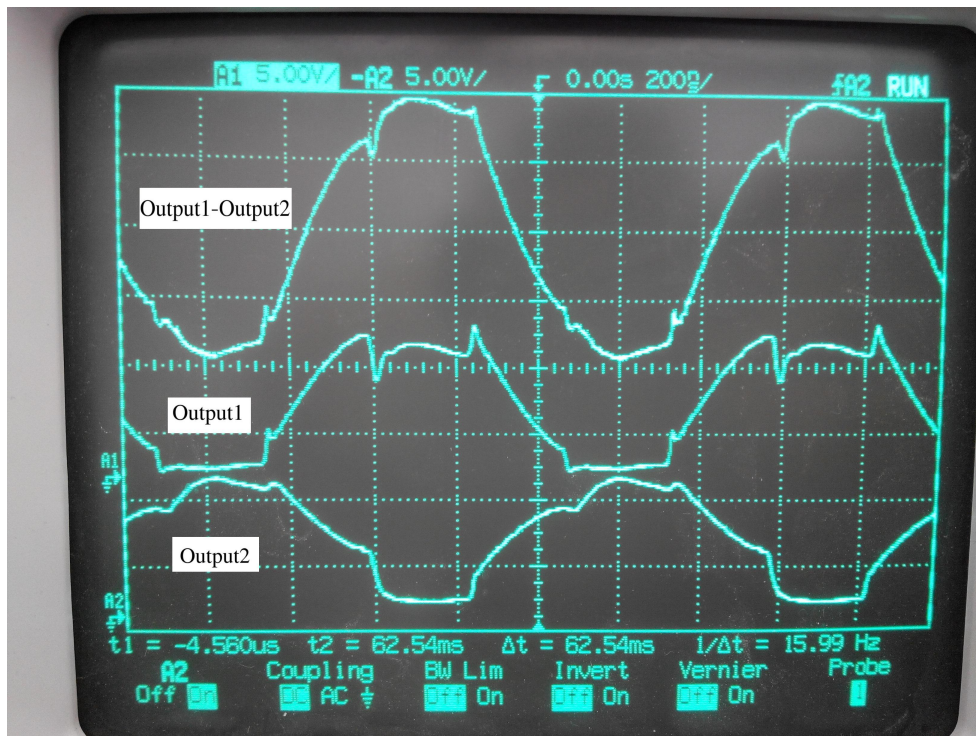


Figure 5.7: Experimental result of driving the transducer by 1036 kHz and 25% duty ratio pulse trains.

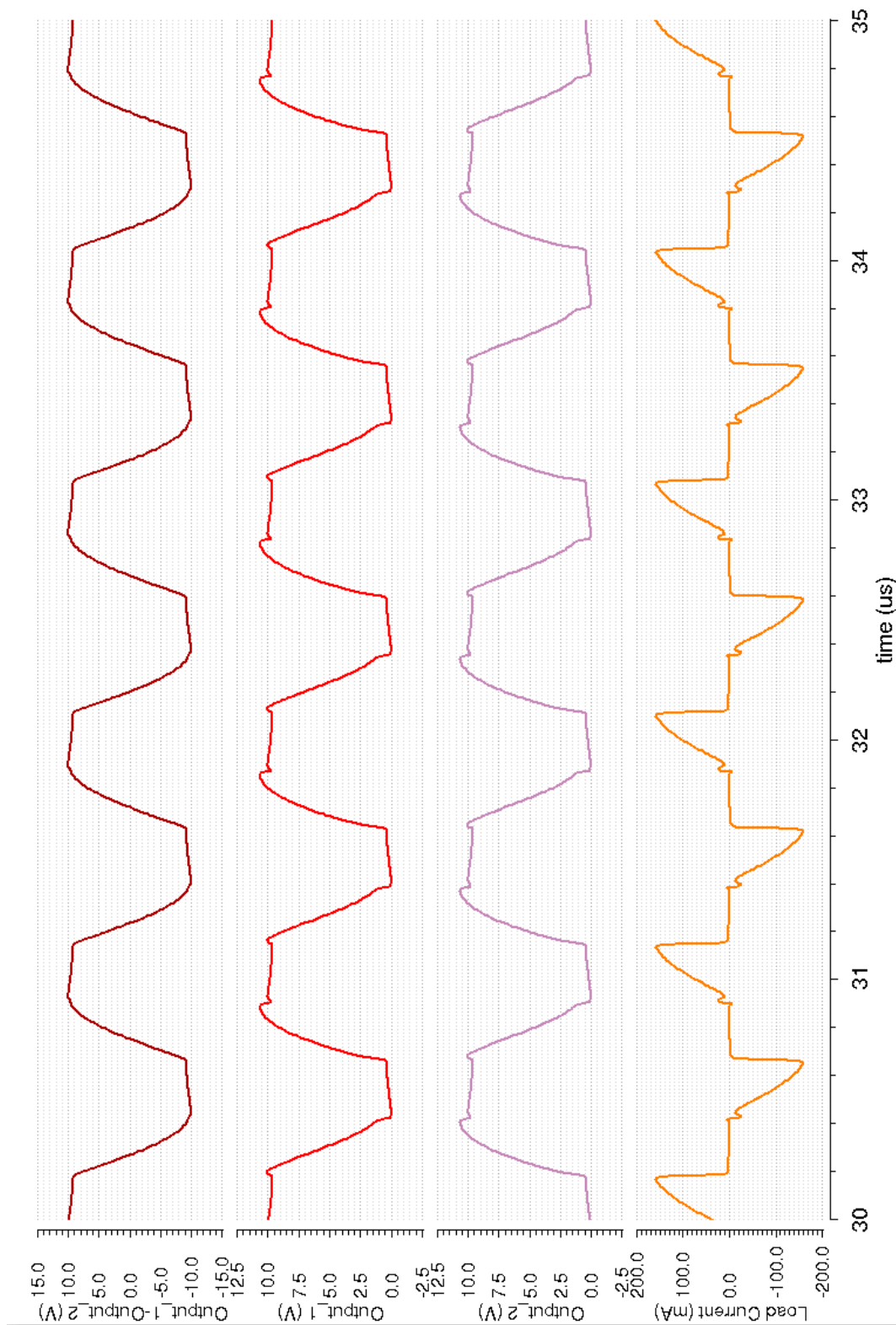


Figure 5.8: Simulation results of driving the transducer with $C_{ext} = 128$ pF by 1036 kHz, 0° phase shift and 25% duty ratio pulse trains. Brown: output voltage (Output1-Output2); Red: potential of Output1; Pink: potential of Output2; Orange: load current

Chapter 6

Conclusions and Future Work

6.1 Conclusions

The objective of this thesis was to design a CMOS driver for an ultrasound transducer array to be installed within the MRI environment. Some design challenges have been met. The driver does not require external matching networks and its die area is 2mm by 1.5mm.

Contrast to the previous half-bridge driver, the new full-bridge driver's switch pulses are generated internally by the chip. Their phase shifts, duty ratios and operation frequencies are digitally programmable. The power that can be delivered to some piezoelectric transducers by the new full-bridge driver is near 4 times to the previous half-bridge one's. Its efficiency is nearly 89.4% which is just slightly lower than the previous design. That might be caused by extra gate drivers, because the number of gate drivers is increased from 2 in previous design to 4 in this new design.

For driving a transducer array, we used an average frequency along each element and their own optimum duty ratios. This strategy can make a better balance between output power and efficiency than other strategies. However, not all transducers may work in Class-DE mode.

6.2 Future Work

There are several issues that need to be fixed:

- Bread boards have high parasitic capacitances that affect the performance of the driver. Further testing of the driver should be made on a printed circuit board.
- It should be determined if the driver with the current package can be used at all inside a MRI environment or not. If this is not possible, some of the remaining loose dies could be packaged

with a non-magnetic package or perhaps mounted directly at the back of transducers.

- The output MOSFETs in this design support a drain-source voltage of 50 V. However the gate oxide in can only support 20 V. Thus the high voltage supply in this driver is limited to 20 V and this limits the output power capacity for some transducers. In a future driver design the gate driver could be re-designed to allow a 50 V supply.
- The digital logic unit that we used in this design is limited to phase shifts from 0° to 180° for the driving pulse trains. The digital logic unit should be re-design to allow 0° to 360° phase shifts to.
- The relations of the Class-DE switching point's sensitivity with temperature, moisture etc. should be determined.
- A future version of the driver should incorporate a current measuring unit to measure the current flow through the MOSFETs of the Class-DE amplifier to monitor output power and send feedback to the array control system.
- In this design, the input clock signal of the counter still needs to be set externally. This signal has a very high frequency and distributing it may cause issues in the MRI environment. A future revision of the driver could use a low-frequency external clock signal along with a phase lock loop(PLL) [12] to produce the high-frequency clock signal internally.

Appendix A

Pin Diagram of the Full-Bridge Class-DE Driver

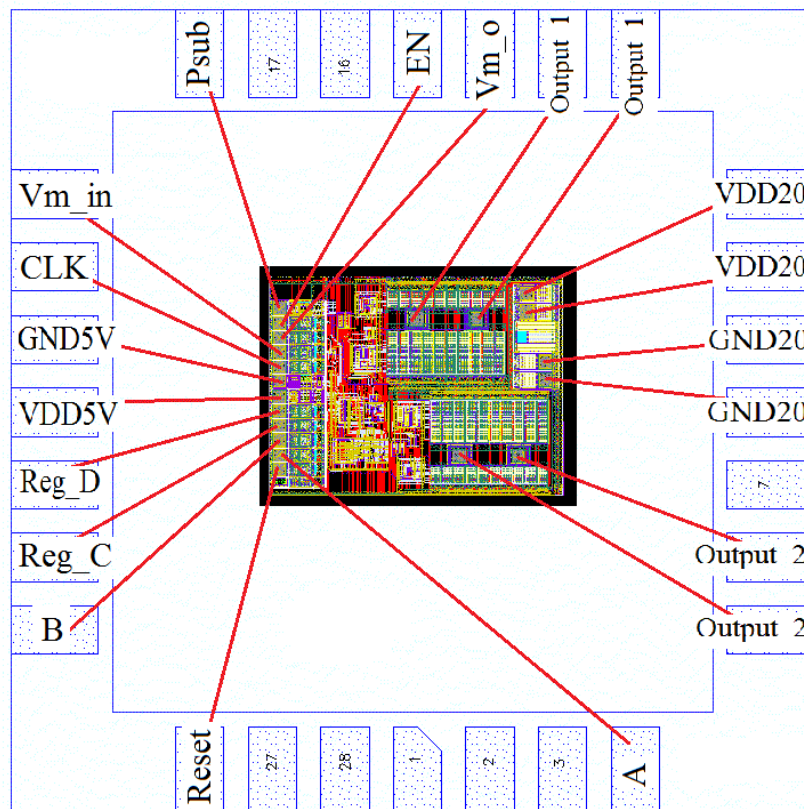


Figure A.1: Pin diagram of the full-bridge Class-DE driver

Appendix B

Parameter Calculations of MOSFETs

B.1 Gate Capacitance of MOSFETs

The gate capacitance of a MOSFET can be calculated by using the following equations [2]:

$$C_{gate} = W \cdot L \cdot C_{ox} + 2W \cdot L_D \cdot C_{ox} \quad (\text{B.1})$$

where the C_{gate} is the gate capacitance of a MOSFET, L_D is the lateral diffusion length of the gate, C_{ox} is the oxide capacitance per unit area and the term $2W \cdot L_D \cdot C_{ox}$ denote the gate-source and gate-drain capacitance of the MOSFET. The C_{ox} can be calculated by using the following equation:

$$C_{ox} = \frac{\epsilon_0 \epsilon_r}{t_{ox}} \quad (\text{B.2})$$

where the ϵ_0 is the permittivity of free space, which is equal to $\frac{10^{-9}}{36\pi} F/m$. The ϵ_r represents the relative permittivity of the silicon oxide, which is equal to 3.97. t_{ox} denotes the gate oxide thickness. But in this technology, the thickness of the gate is not even, so we cannot use this method to find the gate capacitance of the MOSFET.

Another way to get the gate capacitance is using Spectre®simulation, Figure B.1 shows the simulation schematic. If we detect the gate voltage of both the NMOS and PMOS in the full-bridge Class-DE amplifier, we can get the Figure B.2 and B.3, in this two plots, we can get the 10% and 90% of raising time which is shown in Table B.1. In this simulation, the $R_G = 100k\Omega$, so we can

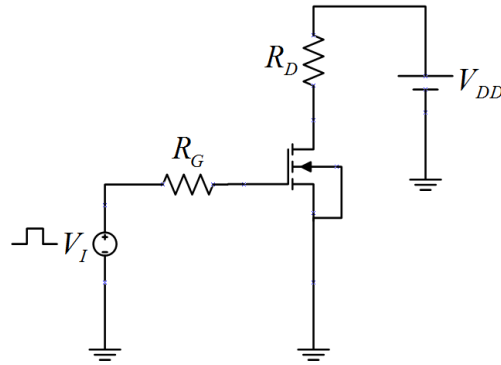


Figure B.1: Gate capacitance extraction circuit

	NMOS	PMOS
10% of raising time($t_{10\%}$)	0.01301 μs	0.01572 μs
90% of raising time($t_{90\%}$)	0.41797 μs	0.23009 μs

Table B.1: Step signal responds of gate voltage of the PMOS and NMOS that used in the amplifier

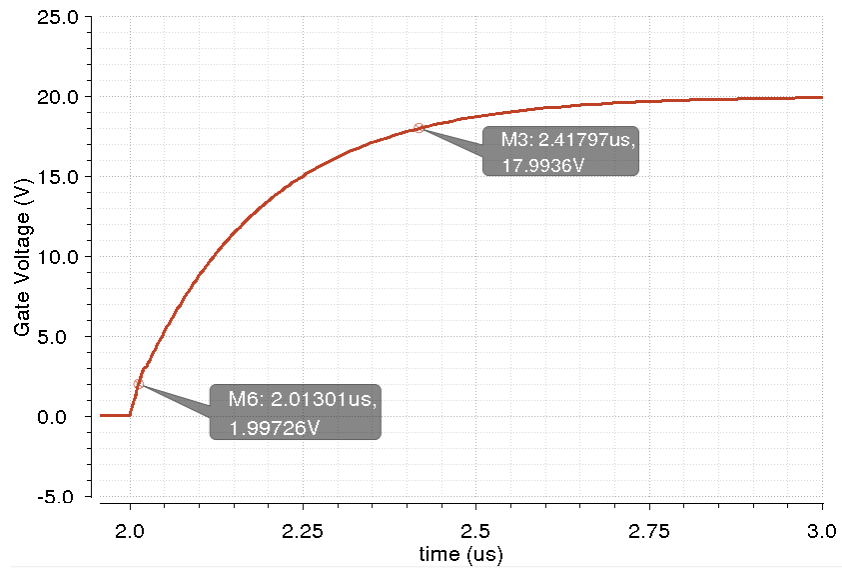


Figure B.2: Gate voltage plot of NMOS

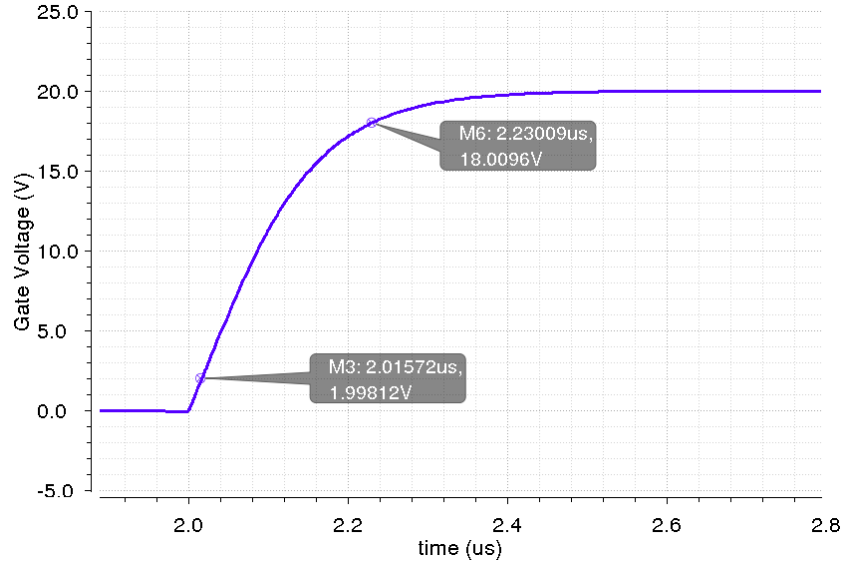


Figure B.3: Gate voltage plot of PMOS

use the following equations to get the value of the gate capacitance C_{gate} :

$$10\%V_{DD} = V_{DD}(1 - \exp(-\frac{t_{10\%}}{\tau})) \quad (B.3)$$

$$90\%V_{DD} = V_{DD}(1 - \exp(-\frac{t_{90\%}}{\tau})) \quad (B.4)$$

where $\tau = R_G \cdot C$. Solving these two equations for both PMOS and NMOS that we used in the amplifier, we can get the gate capacitance of PMOS is 9.76pF and the gate capacitance of NMOS is 18.4pF.

B.2 K' and Threshold Voltage

The technological parameters of a MOSFET, such as k' , V_{th} , can be extracted by using the schematic which is shown in Figure B.4 [2]. This extraction can be done by using Spectre® to simulate the circuit. The theoretical drain current of the MOSFET can be expressed as:

$$I_{Dt} = \frac{k'}{2} \frac{W}{L} (V_{GS} - V_{th})^2 \quad (B.5)$$

where the I_{Dt} is the theoretical drain current of the MOSFET, V_{GS} is the gate-source voltage of the MOSFET. If we make square root of both sides of this equation, we can get:

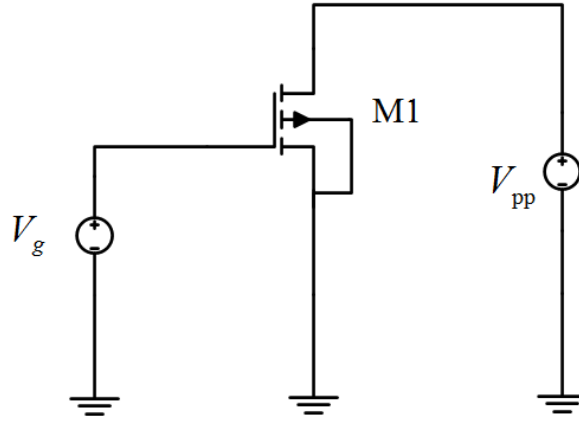


Figure B.4: Schematic of a MOSFET's parameters extraction [2]

$$\sqrt{I_{Dt}} = \sqrt{\frac{k'W}{2L}}(V_{GS} - V_{th}) \quad (\text{B.6})$$

The equation B.6 shows that the $\sqrt{I_D}$ is proportional to V_{GS} . If $V_{GS} = V_{th}$, the $\sqrt{I_D}$ will be equal to 0. The $\sqrt{I_D}$ plots of the real MOSFET and a theoretical model are shown in Figure B.5.

As we can see in the Figure B.5, the theoretical plot of $\sqrt{I_D}$ is same as the real model's plot in the middle part of this curve, so the expression of the real model's plot is almost same as the equation B.6. Near the $V_{GS} = V_{th}$, the expression of the real model's plot can be expressed as [2]:

$$\sqrt{I_D} = \sqrt{\frac{k'W}{2L}}(V_{GS} - V_{th})\sqrt{\frac{1}{1 + \theta(V_{GS} - V_{th})}} \quad (\text{B.7})$$

The factor $\sqrt{\frac{1}{1 + \theta(V_{GS} - V_{th})}}$ is introduced to compromise the behaviour near the end of $\sqrt{I_D}$ versus V_{GS} curve due to mobility degradation [2], as shown in the red line in Figure 4.8. However, when V_{GS} is not too much higher than V_{th} the $\sqrt{\frac{1}{1 + \theta(V_{GS} - V_{th})}} \approx 1$, so we still can use the equation (4.12) to describe the curve when V_{GS} is not very high. In Figure 4.8, the theoretical plot of $\sqrt{I_{Dt}}$ is a straight line and its slope is $\sqrt{\frac{k'W}{2L}}$.

$$\frac{\Delta\sqrt{I_{Dt}}}{\Delta V_{GS}} = Slope = \sqrt{\frac{k'W}{2L}} \quad (\text{B.8})$$

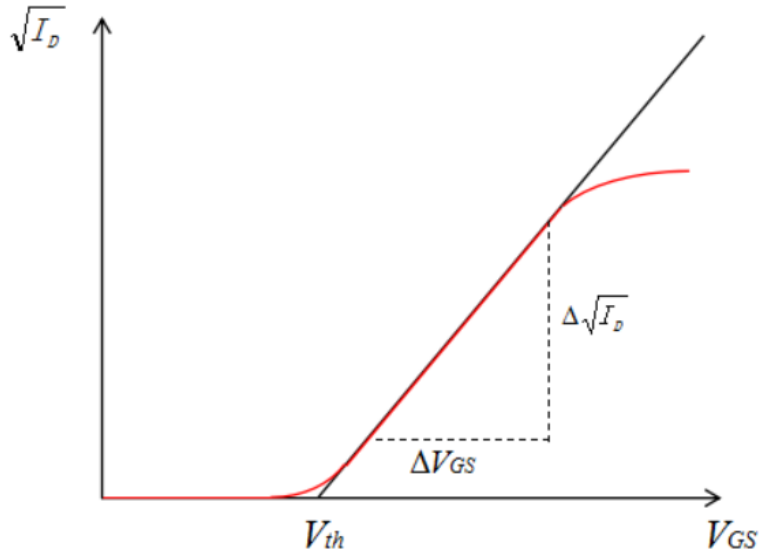


Figure B.5: $\sqrt{I_D}$ plots of a real MOSFET and a theoretical model, the red line is the real MOSFET's plot and the black line is the theoretical model's plot [2]

If we solve the equation (4.14), we have:

$$k' = \frac{2 \cdot L(\text{slope})^2}{W} \quad (\text{B.9})$$

If we use the equation (4.12) by (4.13), we can get:

$$\frac{\sqrt{I_{Dt}}}{\sqrt{I_D}} = \sqrt{1 + \theta(V_{GS} - V_t)} \quad (\text{B.10})$$

then we can solve this equation for θ , θ is true when $V_{GS} \gg V_t$, its expression is:

$$\theta = \frac{I_{Dt} - I_D}{I_D \cdot V_{GS} - I_D \cdot V_t} = \left(\frac{I_{Dt}}{I_D} - 1 \right) \left(\frac{1}{V_{GS} - V_t} \right) \quad (\text{B.11})$$

The Figure B.6 shows the $\sqrt{I_D}$ plot of PMOS and the Figure B.7 shows the $\sqrt{I_D}$ plot of NMOS. When the $\sqrt{I_{Dt}} = 0$, the gate-source voltage is the transistor's threshold voltage, therefore in Figure B.6 and Figure B.7 we can get the threshold voltage of PMOS is -1.52 V and the threshold voltage of NMOS is 2.7 V. The slope of the PMOS's $\sqrt{I_{Dt}}$ is -0.2676 and the slope of the NMOS's $\sqrt{I_{Dt}}$ is 0.1654. So based on equation B.9, the k' value for the PMOS and the NMOS are $5.57 \mu\text{A}/\text{V}^2$ and

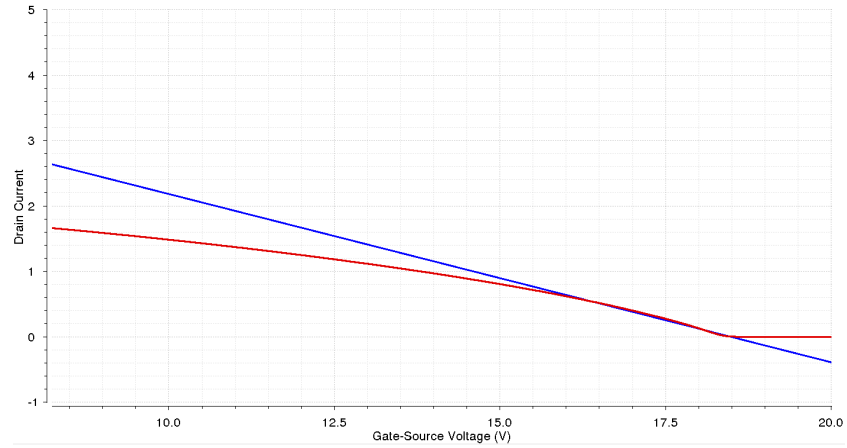


Figure B.6: $\sqrt{I_D}$ plots the PMOS, the blue line is the theoretical square root of drain current $\sqrt{I_{Dt}}$ and the red line is the real model's square root of drain current $\sqrt{I_D}$

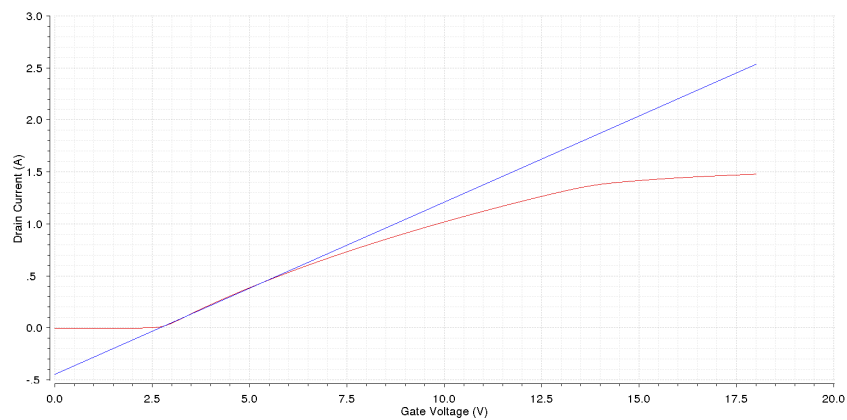


Figure B.7: $\sqrt{I_D}$ plots the NMOS, the blue line is the theoretical square root of drain current $\sqrt{I_{Dt}}$ and the red line is the real model's square root of drain current $\sqrt{I_D}$

$3.91\mu A/V^2$ respectively.

B.2.1 Calculation of on-resistance

The expression of channel resistance is shown below, it is derived from the expression of drain current of a MOSFET that is in triode mode [2].

$$I_D = \frac{k'}{2} \frac{W}{L} \frac{2(V_{GS} - V_t)V_{DS} - V_{DS}^2}{1 + \theta(V_{GS} - V_t)} \quad (\text{B.12})$$

If we simplify this equation, we can get [2]:

$$I_D \approx \frac{k'}{2} \frac{W}{L} \frac{2(V_{GS} - V_t)V_{DS}}{1 + \theta(V_{GS} - V_t)} \quad (\text{B.13})$$

So the expression of the on-resistance of a MOSFET is [2]:

$$R_{ch} = \frac{V_{DS}}{I_D} = \frac{1 + \theta(V_{GS} - V_t)}{\frac{k'}{2} \frac{W}{L} (V_{GS} - V_t)} \quad (\text{B.14})$$

The summary of extracted parameters values of the PMOS and NMOS are shown in Table B.2

	NMOS	PMOS
$k'(\mu A/V^2)$	3.91	5.57
$V_t (V)$	2.7	-1.52
$\theta (V^{-1})$	0.3336	-0.4391
$R_{ch}(\Omega)$	4.17	4.07

Table B.2: Summary of extracted parameters values of the PMOS and NMOS

Appendix C

Schematic Diagrams

The schematic diagrams used in Spectre®.

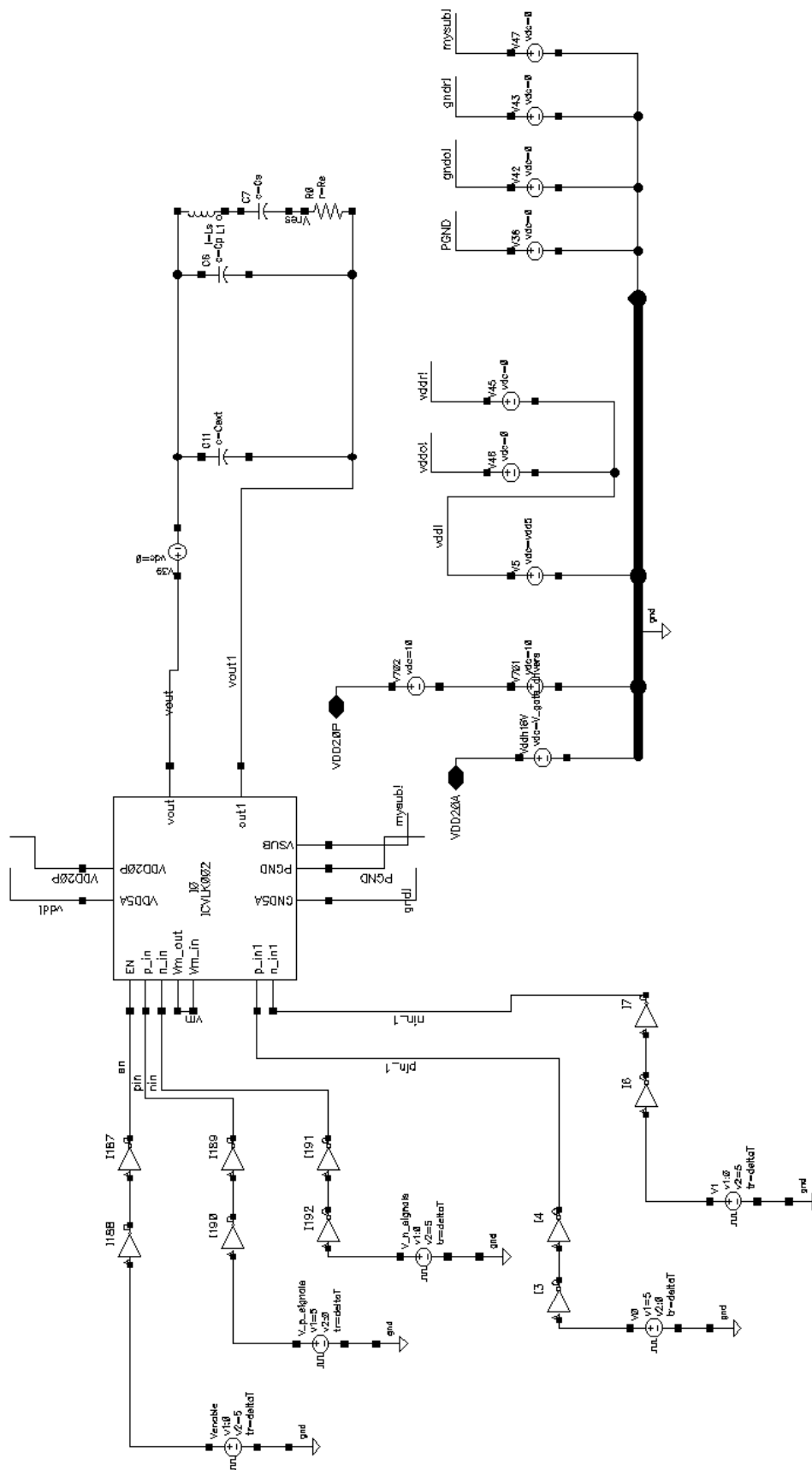


Figure C.1: Block diagrams of simulation circuit of the full-bridge Class-DE amplifier.

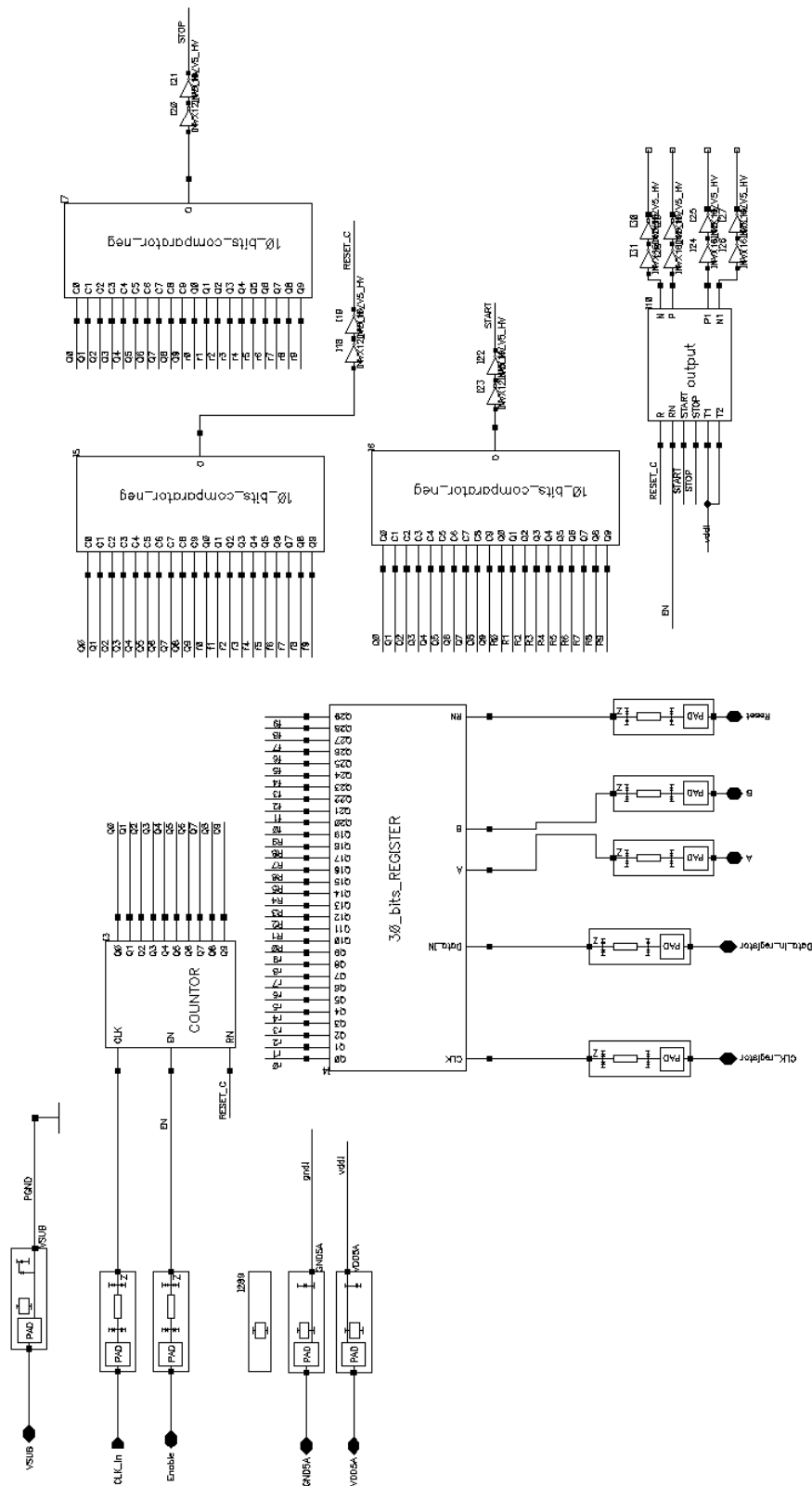


Figure C.2: Block diagrams of the logic control unit

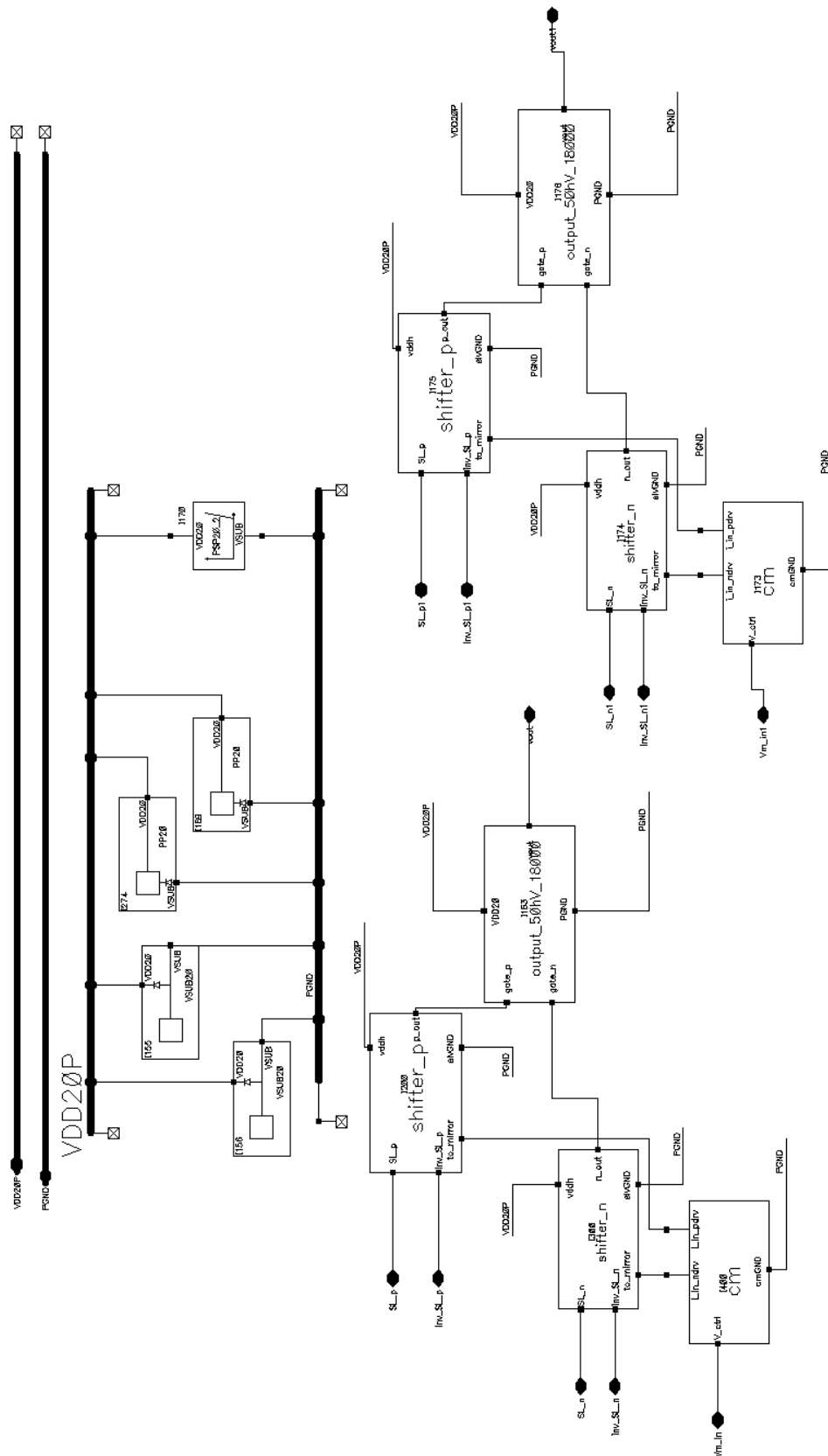


Figure C.3: Block diagrams of the Class-DE amplifier with gate drivers

Appendix D

Layout View

The layout views used in Virtuoso.

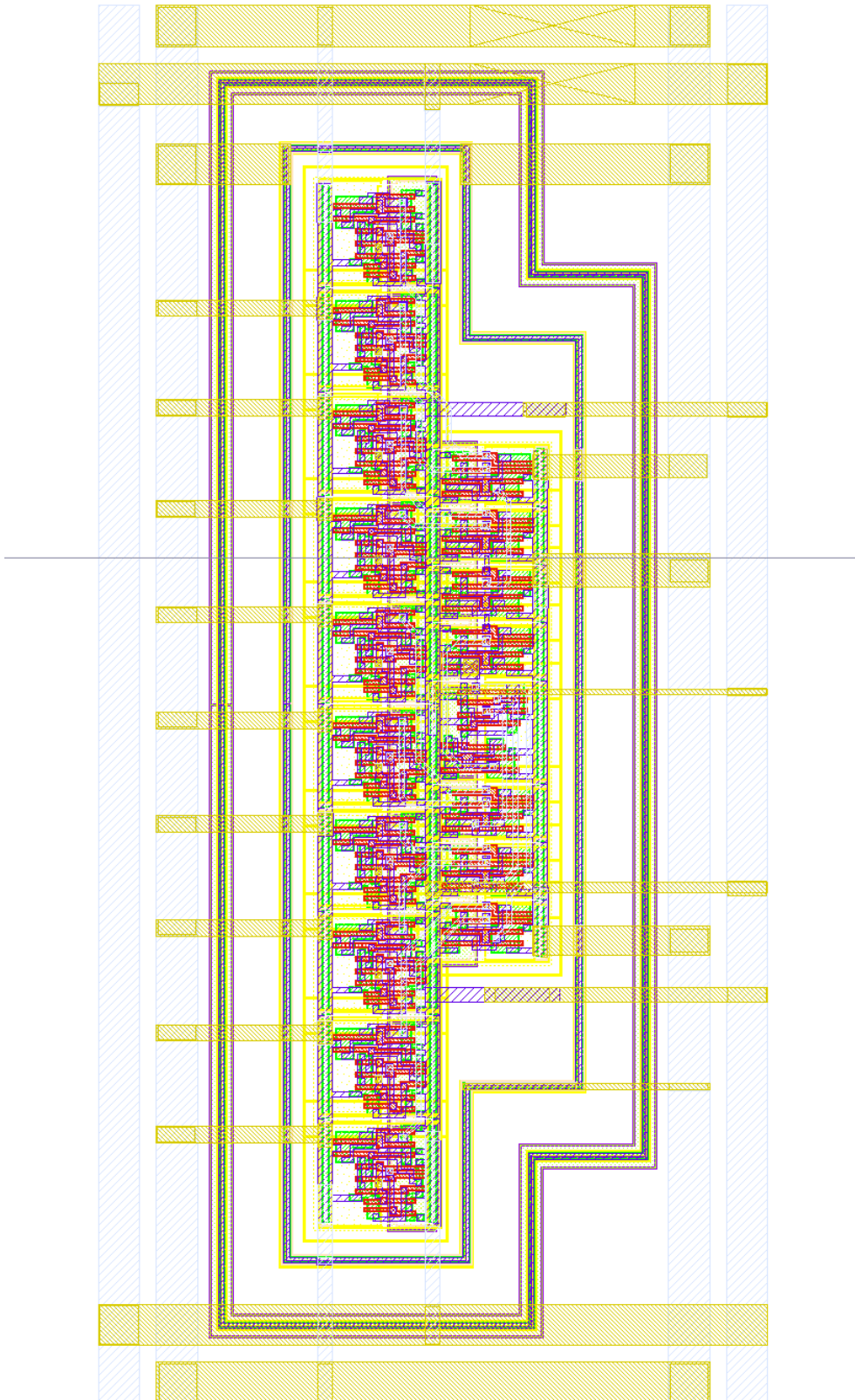


Figure D.1: Layout of the 10-bit-comparator

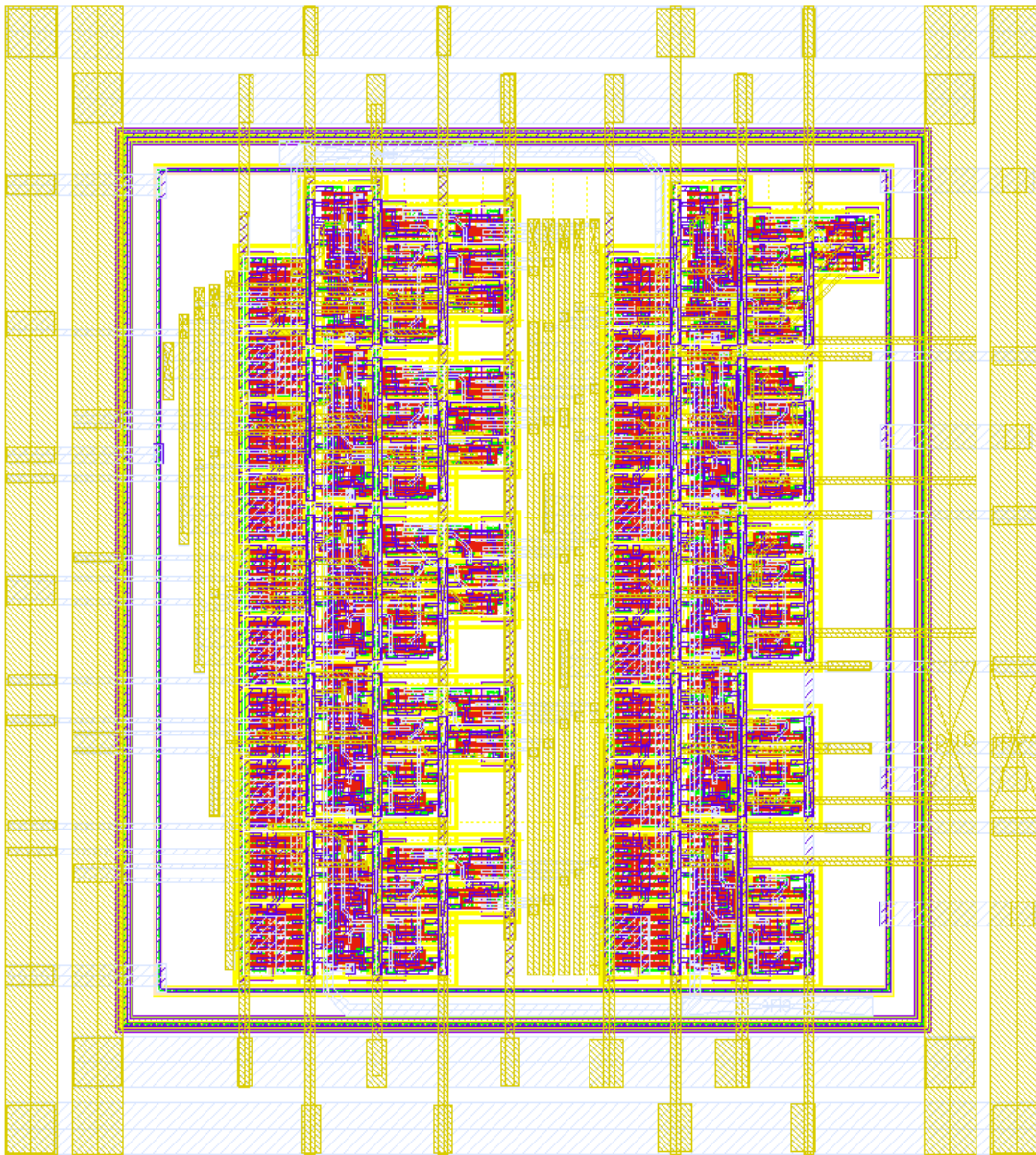


Figure D.2: Layout of the 10-bit-counter

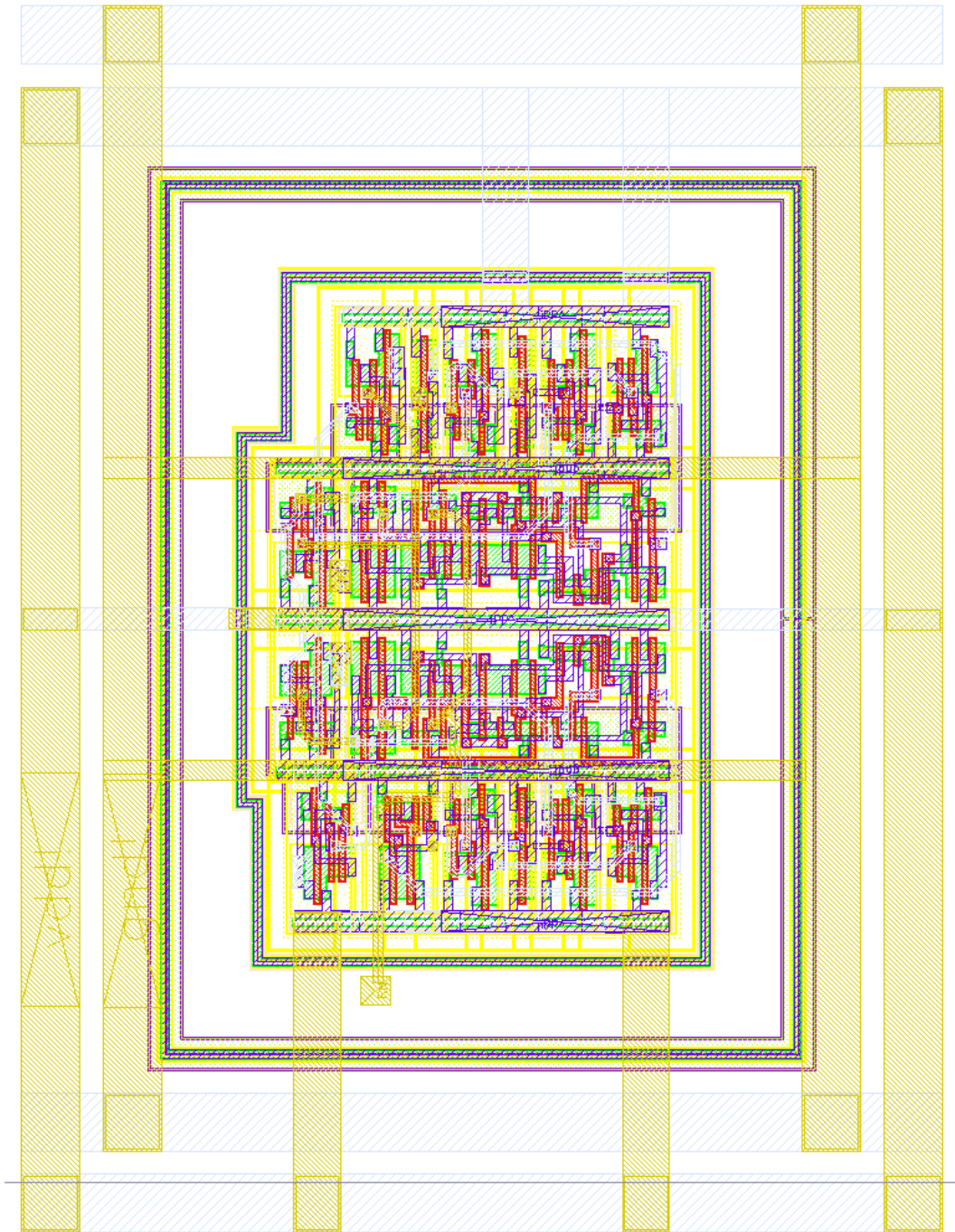


Figure D.3: Layout of the pulse trains generator

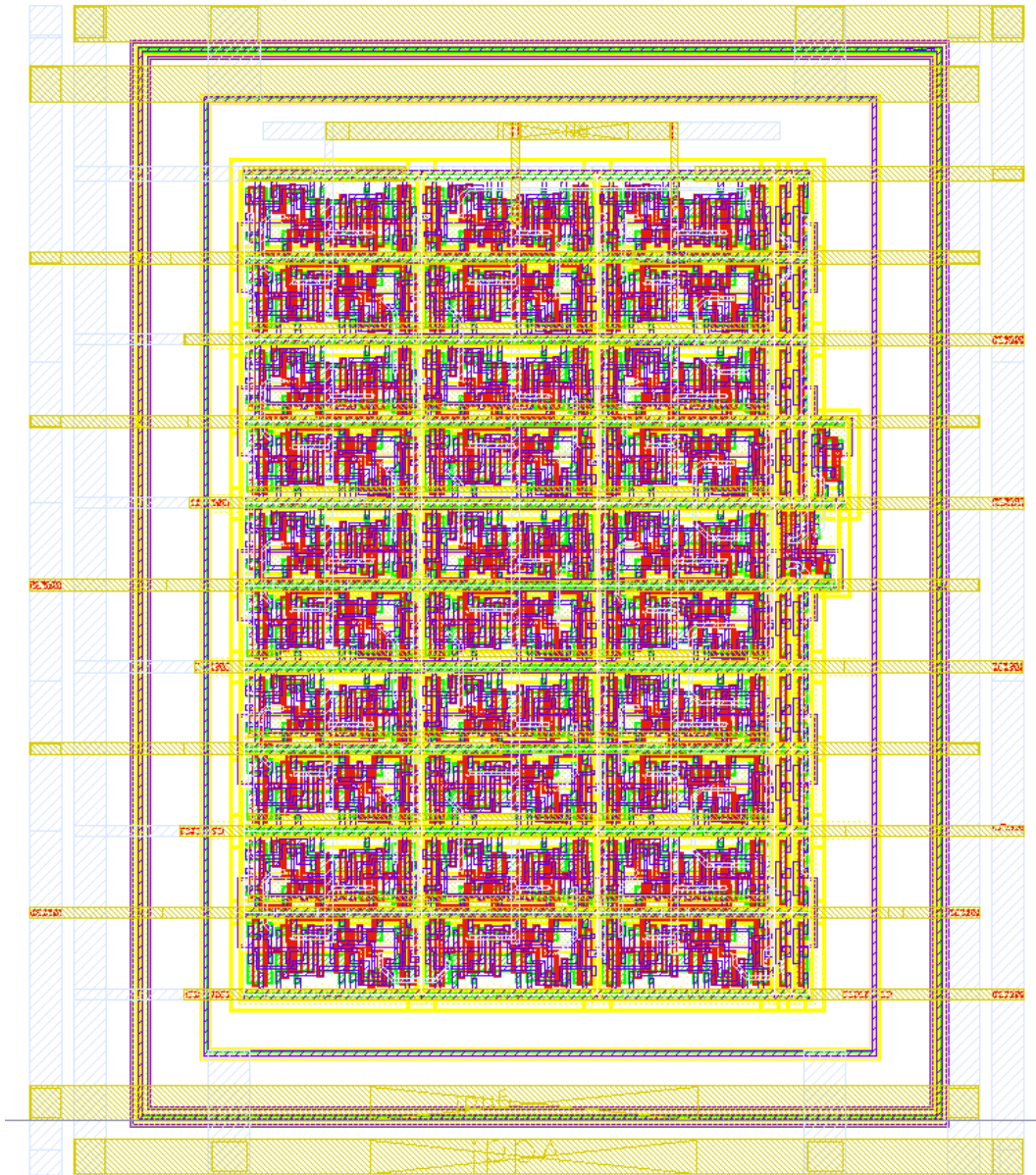


Figure D.4: Layout of the 30-bit-register

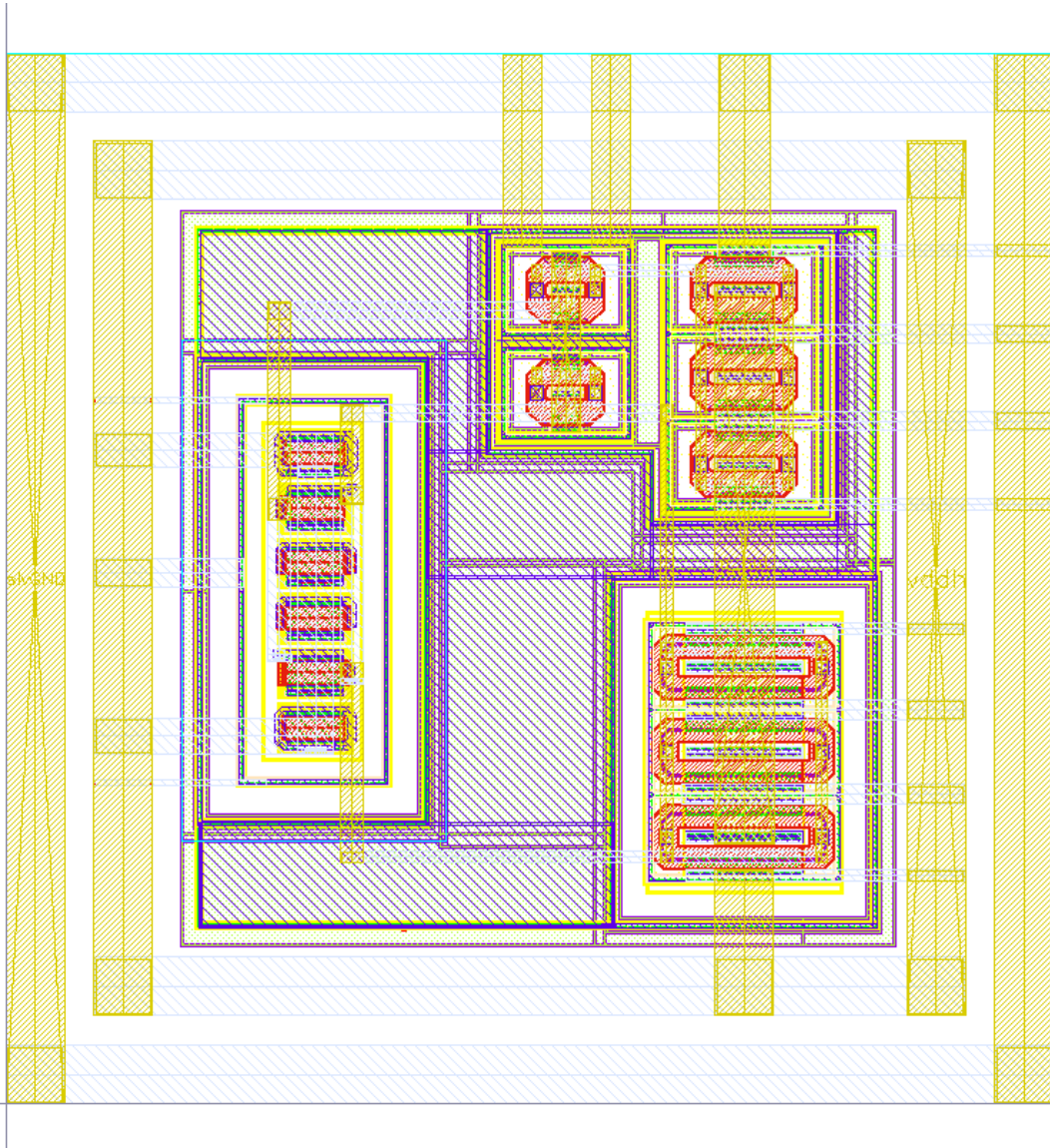


Figure D.5: Layout of the NMOS's gate driver that designed by Wai Wong

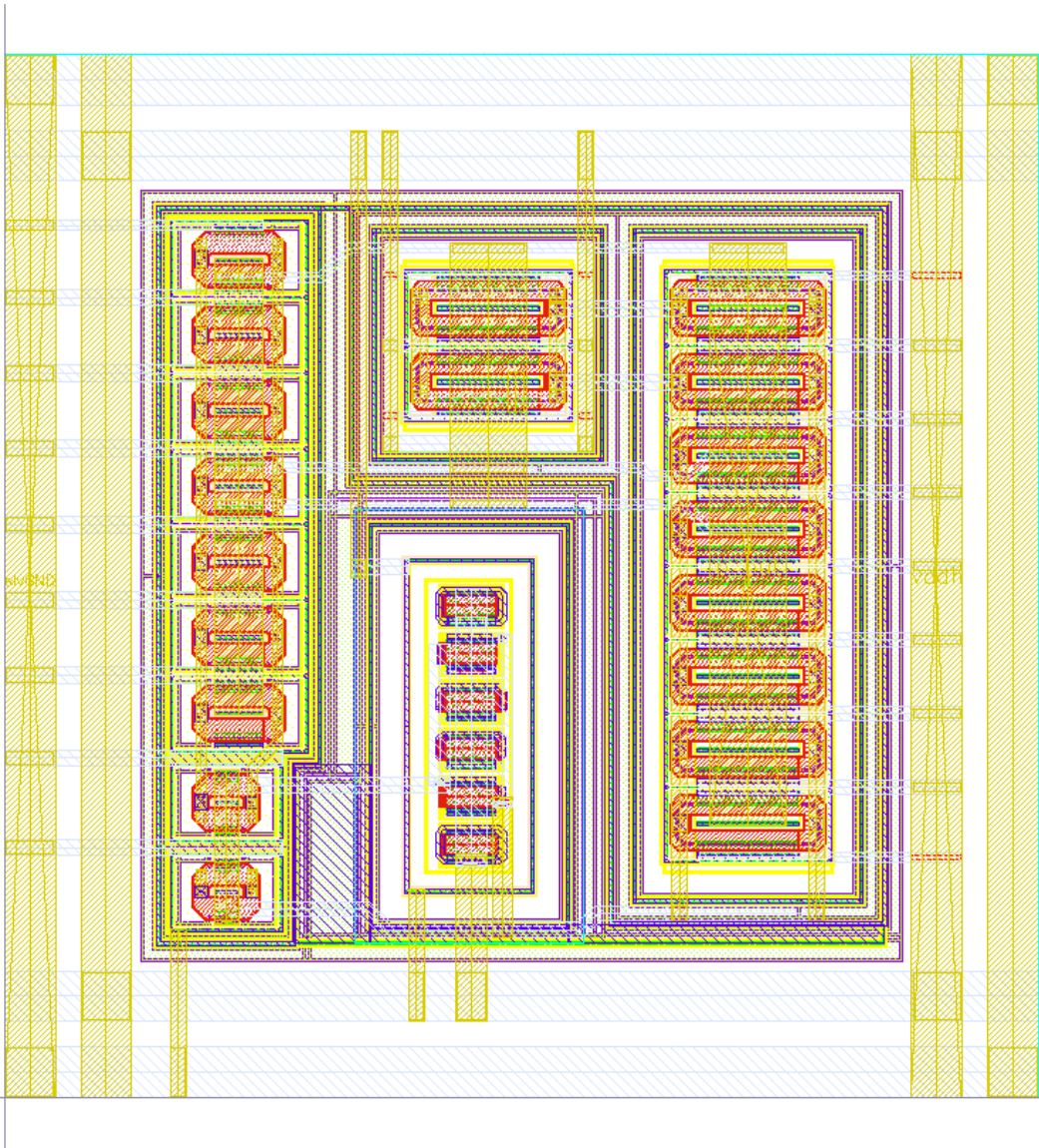


Figure D.6: Layout of the PMOS's gate driver that designed by Wai Wong

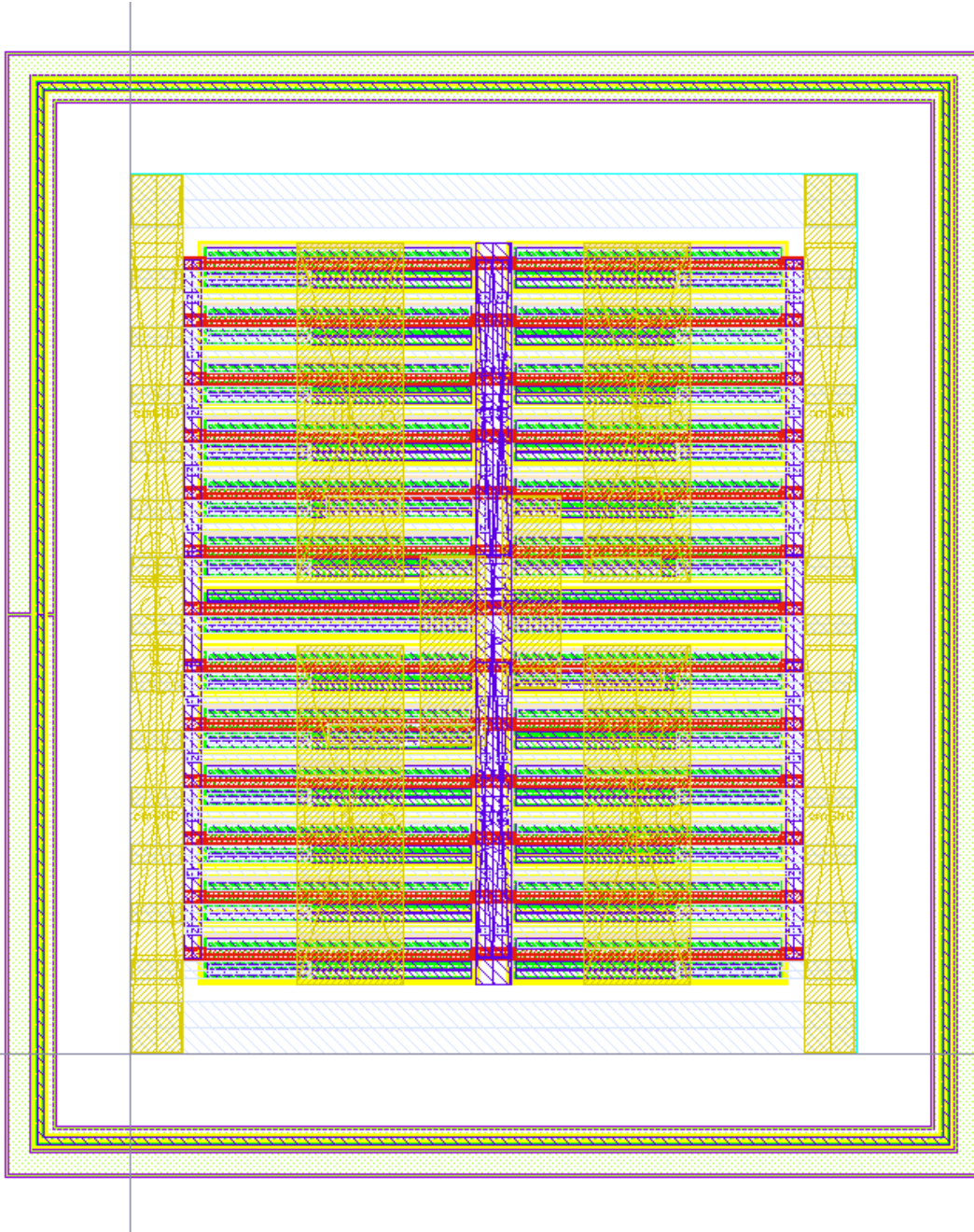


Figure D.7: Layout of the gate drivers' current mirror that designed by Wai Wong

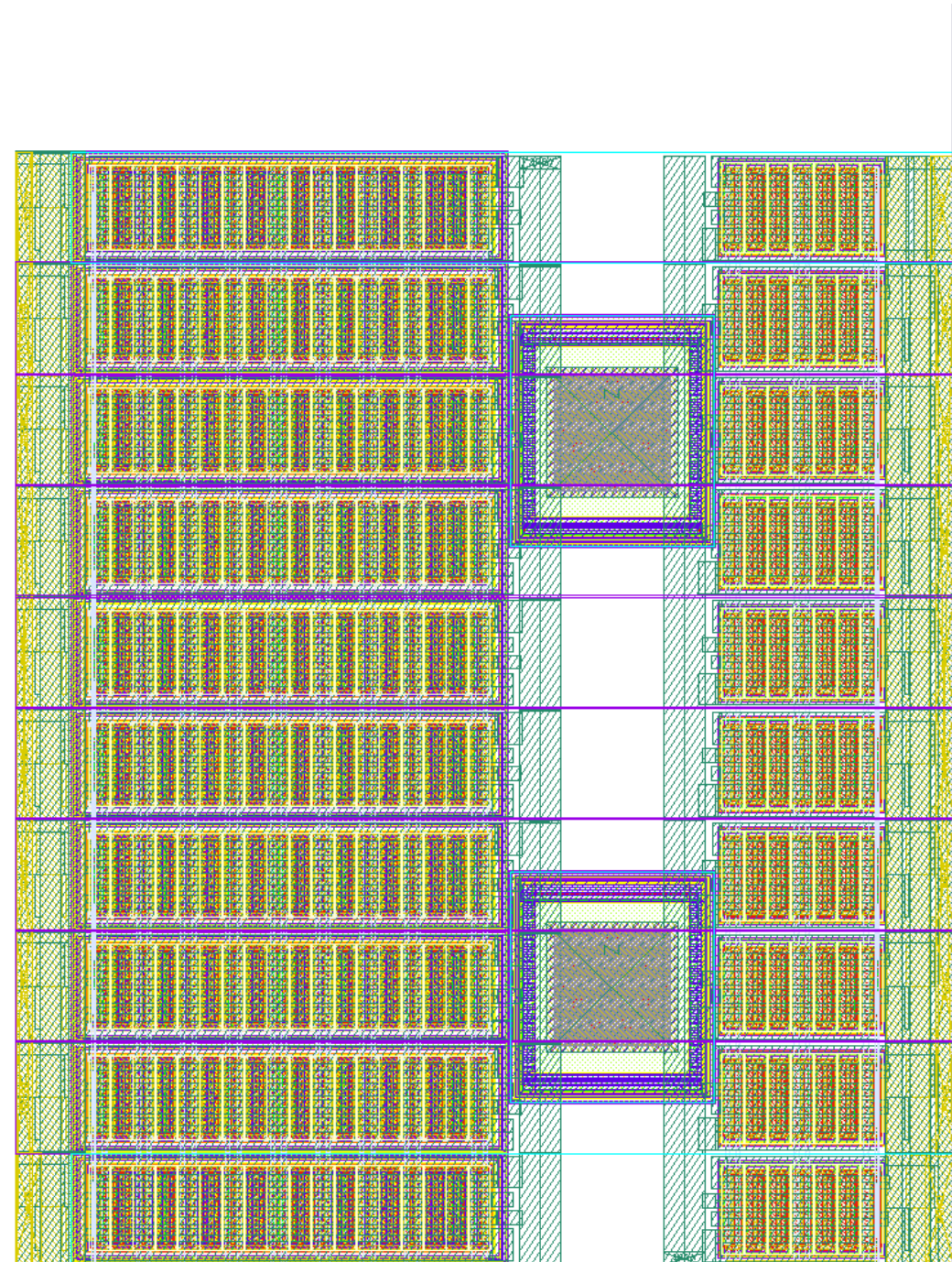


Figure D.8: Layout of a branch of Class-DE amplifier that designed by Wai Wong

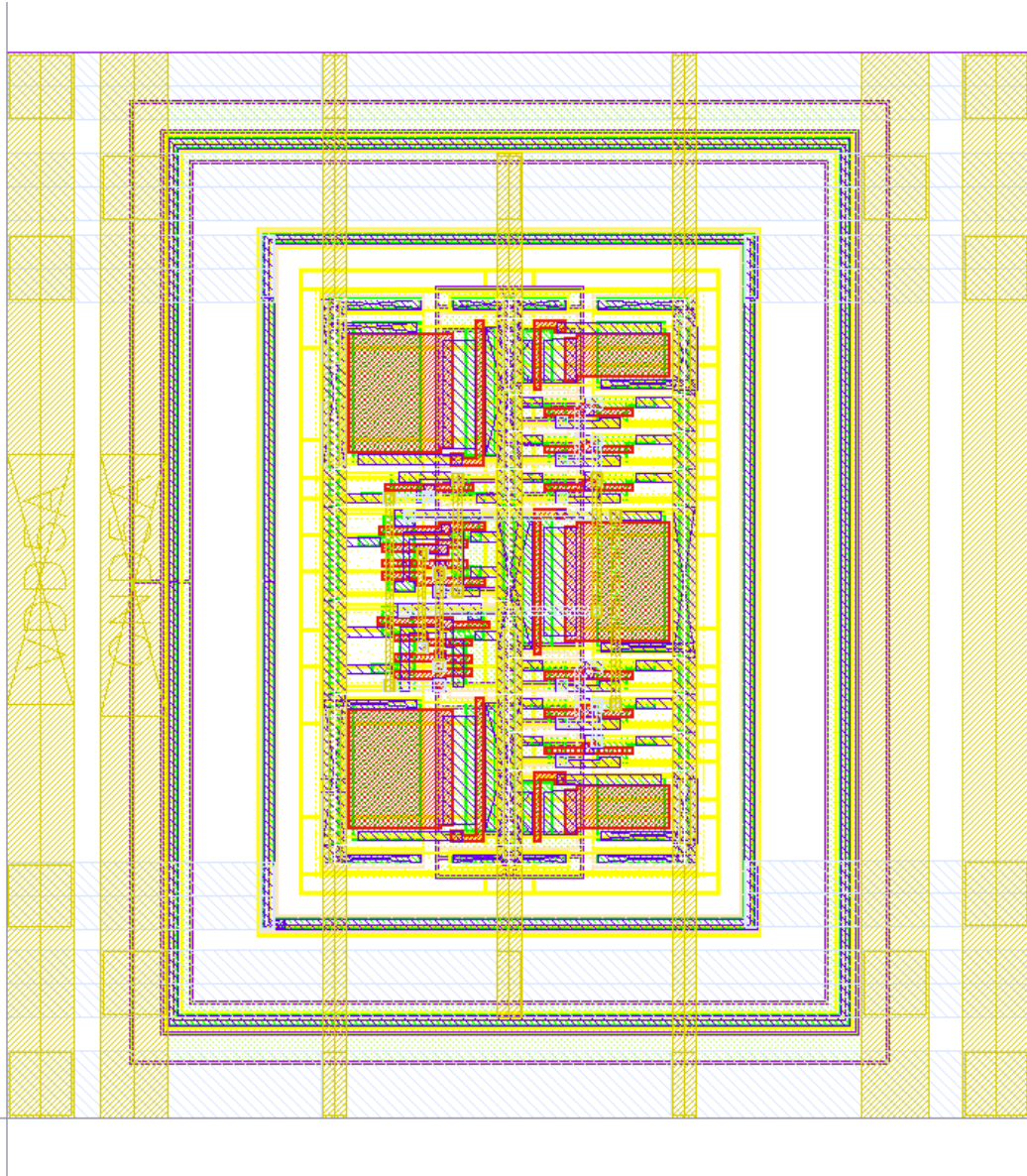


Figure D.9: Layout of the additional safety logic block that designed by Wai Wong

Bibliography

- [1] W. Wong, C. Christoffersen, Samuel Pichardo, Laura Curiel “An Integrated Ultrasound Transducer Driver For HIFU Applications,” *Proc. 2013 IEEE Canadian Conf. on Electrical and Computer Engineering*, 2013, pp. 1–5.
- [2] W. Wong, “An Integrated Ultrasound Transducer Driver For HIFU Applications,” *MSc Thesis Dissertation*, Lakehead University, 2013.
- [3] “IEEE Standard Definitions and Methods of Measurement for Piezoelectric Vibrators,” *IEEE Std No.177*, p. 1, 1966.
- [4] J. L. Kivinen, “A Device for Performing Sonoporation on Adherent Cell Cultures”.*MSc Thesis Dissertation*, Lakehead University, 2014.
- [5] C. Christoffersen, W. Wong, S. Pichardo, G. Togtema and L. Curiel “Class-DE Ultrasound Transducer Driver for HIFU Therapy” *IEEE Transactions On Biomedical Circuits And Systems*, vol.10, issue 2, pp.375-382, May 2015
- [6] M. Kazimierczuk, “Class DE RF Power Amplifier,” in *RF Power Amplifiers*, Chichester, West Sussex, U.K., Wiley, 2008, pp. 251–265.
- [7] S. C. Tang and G. Clement, “A harmonic cancellation technique for an ultrasound transducer excited by a switched-mode power converter,” *IEEE Trans. on Ultrasonics, Ferroelectrics and Frequency Control*, vol. 55, no. 2, pp. 359–367, February 2008.
- [8] L. Svilainis, V. Dumbrava and G. Motiejunas, “Optimization of the ultrasonic excitation stage”, *30th International Conference on Information Technology Interfaces*, 2008. ITI 2008. 2008. pp. 791–796.
- [9] T. Hall and C. Cain, “A Low Cost Compact 512 Channel Therapeutic Ultrasound System For Transcutaneous Ultrasound Surgery,” *AIP Conf. Proc.*, vol. 829, pp. 445–449, May 8 2006.

- [10] L. Yang, L. Xu, T. Yang and B. Zhang, "Class D power amplifier for audio beam system," *International Conference on Mechatronics and Automation*, 2007. ICMA 2007. 2007. pp. 3469–3474.
- [11] D. Zhao; M. T. Tan; H. K. Cha; J. Qu; Y. Mei; H. Yu; A. Basu; M. Je, " High-voltage pulser for ultrasound medical imaging applications" *Integrated Circuits (ISIC), 2011 13th International Symposium* pp.408-411, 2011.
- [12] A. Bozkurt; O. Farhanieh; R. B. Roy; A. S. Ergun, " Design of a driver IC for an ultrasound catheter ablation system" *Ultrasonics Symposium (IUS), 2014 IEEE International*, pp.1536-1539, 2014
- [13] K. Moro; J. Okada; K. Takada; S. Yoshizawa; S. i. Umemura, "Staircase-wave drive circuit to drive therapeutic array transducer" *Ultrasonics Symposium (IUS) IEEE*, pp. 1799-1802, 2010
- [14] D. C. Hamill, "Impedance plane analysis of class DE amplifier," *Electronics Letters*, Vol. 30, Issue 23, pp. 1905–1906, Nov. 1994.
- [15] Samuel Pichardo, Rafael R. C. Silva ,Oleg Rubel, Laura Curiel "Efficient Driving of Piezoelectric Transducers Using a Biaxial Driving Technique" *PLOS ONE*, DOI: 10.1371/journal.pone.0139178, September 29, 2015
- [16] H. Ballan and M. Declercq, "High-Voltage Analog and Digital Output Interfaces," in, *High Voltage Devices and Circuits in Standard CMOS Technologies*, Dordrecht, Netherlands: Kluwer Academic Publishers, 1999, ch. 6, pp. 181-207.
- [17] Yan Shi and Wang Hong , "Synchronous Logical Circuits," in *The fundamental of digital circuit* Beijing, China: Higher Education Press, 2010, ch. 6, pp. 259-354
- [18] "Foundry Design Kit 0.8 μ m 5/20V CMOS Cell Library", Dalsa Semiconductor Inc., Document No. DK08EDS01.04, 2005. 34 D. Clein 1958-, *CMOS IC Layout : Concepts, Methodologies, and Tools* /. Boston : Newnes, c2000.